Development of a Small-Sized Wireless Power Transfer System with High Efficiency for Wireless Charging of Biomedical Implants

シマ アルバサオ アブデルラズ アルシュヘウィ

https://hdl.handle.net/2324/7157365

出版情報：九州大学, 2023, 博士（学術）, 課程博士
バージョン：
権利関係：

Graduate School of Information Science and Electrical Engineering

Development of a Small-Sized Wireless Power Transfer System with High Efficiency for Wireless Charging of Biomedical Implants

By

Shimaa Albasuony Abd-Elrazk Alshhawy

A Doctoral thesis

Submitted to the Graduate School of Information Science and Electrical Engineering in partial fulfillment of the requirements for the degree of Doctor of Philosophy

Department of Electrical and Electronics Engineering

Graduate School of Information Science and Electrical Engineering

Kyushu University, Fukuoka, Japan

2023

ABSTRACT

Wireless power transfer (WPT) is a crucial technology with many practical applications, particularly in the biomedical field. By charging implanted sensors wirelessly, the use of batteries and their associated risks can be avoided. Near-field WPT is the most common technique used in biomedical applications, as it is better suited to compact implanted devices and provides insensitivity to misalignment and electromagnetic compatibility. However, the presence of biological tissue introduces challenges, including the degradation of the system's performance due to misalignment and changes in resonance frequency.

To address these challenges, we developed a frequency-misalignment-insensitive WPT system for use in biomedical applications. Our system is based on short-length inductors and stacked metamaterials that take advantage of the self-shielding and high-coupling properties of the metamaterials. Specifically, our unit cell consists of multi-ring resonators (MRR) that have low magnetic loss and can improve the intensity of the magnetic field. We achieved good performance with our system, which allowed for further reduction in the size of the implanted receiver (RX) while achieving a matching-less rectifier without increasing the system's area.

We evaluated our system in three parts. The first part involved designing a compact and efficient frequency-dependency WPT system using small inductor theory DGS resonator. The transmitter (TX) was 20mm x 20mm with three cooperative DGS resonators, and the RX was 10mm x 10mm and implanted at a 10mm depth. We achieved a measured efficiency of around 62% in tissue and 68% in air.

In the second part, we used stacked metamaterials to improve the system's performance. The MRR unit cell was 20mm x 20mm, and the RX was 7mm x 7mm with three-turn DGS resonators at a 9mm depth inside the tissue. We achieved a measured efficiency of 51%.

In the third part, we integrated the rectifier or voltage Doubler with the RX. The TX was the same as in the second part (MRR 20mm x 20mm), and the RX was 7mm x 7mm. The voltage Doubler was integrated on the backside of the RX substrate, implanted at a 9mm depth. We achieved a measured efficiency of 42% and 39% in air and tissue, respectively, with a load of 1 kΩ.

All of our WPT systems, complied with the IEEE C95.1-1999 specific absorption rate (SAR) standard, which limits the SAR for 1g to 1.6 W/Kg.

Overall, our frequency-misalignment-insensitive WPT system shows promise for use in biomedical applications. We believe that the use of short-length inductors and stacked metamaterials can help overcome the challenges associated with WPT in biological tissue, and we hope that our work will inspire further research in this area.

ACKNOWLEDGMENTS

I begin by praising the Almighty ALLAH SUBHANAHU WA TA'ALA, the Most Magnificent, for granting me the ability to successfully complete my Ph.D. thesis as part of the requirements for my Doctoral study in the Graduate School of Information Science and Electrical Engineering (ISEE), Kyushu University.

I am truly grateful to my advisor, Professor Ramesh K. Pokharel, for his guidance, encouragement, and understanding throughout my research. He has been a constant source of inspiration and motivation for me. I would also like to express my appreciation to Dr. Adel Barakat for his generous contributions of time and knowledge, which have enhanced my research skills and deepened my understanding.

To my fellow lab mates, I offer my sincere thanks for creating a cheerful environment that has made me feel welcome.

To my family, I cannot express in words how fortunate I feel to receive your continuous love, support, encouragement, and prayers. I extend my heartfelt gratitude to my mother and siblings for always being there for me.

Finally, I am deeply grateful to my husband for his unwavering support throughout this journey and for always being there to lend me his shoulder.

List of Figures

List of Tables

Table of Contents

Chapter 1 Introduction

The emergence of wireless power transfer (WPT) systems has revolutionized the way we charge and power our devices. Unlike traditional wired charging methods, which rely on physical connections and limit charging to one device at a time, WPT systems allow for the simultaneous charging of multiple devices without the need for cords or cables. This technology has seen remarkable advancements in recent years, making it a practical and widely adopted solution for device charging across various applications.

One of the key breakthroughs in WPT technology has been the development of resonant magnetic coupling, enabling efficient energy transfer over distances. This innovation has opened up new possibilities for wirelessly charging devices, even when they are not in direct contact with a charging pad. Consequently, WPT systems are now extensively employed in diverse fields such as consumer electronics, automotive, healthcare, and industrial applications.

The advantages of WPT systems are manifold. They eliminate the inconvenience and safety concerns associated with physical connections, offering a more convenient and secure charging experience. Moreover, WPT systems reduce clutter and facilitate a streamlined and efficient charging process. Additionally, these systems can be customized to accommodate various device types and power requirements, making them adaptable and versatile.

1.1 Motivation of Research

The motivation behind researching WPT systems in biomedical applications is the need for an efficient and safe power supply for implanted medical devices. The use of batteries in these devices can pose a risk to the patient due to the need for surgery to replace or remove the battery, the potential for chemical hazards, and the limited lifespan of the battery. WPT offers a non-invasive, safe, and reliable alternative to power these devices, ensuring continuous operation without the need for battery replacement. Furthermore, the use of WPT in medical devices allows for a reduction in device size, which is essential for implantable devices that require miniaturization for safe and comfortable implantation. Overall, the research into WPT in biomedical applications aims to provide a reliable and efficient solution for powering implantable medical devices, improving patient safety and comfort.

1.2 Objective of this Research

The objective of the research on WPT system in biomedical applications is to design and develop a WPT system that is efficient, safe, and reliable for powering implanted medical devices. The research aims to overcome the challenges of WPT system design, such as insensitivity to misalignment, compact size, and electromagnetic compatibility. The objective is to achieve a high level of power transfer efficiency with minimal power loss and minimal risk of adverse health effects on the human body. Additionally, the research aims to optimize the design of the WPT system using advanced techniques such as metamaterials and multi-resonant structures to improve coupling between the transmitter and receiver and to reduce interference with surrounding tissues. Overall, the goal is to provide a reliable and efficient wireless power transfer system that can be used to power implanted medical devices safely and continuously.

1.3 Organization of the Thesis

The thesis work is divided into 6 chapters and each chapter can be described as:

Chapter 1 introduces the research work and outlines the main objectives.

Chapter 2 focuses challenges and considerations related to powering implants, specifically discussing the various energy sources available and the need for a (WPT) system.

Chapter 3 presents the Multi-Input Single Output Resonance Shift Insensitive WPT System, which is proposed as an efficient approach to transmit power to body-implanted sensors.

Chapter 4 discusses the Multi-Ring Resonators stacked metamaterial based WPT system, which is designed to miniaturize the RX. This chapter also explores the use of metamaterials in the design of the WPT system.

Chapter 5 presents the design of an Integrated Matching less Rectifier with the proposed system in chapter 4. This chapter also discusses the use of an isolator in the TX side of the WPT system.

Chapter 6 concludes the thesis work and provides a summary of the research findings. It also suggests some possible directions for future research in the field of WPT systems for biomedical applications.

Chapter 2 Exploring (WPT) for Implantable Sensors"

2.1 Introduction

The use of Wireless Power Transfer (WPT) systems [1-66] in biomedical applications has gained significant attention, mainly due to their ability to overcome the limitations of traditional batteries when it comes to powering implanted medical devices. As depicted in Fig 2.1, WPT systems allow for the wireless transmission of power to implanted sensors, eliminating the need for batteries and the associated surgical replacement procedures. This alternative method of powering implanted sensors ensures their continuous operation, 24 hours a day, without posing any hazardous effects on the human body.

The implementation of WPT technology in the field of implantable medical devices has opened up new avenues for development. It holds great potential in improving the accuracy and reliability of medical data collection and diagnosis. By eliminating the reliance on batteries, WPT systems ensure that implanted sensors function consistently, contributing to more reliable and uninterrupted monitoring of patient health. This continuous power supply enhances the performance and longevity of the implanted devices, leading to more accurate and timely medical assessments.

The benefits of WPT systems in biomedical applications extend beyond their ability to provide uninterrupted power. They also eliminate the need for invasive surgical procedures to replace batteries, reducing the associated risks and complications. This non-invasive power transfer method not only improves patient comfort but also minimizes the potential for infection or other complications that may arise from repeated surgeries. the utilization of WPT systems in biomedical applications offers a promising solution for powering implanted medical devices. By enabling continuous, wireless power transmission to implanted sensors, these systems address the limitations of traditional batteries and enhance the accuracy and reliability of medical data collection and diagnosis. With ongoing advancements in WPT technology, we can expect further improvements in the field of implantable medical devices, leading to enhanced patient care and medical outcomes.

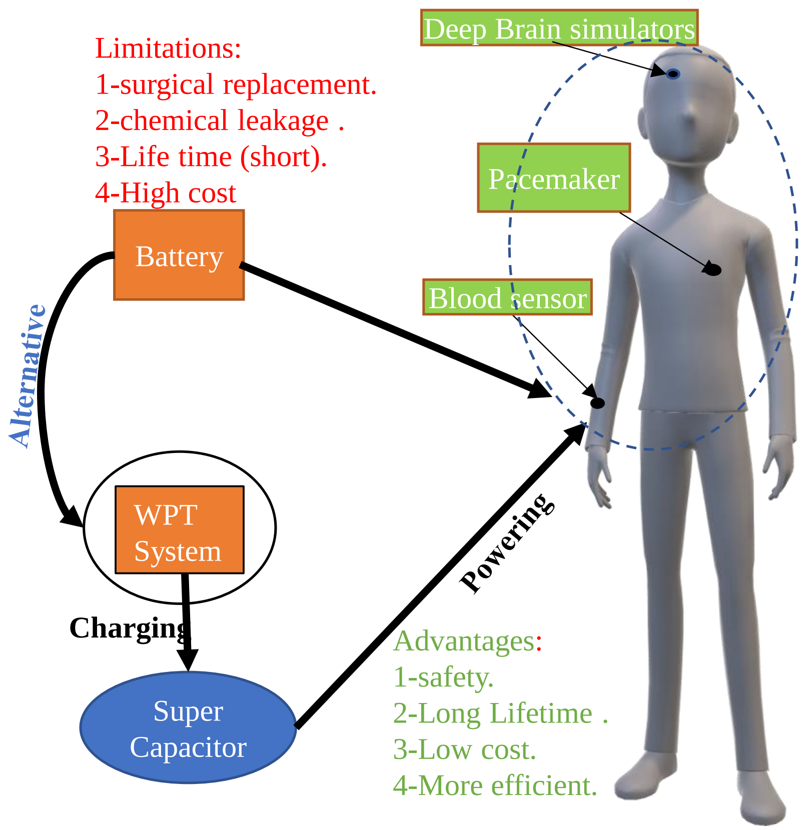

Fig 2. 1 Biomedical implants and sensors showing the need for the WPT technology

2.2 Health Monitoring with Implanted Sensors

Biomedical implants and sensors play a crucial role in various applications, including the monitoring, tracking, and recording of vital signs in the human body. As depicted in Fig 2.1, these implants and sensors enable healthcare professionals to gather essential data for medical diagnosis and treatment.

For instance, let's consider a scenario where a patient is experiencing issues with the pressure of the cerebrospinal fluid surrounding the brain. To monitor and track this pressure, an intracranial pressure sensor can be implanted. This sensor continuously measures and records the intracranial pressure levels, providing valuable information about the patient's condition.

By collecting and analyzing the recorded data from the intracranial pressure sensor, medical doctors can gain insights into the patient's condition and make informed decisions regarding appropriate treatment. They can identify abnormal pressure patterns, detect any critical changes, and develop targeted medication or intervention plans accordingly.

The ability to monitor, track, and record vital signs using biomedical implants and sensors empowers healthcare professionals to diagnose conditions accurately and provide personalized treatment. This approach allows for real-time monitoring, ensuring that any abnormalities or deviations from the normal range are promptly detected and addressed.

By leveraging the recorded data, medical doctors can establish a comprehensive medical history for the patient, enabling them to evaluate the effectiveness of treatments and make informed adjustments as necessary. This data-driven approach enhances the quality of patient care and improves treatment outcomes.

2.3 Conventional Power Source

Conventional power sources typically involve the use of batteries. These batteries are often based on conventional electrochemical technologies, such as lithium-ion or silver-zinc batteries. They store electrical energy and provide power to the implanted device.

The use of batteries as a power source for charging implanted devices has certain advantages. They can provide a reliable and portable source of energy, allowing patients to carry out their daily activities without being tethered to an external power supply. Batteries also offer a stable and consistent power output, ensuring that the implanted device operates efficiently.

However, there are limitations associated with the use of conventional batteries for charging implanted devices. One drawback is the finite lifespan of batteries, which require replacement or recharging over time. This can lead to additional surgeries or interventions for patients, increasing the risk of complications and inconvenience.

Furthermore, the size and weight of batteries can impact the design and comfort of implanted devices. Larger batteries may result in bulkier implants, which can be uncomfortable for patients and affect their quality of life.

The use of conventional batteries also presents challenges in terms of power capacity and energy density. Implantable devices often have power requirements that vary depending on the application, and conventional batteries may not always meet these specific needs efficiently.

As technology advances, there is ongoing research and development to explore alternative power sources for charging implanted devices. This includes exploring the potential of wireless power transfer (WPT) technology, to overcome the limitations associated with conventional battery-based charging methods. WPT has the potential to offer continuous and wireless power supply to implanted devices, eliminating the need for battery replacements, and enhancing patient comfort and convenience. The following sections delve into the advantages of WPT over conventional battery-powered systems.

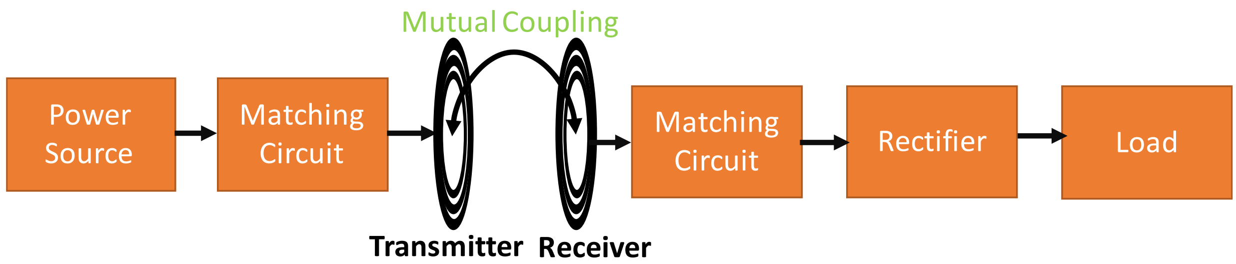

Fig 2. 2 Basic Block diagram of WPT System in near field

2.4 Wireless Power Transfer (WPT)

Wireless power transfer (WPT) technology has a long history, dating back to the experiments conducted by Nikola Tesla in the late 19th and early 20th centuries. However, it is only in recent years that WPT has gained significant research and development efforts for practical applications. The demand for minimally invasive and long-term health monitoring has led to the exploration of WPT as a promising alternative to traditional battery-powered implants [2-28]. The block diagram of a WPT system is shown in Fig. 2.2. A WPT system consists of:

Power source: It is responsible for signal generation in a form that can be transmitted wirelessly.

Transmitter, receiver, and mutual coupling: Their configuration depends on the type of the WPT system. In the case of inductive coupling, the transmitter and receiver are inductive loops, and the mutual coupling is mutual inductance. Types of the WPT systems are explained in the following section.

Matching circuits: These circuits are responsible for matching the system to achieve maximum power transfer at the desired frequency of operation.

Rectifier: It is a circuit that converts the received AC signal into dc power.

Load: It is a representation of the target circuit that requires dc power.

WPT offers the ability to wirelessly transfer power from a source to a load without the need for physical wires, making it particularly suitable for applications where the use of wires is impractical or unsafe, such as medical implants and sensors. Instead of relying on conventional wiring methods, WPT utilizes technologies like magnetic induction, resonant coupling, or radio frequency (RF) radiation to facilitate power transfer between the power source and the load. The potential impact of WPT on the healthcare industry is substantial. By enabling the development of smaller, more efficient, and wirelessly powered medical implants and sensors, WPT has the potential to revolutionize healthcare practices. These advancements can improve patient comfort, reduce the risk of infections or complications associated with invasive surgeries, and extend the lifespan of implanted devices.

Moreover, WPT opens new possibilities for long-term monitoring of patients' health, as it eliminates the need for frequent battery replacements. This translates to enhanced patient convenience, reduced healthcare costs, and improved overall quality of care.

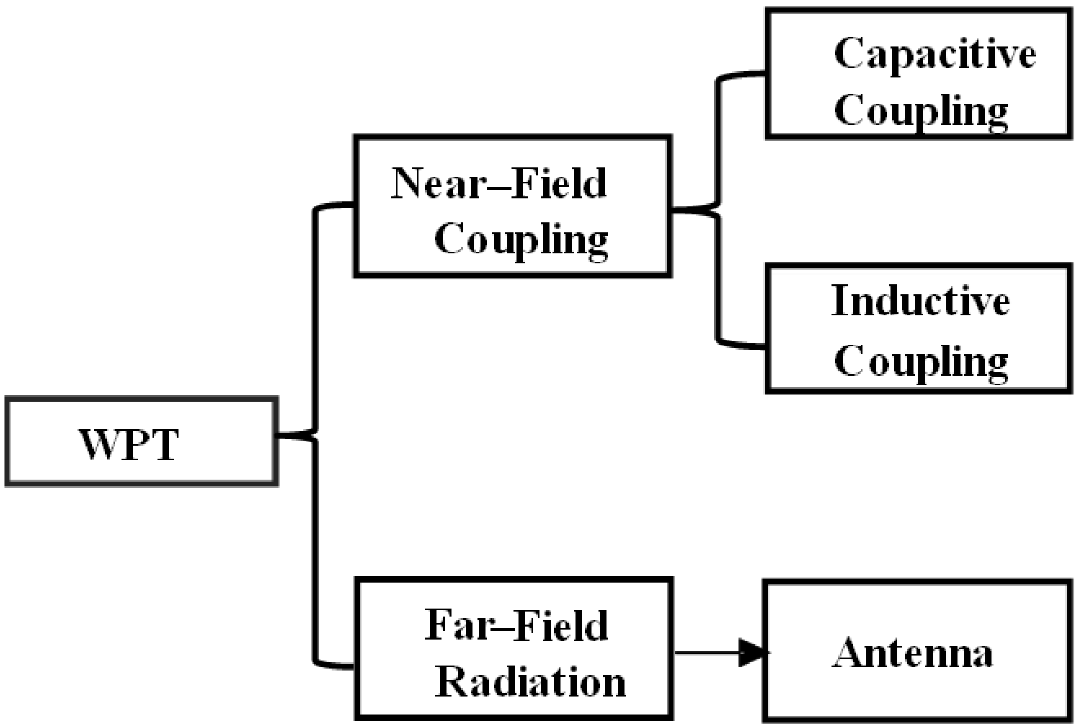

Fig 2. 3 Types of WPT Systems

2.5 Types of Wireless Power Transfer Systems

Wireless power transfer (WPT) techniques vary depending on the application and distance between the transmitter and receiver. Generally, WPT systems can be categorized into two types: Near-Field and Far-Field as shown in the Fig 2.3. Near-Field techniques are suitable for applications that require short to medium-range separation between the transmitter and receiver, such as biomedical implants and sensors [2], [5]. In contrast, Far-Field techniques are used for applications that require a larger separation distance between the transmitter and receiver, such as wireless charging for electronic devices [33-34].

2.5.1 Near-Field WPT

Near-field Wireless Power Transfer (WPT) is a type of wireless power transfer that operates over short distances (typically within a few centimeters to a few meters). Unlike traditional far-field WPT technologies, which rely on electromagnetic radiation to transmit power over long distances, near-field WPT utilizes the principle of magnetic induction or electric field coupling to transfer power between two coils that are within striking distance of each other.

In near-field WPT, the transmitter and receiver coils are typically designed as resonant structures, which allows them to efficiently exchange energy at a specific resonant frequency. The separation distance between the coils depends on the coupling type used, which can be either capacitive or inductive. Capacitive coupling [27], [29] is achieved by placing two parallel plates close to each other, while inductive coupling [4,11,22,23,30,37,44,45,50,54] is achieved by placing two coils close to each other.

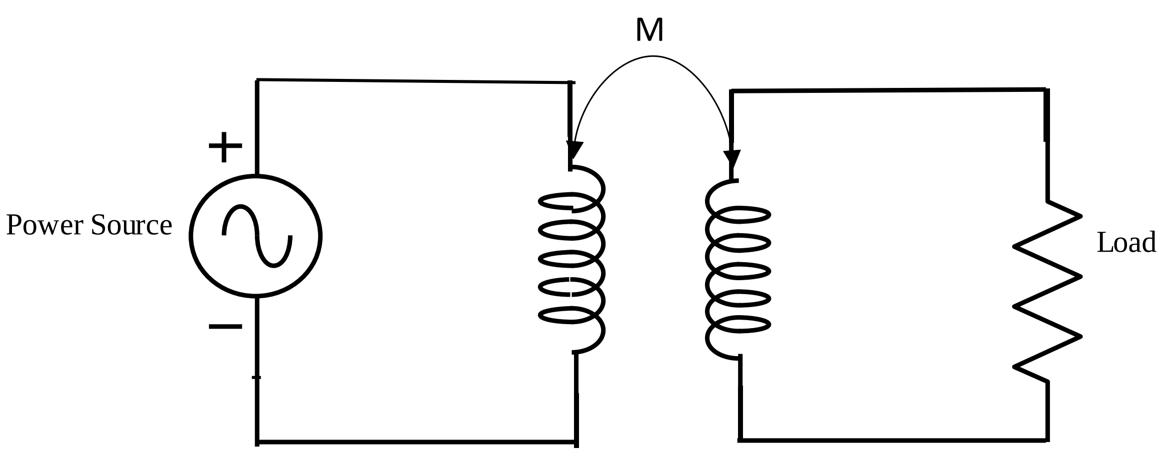

Fig 2. 4 Basic circuit of Inductive Coupling

2.5.1.1 Inductive Coupling:

The use of planar spiral coils in near-field WPT based on inductive coupling is becoming increasingly popular in biomedical applications due to their small size and potential for efficient power transfer. Planar spiral coils consist of a thin, flat conductor that is wound in a spiral pattern, typically on a printed circuit board or other substrate. This design allows for a larger surface area than solenoid coils, which can result in better coupling and higher efficiency. Harrison et al. [4] introduced a technique for analyzing and optimizing the inductive power link between planar spiral "pancake" coils in the 100 kHz to 10 MHz frequency range. They used a combination of analytical modeling and experimental measurements to characterize the performance of the coils, including their resonant frequency, quality factor, and coupling coefficient. They also investigated the effect of various design parameters, such as the coil size, number of turns, and substrate material, on the performance of the system. The results of their study showed that planar spiral coils can achieve high efficiency in the near-field range, with a maximum power transfer efficiency of around 70% at a distance of a few millimeters. They also found that the coupling coefficient and resonance frequency of the coils can be optimized by adjusting their design parameters. Overall, the use of planar spiral coils in near-field WPT based on inductive coupling offers several advantages for biomedical applications, including small size, high efficiency, and minimal interaction with the human body. Ongoing research is focused on further improving the performance and reliability of these systems for various applications in the medical field.

The efficiency of a near-field WPT system based on inductive coupling is typically defined by the coupled quality factor, also known as the kQ-product [16] as illustrate in equation 2.6.11. The kQ-product is a measure of the efficiency of energy transfer between the transmitting and receiving coils and depends on several factors, including the size and geometry of the coils, the distance between them, and the presence of any magnetic materials.

$$\eta_{max} = \left\{\frac{kQ}{1+\sqrt{1+(kQ)^2}}\right\}^2 \tag{2.6.1.1}$$

k is the coupling coefficient between the coupled inductors and can be determined as

$$k = \frac{M}{\sqrt{L_{TX}L_{RX}}} \tag{2.6.1.2}$$

Where L_{TX} and L_{RX} are the self-inductances of the transmitting and receiving inductors, respectively. Q is the average quality factor of L_{TX} and L_{RX} ($Q = \sqrt{Q_{TX}Q_{RX}}$), which are determined as

$$Q_{TX} = \frac{\omega_0 L_{TX}}{R_{TX}} \tag{2.6.1.3a}$$

$$Q_{RX} = \frac{\omega_0 L_{RX}}{R_{RX}} \tag{2.6.1.3b}$$

Where ω_0 is the resonance frequency, and R_{TX}/R_{RX} is the loss resistance of L_{TX}/L_{RX}.
In general, higher kQ-products correspond to higher efficiency in WPT systems, indicating a greater ability to transfer energy between the coils. However, achieving high kQ-products can be challenging due to factors such as coil misalignment, losses in the transmission medium, and electromagnetic interference. Hence, the KQ product equation can be rewriten as:

$$KQ = \frac{\omega_0 M}{\sqrt{R1 \times R2}} \tag{2.6.1.3c}$$

According to equation (2.6.1.3c) we can improve KQ product by:

1- Increasing the mutual inductance (M) is indeed a key factor in enhancing the power transfer efficiency and KQ product in inductive coupling Wireless Power Transfer (WPT) systems. However, as the conventional approach of increasing the number of turns in the TX and RX coils can lead to undesirable effects such as an increase in specific absorption rate (SAR) and electromagnetic radiation.
2- Increasing frequency, while increasing the frequency in Wireless Power Transfer (WPT) systems can enhance the KQ product and power transfer efficiency, it is important to consider the specific absorption rate (SAR) as a limiting factor, especially in biomedical applications which we explained in detail in Section (2.7.3). At higher frequencies, resistive losses can become more significant due to the skin effect and proximity effect. The skin effect causes current to be concentrated near the surface of the conductor, leading to increased resistance and higher power dissipation. Similarly, the proximity effect occurs in conductors placed close together, resulting in additional resistive losses. Resistive losses can lead to reduced power transfer efficiency and a decrease in the KQ product. These losses can be especially pronounced in high-frequency WPT systems, where the smaller size of the coils and the closer proximity of the conductors exacerbate the effects of resistive losses. The third effect is on the discrete capacitors. At high frequencies, the Q-factor of the discrete capacitors reduces significantly as $Q_c = (\omega R_s C)^{-1}$ because of the increase of the associated series resistance (R_s) and the inversely proportional relation with the frequency.
3- By decreasing the resistance.

Enhancing the KQ product in Wireless Power Transfer (WPT) systems can be achieved by reducing the resistive loss. However, when using the same material, reduction of resistive loss comes always with degradation of the mutual coupling, i.e., it requires compensation between both factors (resistive loss and mutual coupling) based on the design requirements. Moreover, the use of superconductors can maintain the level of mutual coupling while eliminating reducing the resistive loss. Despite these advantages, using superconductors I not suitable for biomedical applications because the need for low temperature operation to excite superconductivity. Such a low temperature be harmful to the human body.

In summary, choosing the frequency of operation for a WPT system is a crucial decision that involves considerations of efficiency, component availability, and size constraints. In this case, the decision to operate the WPT system at 50 MHz was influenced by two main reasons:

- *Commercial Capacitor Quality Factor:* At frequencies below 70 MHz, many commercial surface-mount capacitors exhibit relatively high Q-factors. By operating at 50 MHz, the system can take advantage of the high-quality factors of commercial capacitors, which contribute to increased overall power transfer efficiency. As the frequency increases beyond this range, the effective quality factor of commercial capacitors decreases, which can lead to reduced efficiency when combined with inductors in the system.
- Size Constraints and Efficiency Tradeoff: The second reason for selecting 50 MHz is related to the size constraints of the receiver (RX). In WPT systems, smaller receiver coils are desirable, especially for biomedical applications where implantable devices require compact and unobtrusive designs. At lower frequencies, such as 13.56 MHz, achieving a high KQ factor can be challenging due to the larger size requirements of the receiver coil. However, by increasing the frequency to 50 MHz, a tradeoff between efficiency, maximum power transfer, and specific absorption rate (SAR) can be achieved. Operating at 50 MHz allows for a good level of efficiency while maintaining a smaller RX size and a lower SAR within acceptable input power limits.

Overall, the selection of 50 MHz as the operating frequency for the WPT system balances the advantages of commercial capacitor performance at this frequency range and the ability to achieve a more compact RX design. By carefully considering these factors, the WPT system can optimize power transfer efficiency and meet the requirements of the biomedical implantable devices.

2.5.1.2 Capacitive Coupling

WPT systems based on capacitive coupling rely on mutual capacitance between two nearby sets of plates, as shown in Fig. 2.5. The capacitance, C_m, between the plates depends on factors such as their size and structure, the distance between them, and the presence of any dielectric material. Capacitive coupling is most effective at small separation distances between the plates, and these systems can achieve good efficiency under these conditions [27], [29-30].

However, for biomedical applications, capacitive coupling is not typically recommended due to the short distances involved. Additionally, human tissue has electrical characteristics that can potentially interfere with the resonance of a WPT system based on capacitive coupling [27]. As with systems based on inductive coupling, WPT systems based on capacitive coupling can also be susceptible to misalignment effects that can reduce their efficiency. Therefore, while capacitive coupling has its advantages in certain applications, it may not be the most practical choice for many biomedical WPT applications.

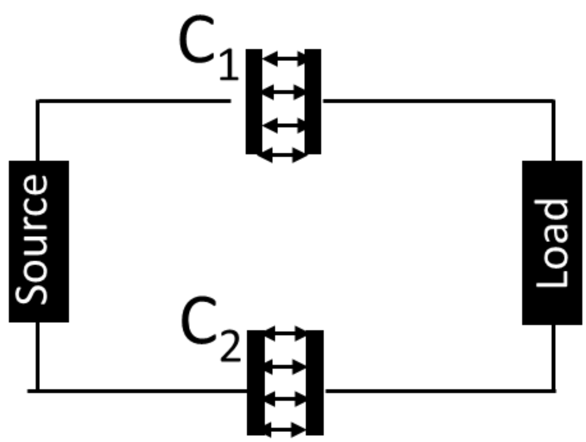

Fig 2. 5 Basic circuit of Capacitive Coupling

Jegadeesan et al. [27] conducted an experiment using near-field capacitive coupling WPT to supply power to a receiver placed in a Non-Human Primate (NHP) cadaver. The results showed that 100mW of power could be safely and successfully transferred to the NHP cadaver with an operating efficiency of 50%. However, the power transfer distance was limited compared to the magnetic coupling technique. In addition, the deformation property of the transmitter and receiver resonator was analyzed to demonstrate the reliability of the capacitive coupling link. Meanwhile, Huang et al. [32] presented a capacitive WPT method that utilized Z-impedance compensation. In order to, compensate the circuit and enhance the WPT characteristics, an inductor is often used. However, this can lead to a high voltage spike in the event of an open or short-circuited load. To address this issue, the Z-impedance compensation technique has been developed to increase the circuit's immunity to these load conditions. This technique has been shown to boost the output voltage by 50% and improve power transfer efficiency to over 80%.

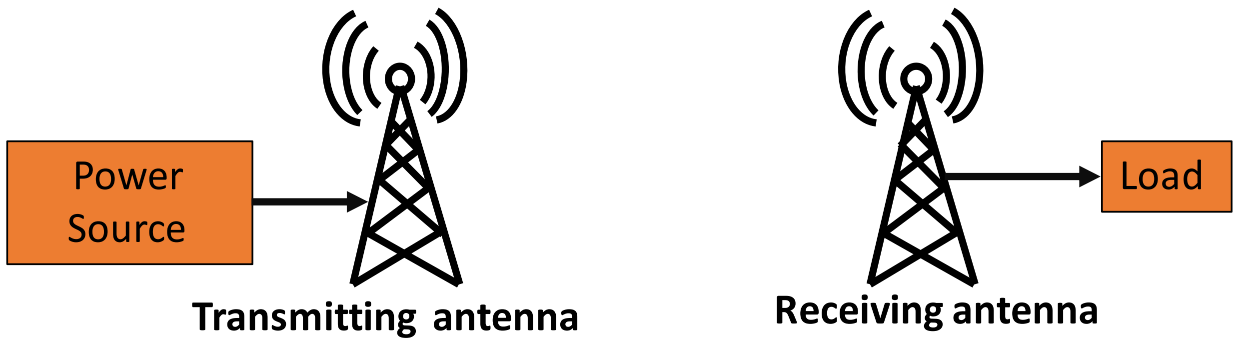

Fig 2. 6 Basic block diagram of a far-field WPT system

2.6 Far-Field WPT technology

Far-field WPT systems rely on the transmission of radiated plane waves from a transmitting antenna to a receiving antenna. This type of WPT system is suitable for longer transmission distances. The amount of power received by the receiving antenna (P_r) can be calculated using Friis's formula (2.4) [31] for aligned, line-of-sight, and same polarization antennas in free space. The formula takes into consideration the transmitted power (P_t), the gain of the transmitting (G_t) and receiving (G_r) antennas, the operating wavelength (λ), and the distance between the two antennas (d).

$$P_r = P_t G_t G_r \left(\frac{\lambda}{4\pi d}\right)^2 \tag{2.7.1}$$

Hence, the efficiency of a far-field WPT system (η_{FF}) can be calculated as

$$\eta_{FF} = \frac{P_r}{P_t} = G_t G_r \left(\frac{\lambda}{4\pi d}\right)^2 \tag{2.7.2}$$

Far-field WPT systems have the advantage of being able to transfer power over long distances of kilometers by focusing the electromagnetic radiation into beams. These systems are typically designed to operate at GHz frequencies to achieve small size. Far-field WPT systems are commonly used for energy harvesting, where a non-dedicated source of power is available. However, these systems also have several disadvantages. Firstly, the efficiency of power transfer is typically poor when using a single receiving antenna. Secondly, when using MHz frequencies, the size of the system can become quite large. Finally, there can be a high degree of interaction between the electromagnetic waves and the human body, making it unsuitable for biomedical applications.

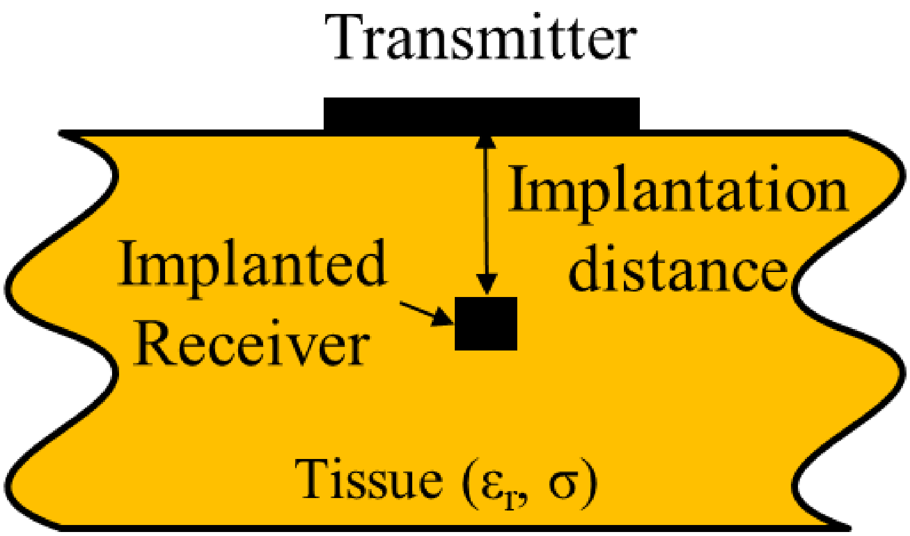

Fig 2. 7 Conventional WPT system in Tissue

2.7 Challenges of the Conventional inductive coupled WPT System

While conventional inductive coupled WPT systems offer several advantages, they also face some challenges. One of the primary challenges is the limited range of operation. As mentioned earlier, the efficiency of inductive coupled WPT systems is highest at medium distances, which is typically around the diameter of the inductors. Beyond this distance, the power transfer efficiency drops significantly. Moreover, the system is highly sensitive to misalignment between the transmitting and receiving inductors.

Another challenge is the sensitivity of the system to changes in the load impedance. Any change in the load impedance can significantly affect the power transfer efficiency, and the system may require frequent tuning to maintain optimal performance.

Furthermore, the use of inductive coupling can result in significant electromagnetic interference

(EMI) that can affect nearby electronic devices. The electromagnetic fields generated by the inductors can also have harmful effects on the human body, making it unsuitable for some medical applications.

Overall, while inductive coupled WPT systems have several advantages, they also face several challenges that limit their effectiveness in certain applications. Ongoing research is focused on addressing these challenges and developing more efficient and reliable WPT systems for a wide range of applications.

2.7.1 These challenges are:

2.7.1.1 Compact Size of the Receiver

When designing biomedical receivers for implantation in the human body, researchers have emphasized the importance of size as a crucial factor. To ensure compactness and efficiency, they have suggested the use of multi-turn spiral inductors operating in the MHz frequency range. This choice of frequency range helps to prevent any risk of electromagnetic absorption by the body, and the multi-turn spiral inductor configuration allows for a more compact design. By implementing these design choices, researchers hope to create receivers that are both safe and effective for use in biomedical applications.

2.7.1.2 Electromagnetic (EM) Compatibility

Designing a wireless power transfer (WPT) system for biomedical applications involves several critical considerations, including frequency, efficiency, and power levels, which are crucial to ensuring the safety of the human body. Specifically, the system's design must aim to prevent excessive tissue heating due to electromagnetic absorption. In addition, ensuring electromagnetic compatibility (EMC) is equally important to avoid interference with other medical devices and any adverse effects on the patient's health. Therefore, careful attention must be paid to these factors during the WPT system's design process to ensure its safety and effectiveness for use in biomedical applications.

2.7.1.3 Misalignment

Inductively coupled wireless power transfer (WPT) systems commonly face the challenge of misalignment, which can arise due to factors like movement of the transmitting or receiving device or improper placement during manufacturing. Misalignment leads to changes in the mutual inductance between the inductors, resulting in a decrease in power transfer efficiency. To mitigate the effects of misalignment, suitable compensation techniques are necessary for the WPT system. Misalignment can be categorized into three types based on the nature of the location change: angular misalignment, separation misalignment, and lateral misalignment. Each type of misalignment can have different effects on the performance of the WPT system. Therefore, a detailed understanding of these types is essential for developing effective compensation techniques. In the following sections, we will discuss each type of misalignment and its impact on the WPT system in detail.

2.7.1.3.1 Angular Misalignment

Angular misalignment occurs in inductively coupled wireless power transfer (WPT) systems when the angle of the receiver changes in either the horizontal ($\emptyset$) or vertical (θ) directions, assuming the transmitter is fixed in its original position. As the inductor is typically symmetrical around $\emptyset$, the mutual inductance remains unchanged with respect to this angle.

In contrast, misalignment with respect to θ, as illustrated in Fig 2.8, may cause variations in the mutual inductance (M) due to changes in the receiver's location. Therefore, the impact of angular misalignment on the WPT system's performance is primarily determined by changes in θ. It is important to consider these effects when developing compensation techniques to mitigate the impact of angular misalignment on the WPT system's efficiency.

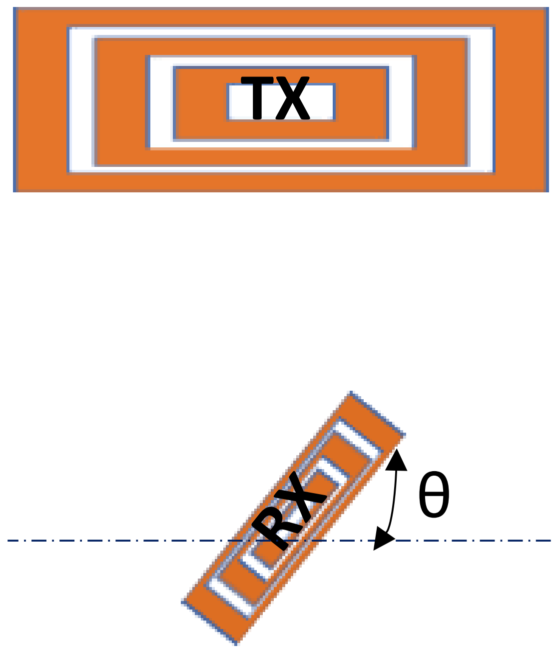

Fig 2. 8 Explanatory diagram for Angular Misalignment with the angle θ.

2.7.1.4 Separation Misalignment

Separation misalignment occurs when the receiver moves closer to or farther away from the fixed transmitter by a distance of Δd, as shown in Fig 2.9. When the receiver approaches the transmitter, the mutual inductance between the inductors increases, resulting in an enhancement of the kQ-product and corresponding maximum efficiency (η_{max}). Conversely, when the receiver moves away from the transmitter, the mutual inductance decreases, leading to a degradation of both the kQ-product and η_{max}. However, in both cases, mismatch loss occurs, and the overall efficiency of the WPT system decreases.

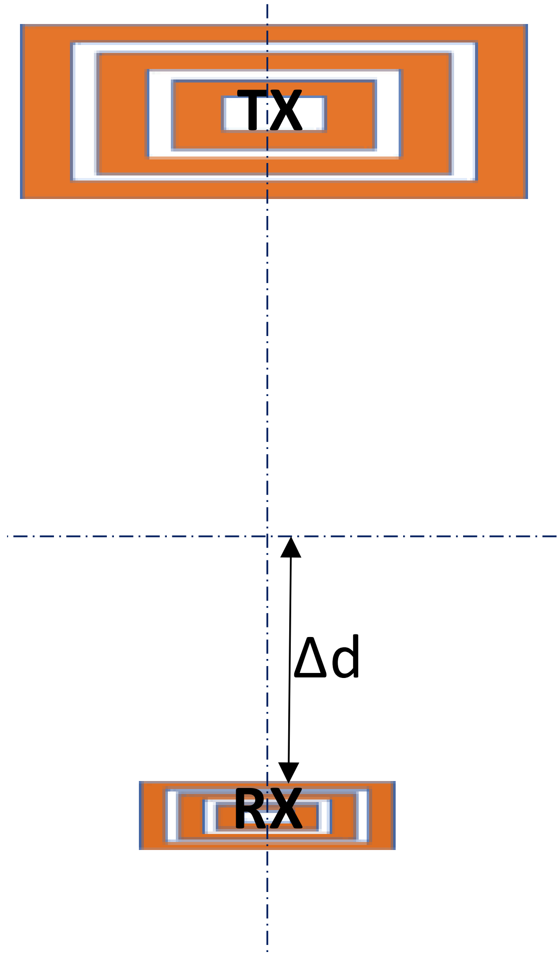

Fig 2. 9 Explanatory diagram for separation misalignment (Δd)

2.7.1.5 Lateral Misalignment

Assuming the transmitter is fixed in its original position, lateral misalignment occurs when the receiver moves away from the transmitter in the x- or y-directions while maintaining the same separation and angle. Fig 2.10 shows an example of lateral misalignment with a displacement Δx in the x-direction.

At no misalignment ($\Delta x=0$), the axes of the transmitter and receiver are identical, and the mutual coupling is at its peak. However, when a lateral misalignment ($|\Delta x|>0$) occurs, the mutual coupling between the inductors decreases, leading to a degradation of both the kQ-product and corresponding maximum efficiency (η_{max}). Moreover, mismatch loss occurs, and the overall efficiency of the WPT system decreases.

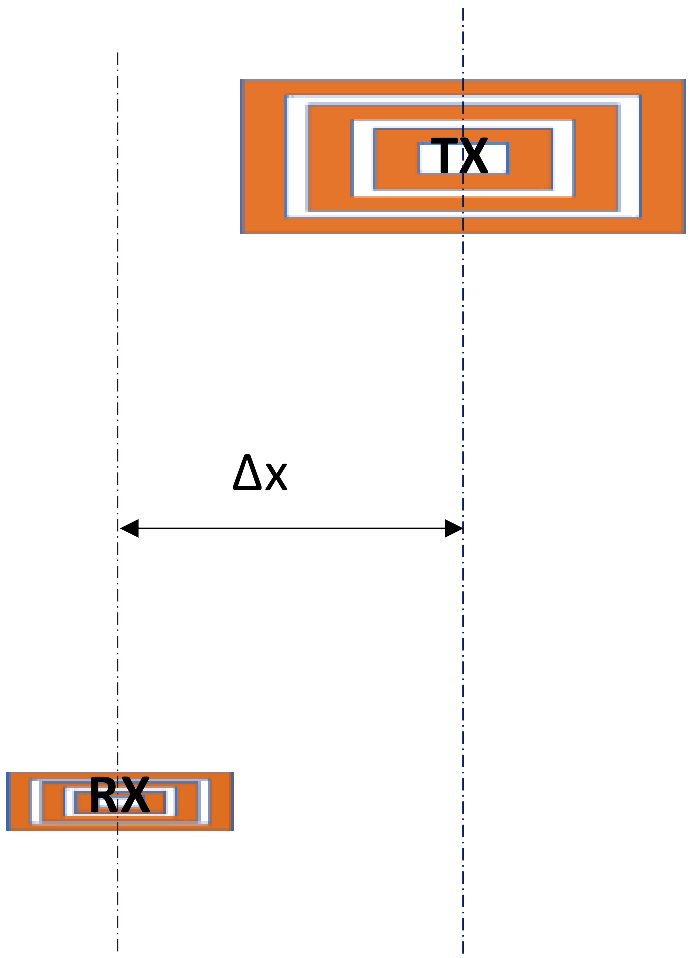

Fig 2. 10 Explanatory diagram for separation misalignment (Δx)

2.7.2 Effect of the body characteristics

The human body's electrical properties can significantly impact the performance of wireless.
power transfer (WPT) systems that use different coupling mechanisms. In the context of biomedical applications, it is crucial to ensure that WPT systems are electromagnetically compatible with the human body to guarantee the safety of patients and operators.

In WPT systems that use inductive coupling, the presence of the human body can alter the coupling coefficient between the transmitter and receiver coils, which can result in reduced efficiency. Additionally, the human body can absorb electromagnetic energy and convert it into heat, potentially causing tissue damage or discomfort.

Capacitive coupling WPT systems may be affected by the human body, as it can act as a dielectric material and alter the capacitance between the transmitter and receiver plates. This can cause changes in the resonance frequency of the system, leading to reduced power transfer efficiency.

In far-field WPT systems, the human body can interfere with the electromagnetic waves and cause scattering and reflection, which can reduce efficiency and pose potential harm to the body. Therefore, selecting an appropriate frequency to minimize the interaction with the human body is crucial.

Overall, to ensure safe and efficient operation in biomedical applications, it is vital to consider the impact of the human body on WPT systems during the design phase. Appropriate solutions must be adopted to address the challenges posed by different coupling mechanisms.

2.7.3 Specific Absorption Rate (SAR)

SAR stands for Specific Absorption Rate, and it is a measure of the rate at which electromagnetic energy is absorbed by the human body when exposed to radiofrequency (RF) electromagnetic fields. SAR is typically expressed in watts per kilogram (W/kg) and is used to evaluate the potential health effects of RF exposure, especially in the context of wireless communication devices, including cell phones and wireless power transfer systems. When a human body is exposed to RF radiation, some of the electromagnetic energy is absorbed by body tissues, and SAR quantifies the amount of energy absorbed per unit mass of body tissue. SAR values are important in determining compliance with safety guidelines and regulations related to RF exposure. Regulatory bodies around the world, such as the Federal Communications Commission (FCC) in the United States, set SAR limits to ensure that RF exposure remains below levels that could cause adverse health effects. For WPT systems, SAR is a critical consideration, especially in the context of biomedical implants or wearable devices that come into close proximity to the human body. The SAR level should be kept within safe limits to avoid any potential harm to human tissues. Engineers and researchers designing WPT systems for biomedical applications carefully assess and control the electromagnetic energy emitted by the system to ensure that SAR values remain well below established safety limits. By considering SAR and complying with relevant regulations, WPT systems can be designed and optimized to deliver wireless power safely and efficiently without posing any risks to human health.

When designing a Wireless Power Transfer (WPT) system, the size of the transmitter (TX) and receiver (RX) coils is indeed related to Specific Absorption Rate (SAR), especially in the context of biomedical applications where the system operates in close proximity to the human body. SAR is a crucial consideration in ensuring the safety of wireless power transfer to avoid potential harm to human tissues. Here are some key points to consider when choosing the size of the TX coil based on the RX size and its relation to SAR:

- *RX Implant Size*: The size of the RX coil is often constrained by the available space within the human body, especially for biomedical implants. The RX size is carefully chosen to fit the implantable device without causing discomfort or interfering with bodily functions.
- *Energy Transfer Efficiency*: The size of the TX coil should be appropriately matched to the RX size to ensure efficient power transfer. If the TX coil is too large compared to the RX coil, it may lead to energy wastage and increased SAR levels due to excess radiation.
- *Magnetic Field Concentration*: A larger TX coil may create a more concentrated magnetic field around the RX coil, which could result in localized hotspots and higher SAR levels. Optimizing the TX coil size to provide a well-distributed magnetic field around the RX coil can help mitigate this issue.
- *Alignment and Coupling*: Proper alignment and coupling between the TX and RX coils are essential for efficient power transfer. Choosing an appropriate TX size that allows for optimal alignment and coupling with the RX coil can enhance system performance and reduce unnecessary RF radiation.
- *Simulation and Safety Analysis*: Performing simulations and safety analysis of the WPT system, including SAR calculations, can help determine the ideal TX size based on the specific RX dimensions and operating frequency. These analyses can ensure that SAR levels remain within safe limits while maintaining efficient power transfer. Regulatory Compliance: Compliance with SAR regulations and safety guidelines is crucial for biomedical applications. The chosen TX size should adhere to established SAR limits to ensure the safety and well-being of the patient or user.

Overall, the size of the TX coil should be carefully chosen in relation to the RX size and its proximity to the human body to maintain efficient power transfer while keeping SAR levels within safe limits. A balanced design approach, including simulation, safety analysis, and adherence to regulatory requirements, is vital for successful implementation of WPT systems in biomedical applications. Based on the finding in [13], side length of the Tx for optimal coupling should not exceed 2.8 times the separation distance to the RX. So, considering all these facts, after careful consideration and design optimization, the transmitter with a size of 20x20 mm^2 and the receiver with a size of 10x10 mm^2 and 7x7 mm^2 for a separation distance ≈10 mm has been identified as the best combination.

Chapter 3 Multi Output Single Input WPT System Insensitive to Resonance Frequency Shifting

3.1 Introduction

Implanting the receiver (RX) of a wireless power transfer (WPT) system inside tissue can lead to two undesirable effects. The first effect is a shift in the self-resonance frequency of the transmitter (TX), resulting in a mismatch loss that causes a position-dependent reduction in efficiency. Several approaches have been proposed to address this issue and improve the coupled quality factor in cases where the RX is embedded in tissue. Our team was the first to investigate the problem of resonance frequency shift.

The second effect of implanting the RX in tissue is a reduction in the kQ product due to the tissue's dielectric and conduction losses. To mitigate this phenomenon, a small electrical-length theory is employed.

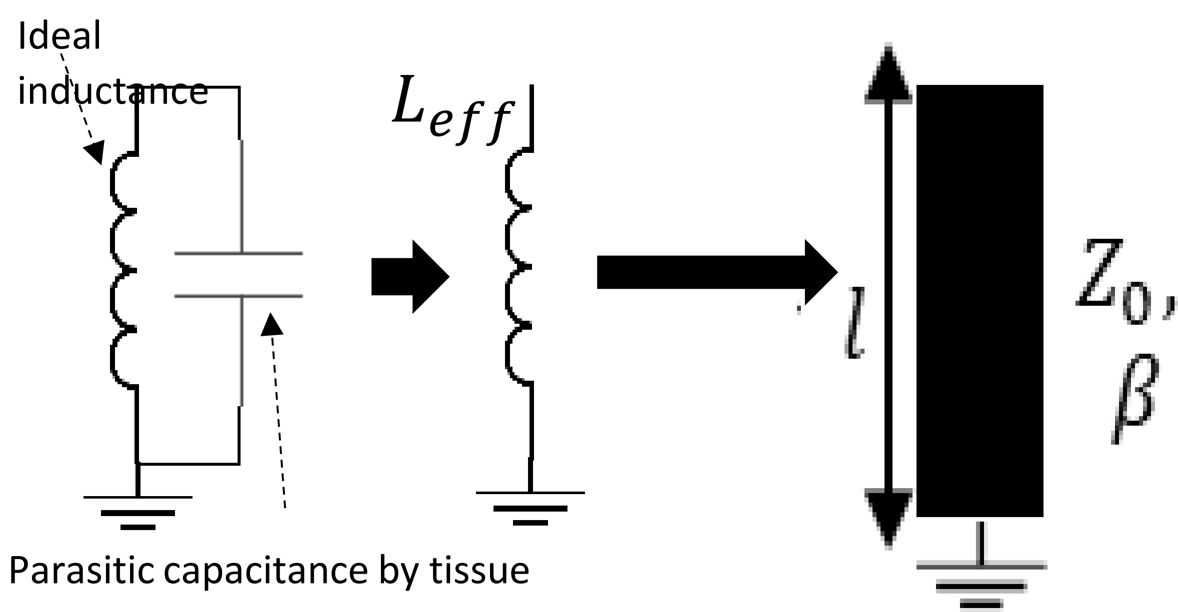

Fig 3. 1 the effective inductance and its high impedance transmission line equivalent

3.2 Small inductor theory

The small inductor theory, also known as the lumped element model, is a simplification of the behavior of an inductor in an electrical circuit. In this theory, an inductor is modeled as a single lumped element with a value of inductance, regardless of its physical size and the distribution of its windings.

According to this theory, an inductor behaves as a pure inductance element and does not exhibit any parasitic capacitance or resistance. This simplification is valid when the physical size of the inductor is much smaller than the wavelength of the electrical signal passing through it.

The small inductor theory is a useful tool in circuit analysis and design as it allows for a simplified representation of inductors in electrical circuits. However, it is important to note that the theory is only valid within certain frequency ranges and that inductors can exhibit more complex behavior at higher frequencies or when their physical dimensions are not small relative to the wavelength of the signal.

When designing a wireless power transfer (WPT) system, the inductor used is not a pure inductor and contains a parasitic capacitance that is independent of the dielectric medium. However, the presence of a nearby dielectric, such as the human body, can increase the parasitic capacitance and result in a change in the effective inductance on that dielectric. The effective inductance is a combination of the intrinsic inductance and the parasitic capacitance from the surrounding medium, as shown in Fig 3.1. The self-resonance of this inductance decreases from 300 MHz to 175 MHz, and the effective inductance at the target frequency of 50 MHz increases by 10 nH (3.6%) due to the change in the medium, as shown in Fig 3.2.

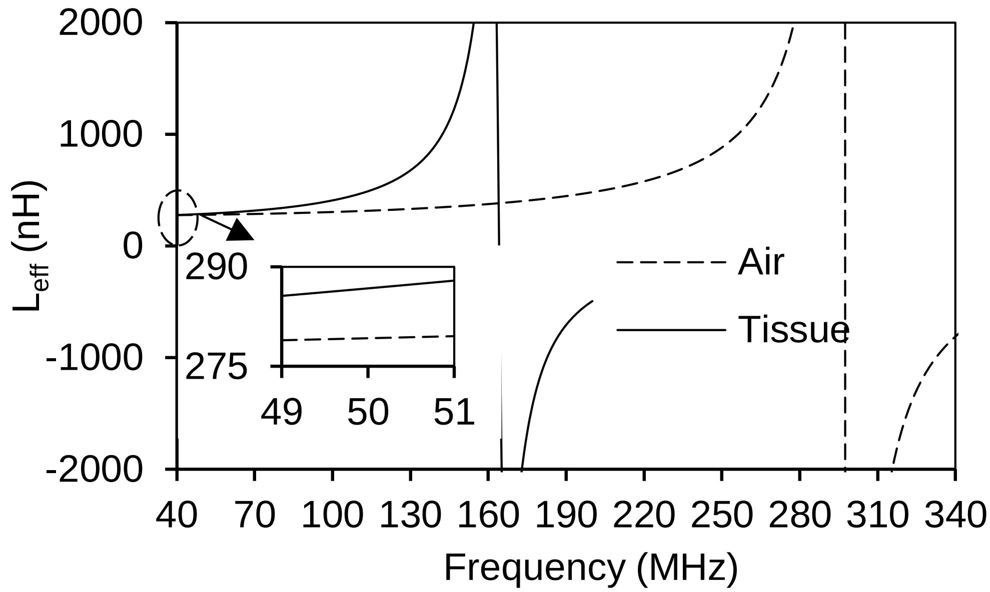

Fig 3. 2 the effect of the tissue on the effective inductance versus frequency.

In order to investigate the cause behind the variation in effective inductance and to seek a resolution, we carried out a parametric analysis on the physical length (l) of the inductor. The calculation of the physical length was performed using equation (3.2.1), and we examined the impact of tissue on the inductance and its associated Q-factor. This study involved placing the inductor in two different scenarios: either in the air or directly on the surface of the tissue. We conducted the study with varying numbers of turns (N), while maintaining D = 20 mm, W = 0.75 mm, and S = 0.5 mm as constant parameters.

$$l = 4\sum_{i=1}^{N} D - (2N-1) \times W - 2(N-1) \times S \tag{3.2.1}$$

Fig 3.2. demonstrates that for short lengths of l, the effective inductance remains unaffected by the surrounding medium. However, as the length l increases, the dependence of the effective inductance on the proximity of the tissue becomes more prominent. Specifically, when a small number of turns is utilized in constructing the inductor, the effective inductance can be represented as a high impedance transmission line, as depicted in Fig 3. 1.

The effective inductance is calculated as:

$$L_{eff} = \frac{Z_0 \times \sin \omega\beta l}{\omega} \tag{3.2.2}$$

where Z_0, μ, β, l, and ε are the characteristic impedance ($Z_0 = \sqrt{\mu/\varepsilon}$), permeability, phase constant ($\beta = \omega\sqrt{\mu\varepsilon}$), transmission line length, and permittivity, respectively. The parasitic capacitive effect of the surrounding medium can be attributed to a reduction in the characteristic impedance and an increase in the electrical length (βl) of the inductor. Since both air and biomedical tissue have the same permeability (μ), we can reduce the dependence on permittivity (ε) by minimizing βl in the medium with the higher value of ε. As a result, for βl≪1 at the interface between the biomedical tissue and air, sinβl ≈ βl. Thus, we can rewrite Equation (2) as follows:

$$L_{eff} \approx \frac{\sqrt{\mu/\varepsilon} \times \omega\sqrt{\mu\varepsilon} \times l}{\omega} \approx \mu l \tag{3.2.3}$$

Hence, L_{eff} is dielectric medium independent by satisfying the condition $\beta l \ll 1$ in the biomedical tissue/air interface, which is roughly 18° and corresponds to a physical length of 96 mm at the frequency of operation, i.e., 50 MHz. We would like to highlight, (3.2) and (3.3) are introduced here for illustrating the medium independent characteristics i.e., not for inductance calculation, which is done usually using the modified Wheeler formula.

By using this study for more confirmation, here are the dimensions and capacitor values for the conventional WPT systems with three-turns and the proposed WPT system with one-turn, for both the transmitter (TX) and receiver (RX) coils. The systems were tested with both tissue and air as the medium.

Table 3. 1 Dimensions and Capacitors of Conventional and Proposed WPT Systems

Parameter	**Three-turns TX**	**Three-turns RX**	**One-turn TX**	**Three-turns RX**
D	20	10	20	10
N “turns”	3	3	1	3
w	0.75	1	0.75	1
s	0.5	0.5	-	0.5
Cp (pF)	23	175	158	180

Cs (pF)	10	35	23	30

In Fig3.3, it can be observed that the proposed method effectively addresses the resonance shift problem. However, another issue caused by the presence of tissue is the reduction of KQ due to radiation at the interface. As shown in Fig 3.5, the quality factor degrades as the radiation near the tissue and air changes. According to equation (3.4), Q depends on the value of R, which is proportional to the effective dielectric. In air, the dielectric is 1, but it becomes very high near the tissue.

Unfortunately, despite the implementation of the proposed method, the radiation issue remains unsolved, as depicted in Fig 3.5. The presence of radiation had a detrimental impact on the small inductor, leading to a substantial degradation in the quality factor. Consequently, the KQ value suffered a decline, resulting in diminished efficiency.

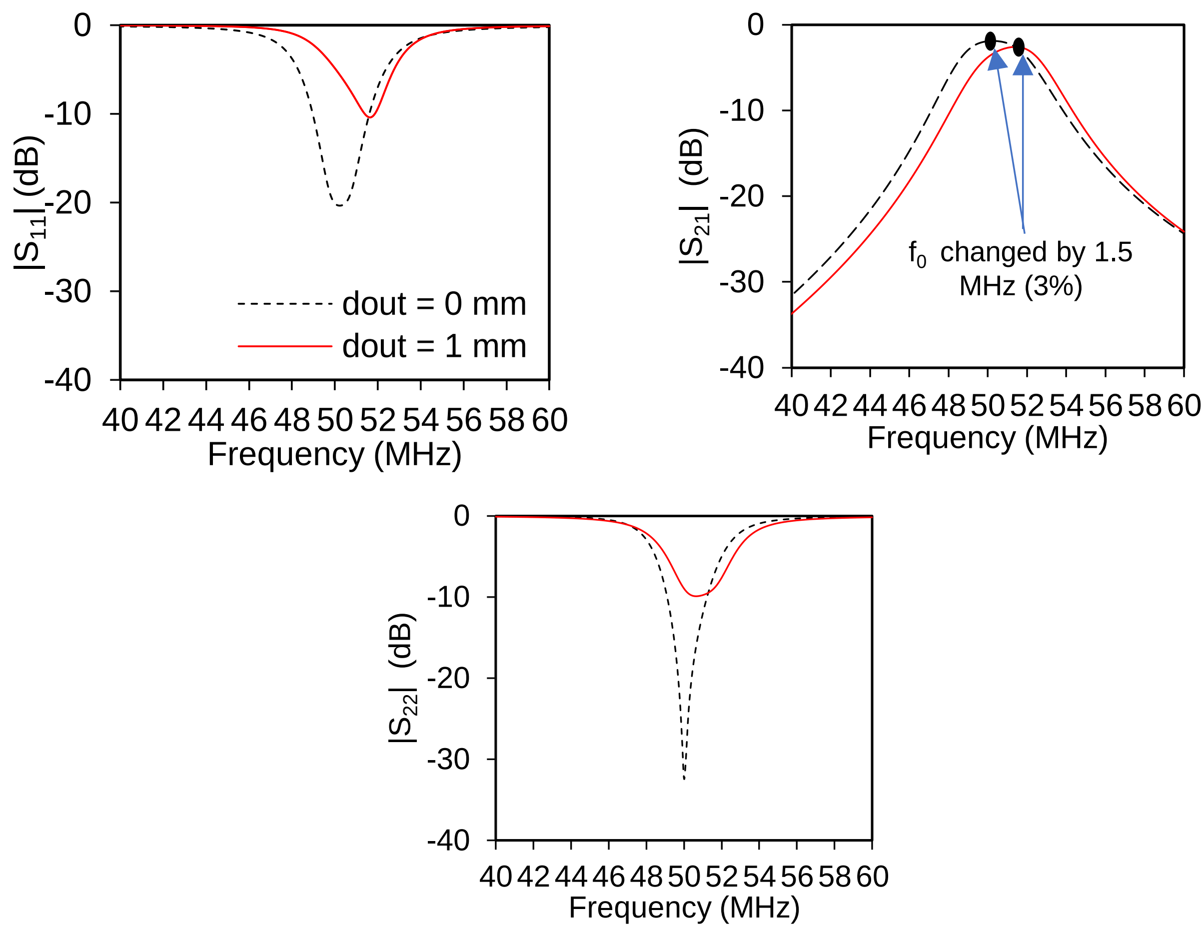

(a)

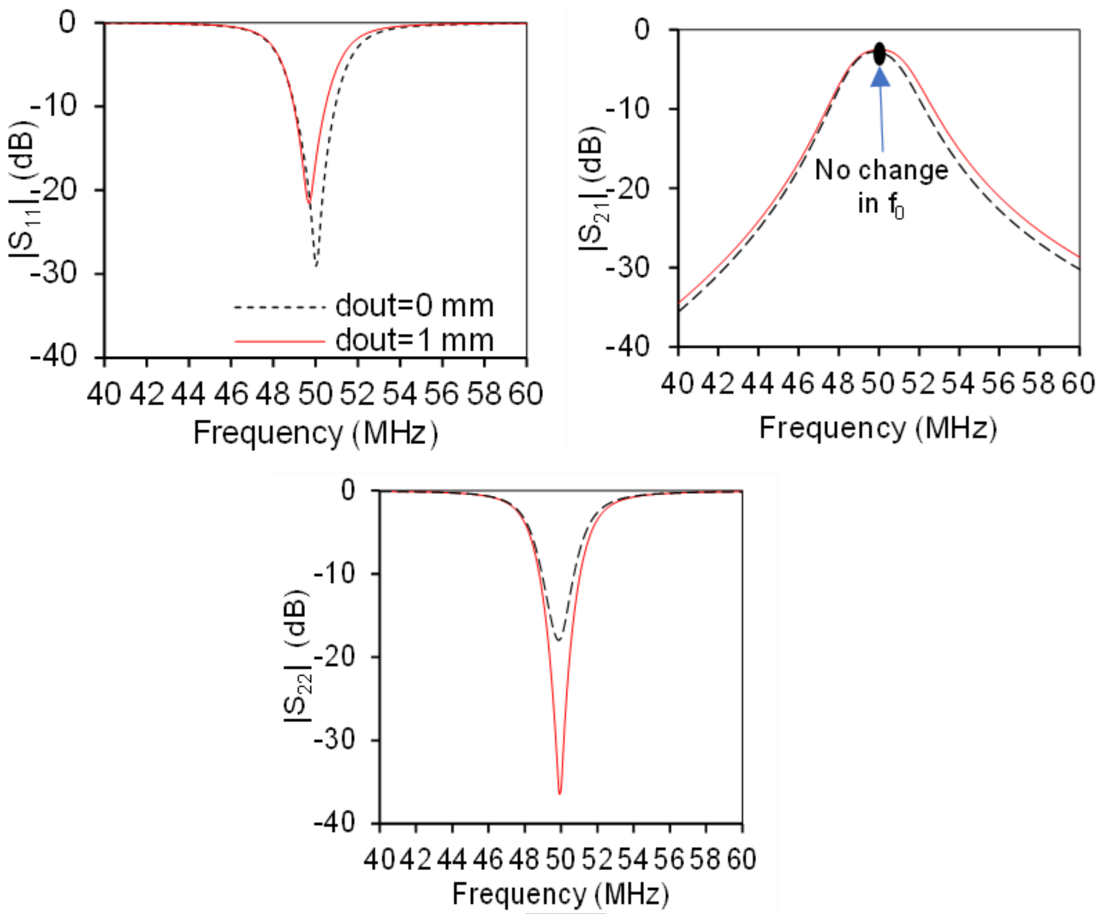

(b)

Fig 3. 3 S-parameters results of WPT systems using (a) Conventional and (b) using proposed inductor.

$$Q = \frac{\omega L}{R} \tag{3.4}$$

$$R = R_{conductivity} + R_{radiation}$$

$$R_{radiation} \alpha\, \varepsilon_{\text{eff}}^{4}$$

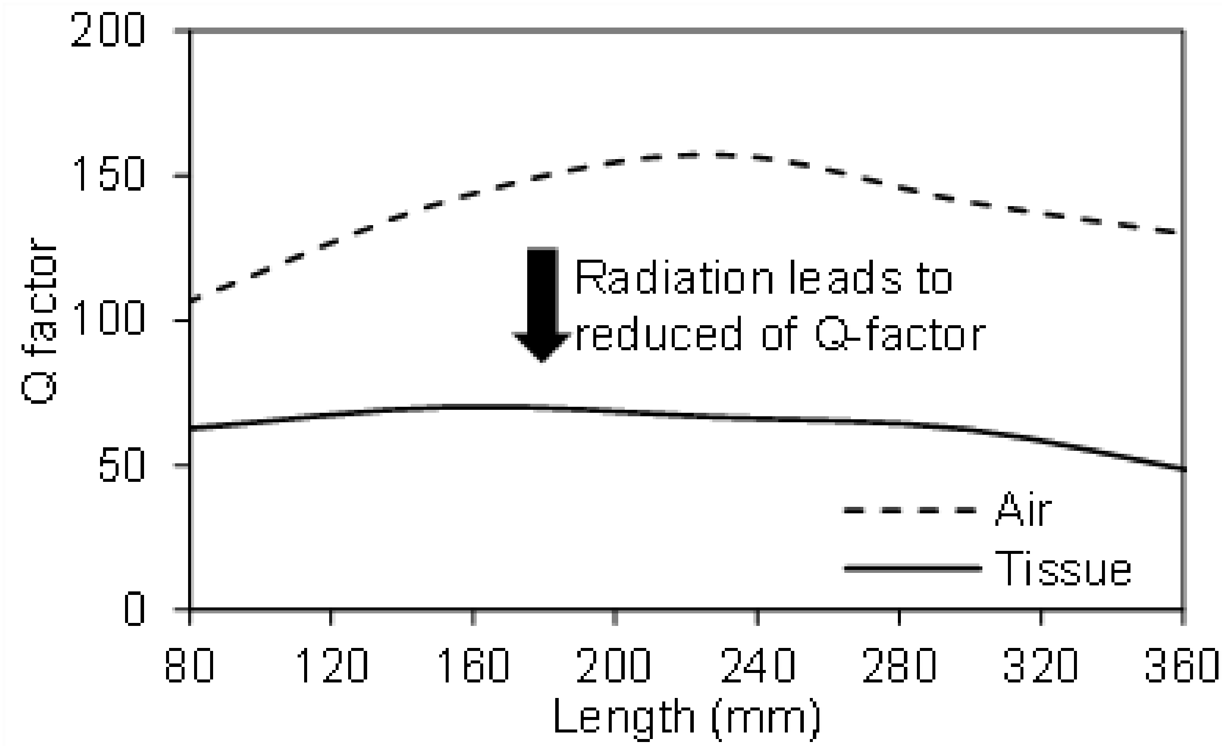

Fig 3. 4 The effect of the tissue on the quality factor

3.3 Proposed DGS resonators.

In the previous section, we discussed the use of a small electrical-length inductor to address the resonance-shift phenomenon and improve the KQ product. However, this approach has a limitation when it comes to achieving peak efficiency due to the low KQ-product. In this section, we propose the use of cooperative DGS resonators in a multi-input-single output (MISO) WPT system [15]. This approach not only achieves high efficiency but is also insensitive to the resonance shift, as demonstrated in Fig 3.5.

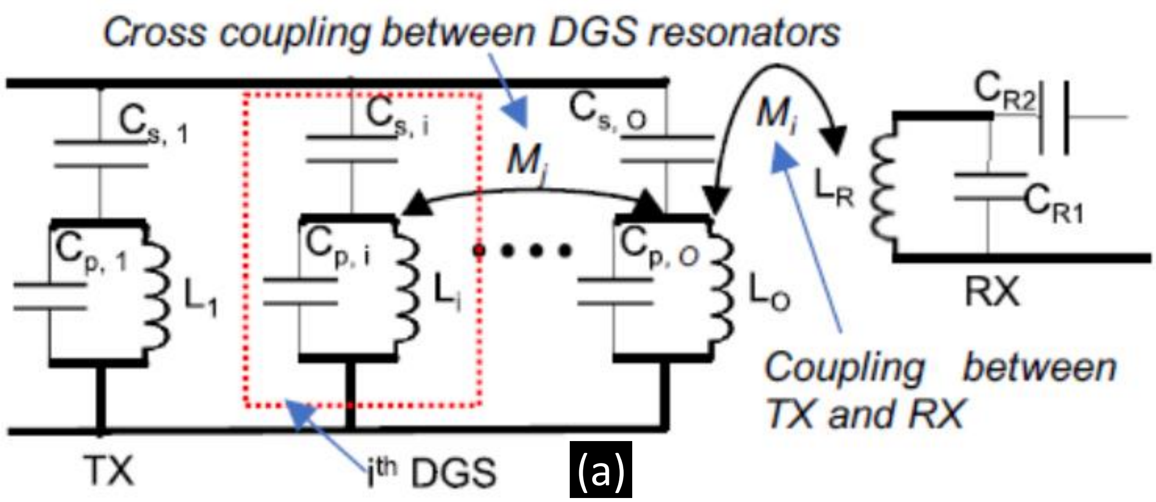

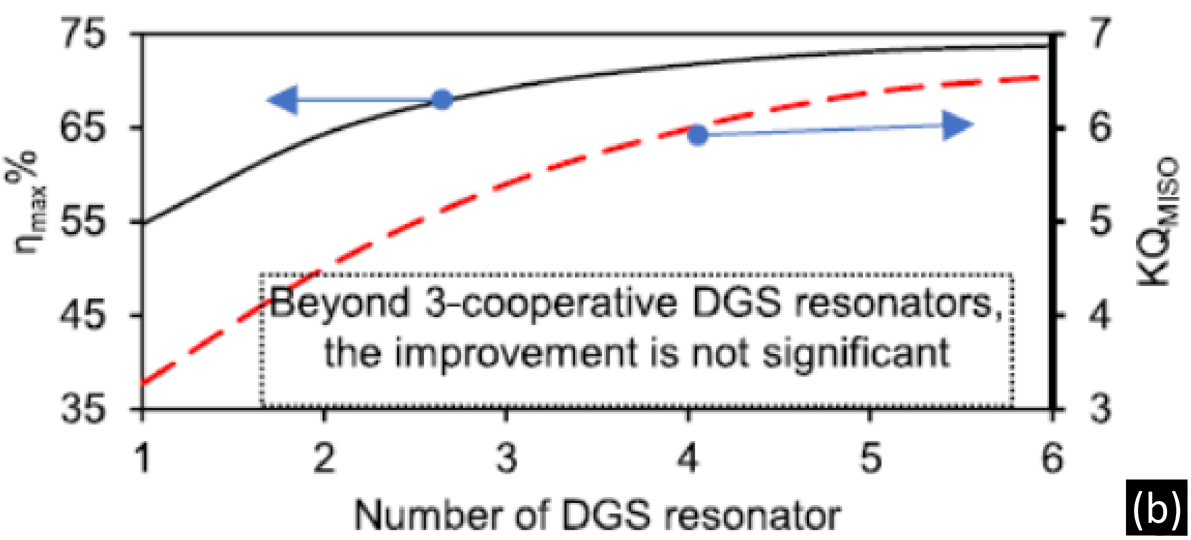

Fig 3. 5 The Proposed solution for improving KQ product (a) Cooperative DGS system. (b) KQMISO and ηmax of a different number of cooperative DGS resonators.

The system proposed in this study is illustrated in Fig 3.5(a), and it comprises an O number of cooperative DGS resonators and a DGS RX. Each cooperative DGS resonator has a small electrical length to mitigate the resonance shift problem. The proposed system is a MISO WPT system, and the overall kQ-product (KQMISO) of an O cooperative DGS resonator is calculated using equation (5). This calculation is not affected by the intra-mutual coupling, as described in [15]. Here, ki represents the coupling coefficient between the i_{th} cooperative DGS resonator and the RX, $Q_{TX,i}$ is the unloaded quality factor of the i_{th} cooperative DGS resonator, and Q_{RX} is the unloaded quality factor of the RX. The corresponding maximum obtainable efficiency is calculated as:

$$\eta_{max} = \left(kQ_T/\left[1+\sqrt{1+(\,kQ_T)^2}\right]\right)^2.$$

$$KQ_T = \sqrt{\sum_{i=1}^{O}(KQ_{\mathrm{i}})^2} \tag{3.3.1}$$

Fig 3.5 (b) shows KQ_T and η_{max} for 20 mm × 20 mm TX. The width of each cooperative DGS resonator is 0.75 mm and the spacing between two sub-TXs is 0.5 mm. The RX has the same dimensions as the RX used in the previous comparison Table I. η_{max} increases as the number of cooperative DGS resonators increases. Still, beyond three cooperative DGS resonators, no significant improvement. is achieved because of the limited increase in the KQ_T after three cooperative DGS resonators. So, we decided to implement the WPT used three cooperative DGS resonators. The shown Fig 3.6 is the proposed system to overcome the two mentioned issues.

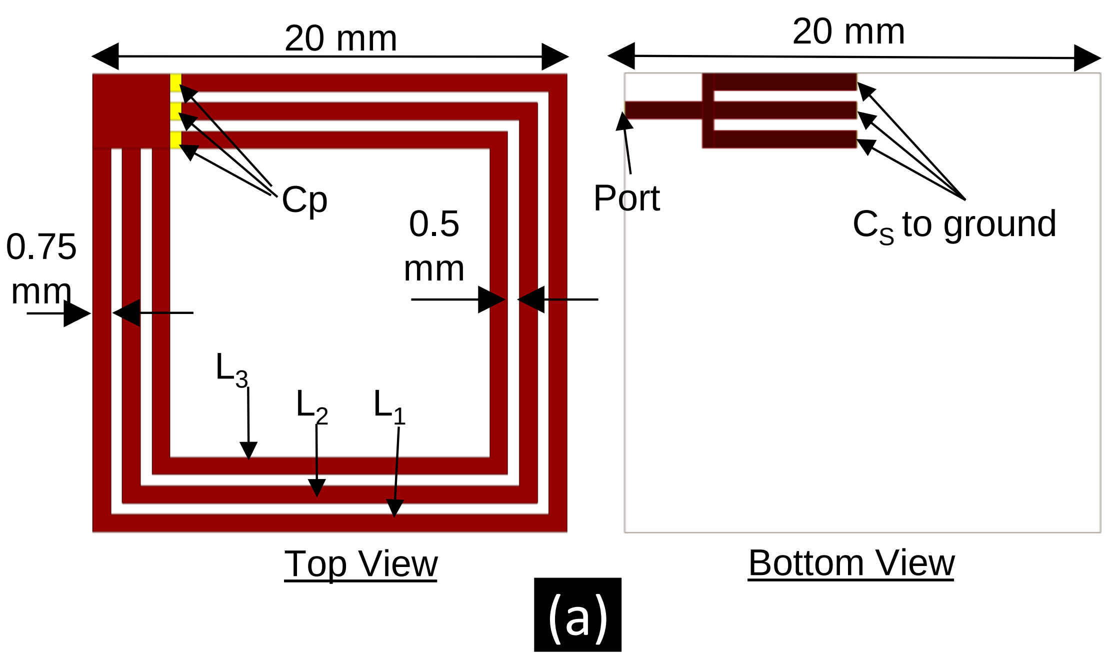

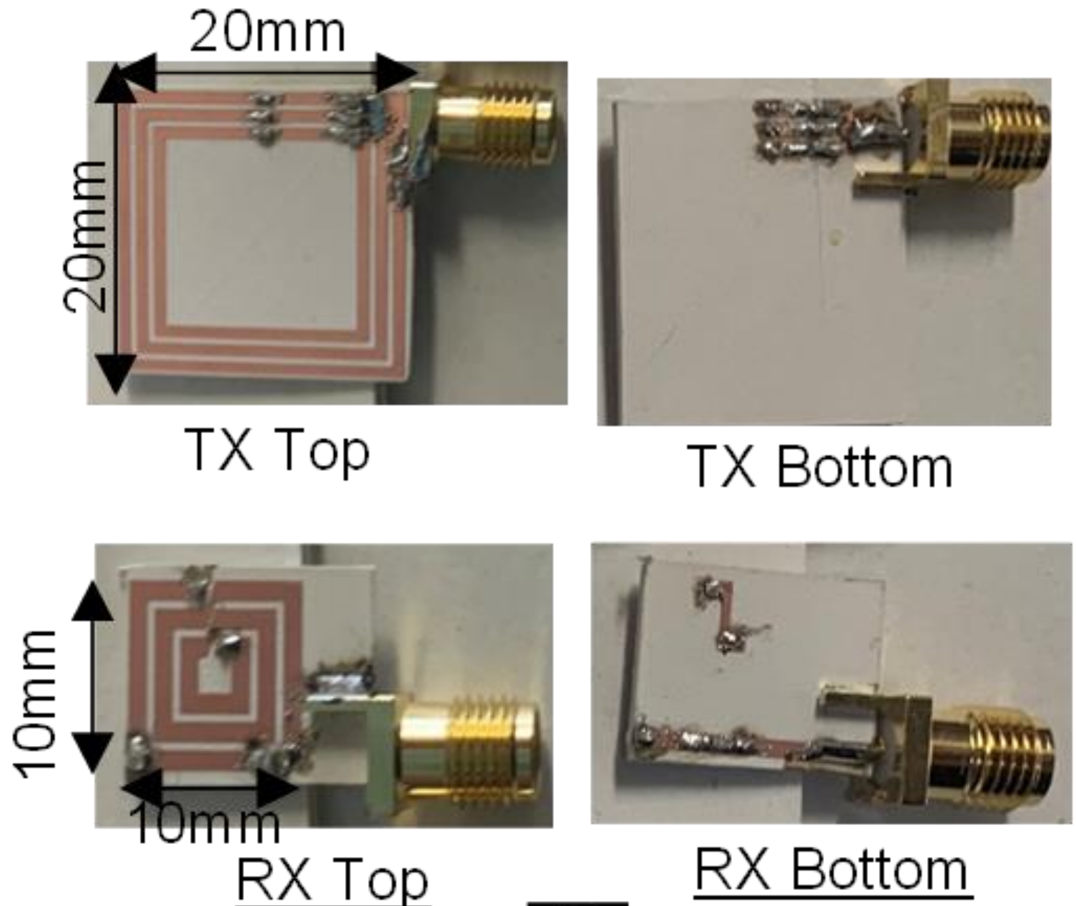
20mm
20mm
TX Top
TX Bottom
10mm
10mm
RX Top
RX Bottom

(b)

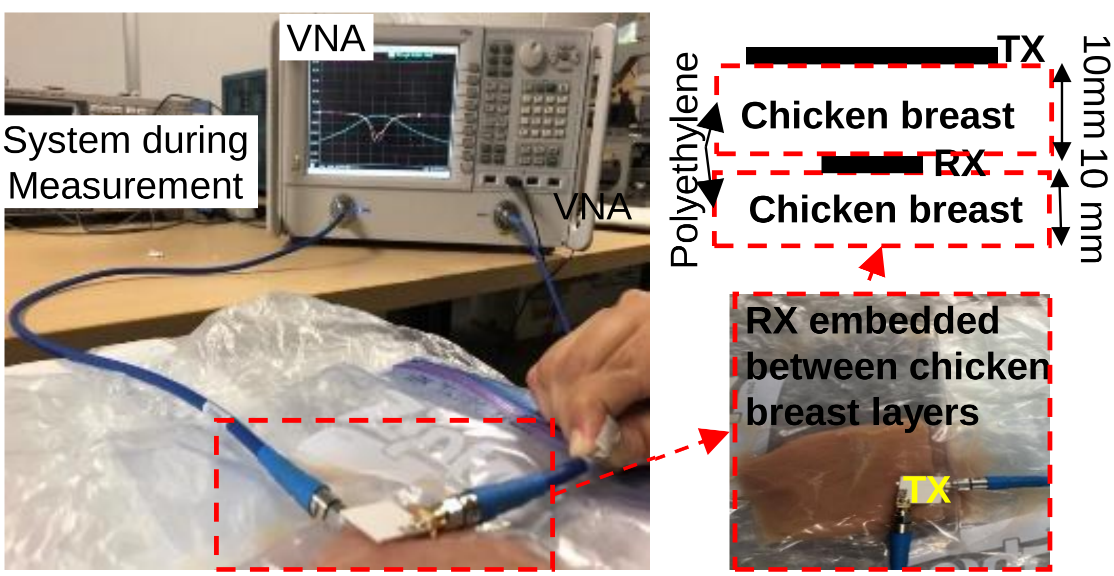
VNA
System during Measurement
VNA
TX
Polyethylene
Chicken breast
RX
Chicken breast
10mm 10 mm
RX embedded between chicken breast layers
TX

(c)

Fig 3. 6 The proposed system (a) Proposed TX layout. (b) The fabricated WPT system. (c) the measurement setup.

Fig 3.6(a) shows the layout of the proposed TX, which is the same as the one explained in the previous section. On the other hand, Fig 3.6(b) shows the fabricated system with dimensions and capacitor values specified in Table 3.2.

3.4 Fabrication and Measurement

The proposed system was fabricated using the MITS FP-21T Precision machine in this section. The fabricated system is presented in Fig 3.6(b). S-parameters were measured using a vector network analyzer (Keysight PNA series, part number: N5222A) in air and chicken breast. The measurement setup in chicken breast is shown in Fig 3.6(c), where the RX is positioned between two layers of chicken breast. To avoid any physical contact between the system and the tissue, the layers of chicken breast are placed inside polyethylene bags with a 10mm thickness for both layers.

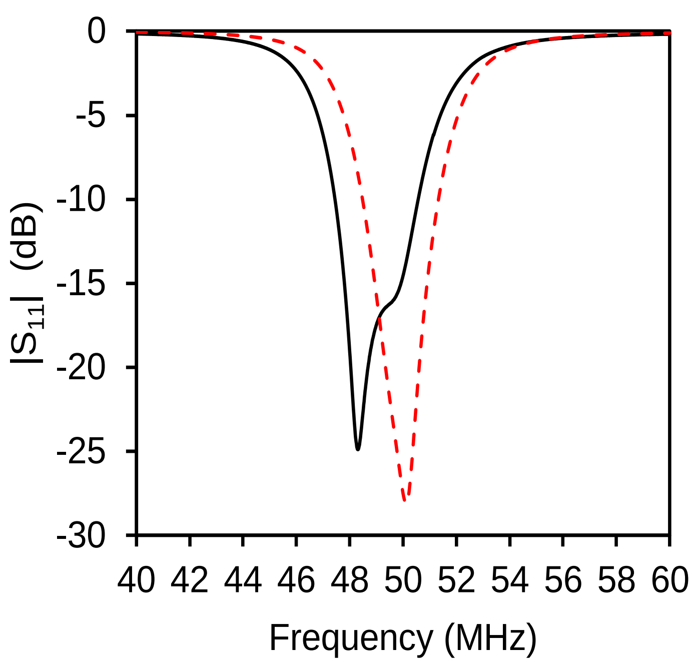

(a)

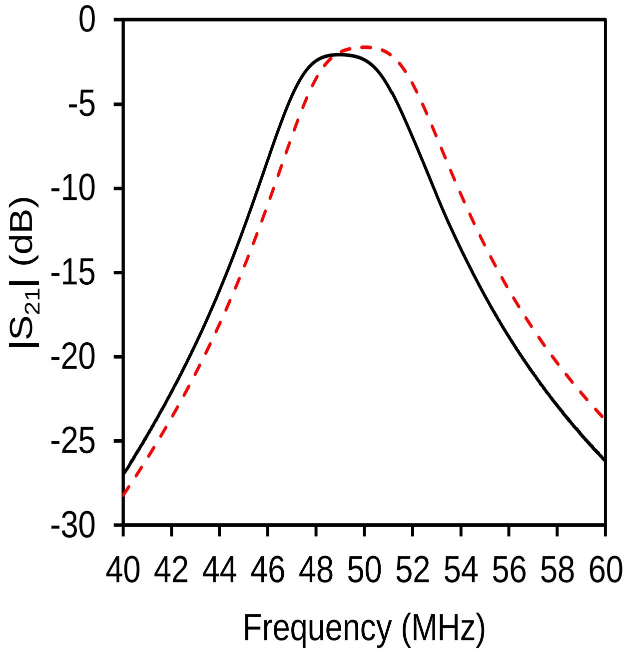

(b)

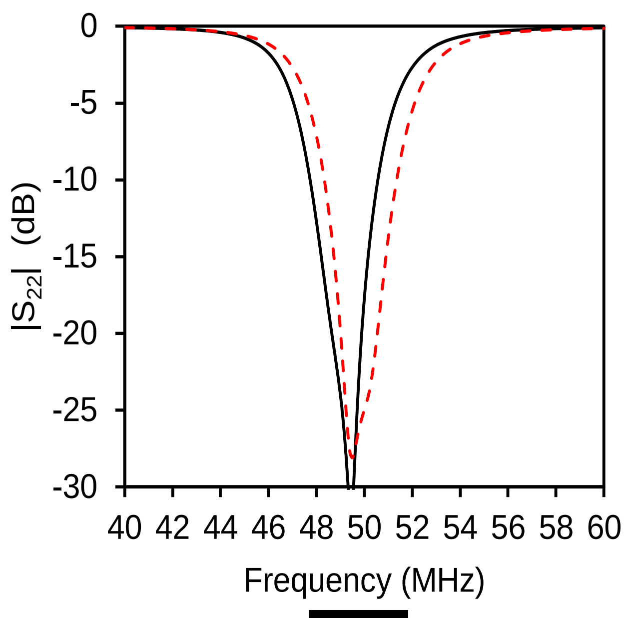

(c)

Fig 3. 7 The comparison between the measured and simulated S-parameters results. (a) TX reflection coefficient (|S11|). (b) Transmission coefficient (|S21|). (c) RX reflection coefficient (|S22|).

Table 3. 2 Capacitor (in pF) used in simulation and Measurements

	TX (20×20) mm^2		RX (10×10) mm^2	
	Cs	Cp	CR1	CR2
Simulation	16	100	180	33
Fabrication	16	103	183	33

The comparison between the measured and simulated S-parameters of the chicken breast medium is illustrated in Fig 3.7. The system's efficiency (η) is calculated from the S-parameters using $|S_{21}|^2$, which is presented in Fig 3.7(b). The simulated efficiencies at 50 MHz are 74% in air and 68% in tissue, while the measured efficiencies at 49 MHz are 68% in air and 62% in tissue. The simulated center frequency is 50 MHz, but the measured center frequency is slightly reduced to 49 MHz This discrepancy between the measured and simulation results is mainly attributed to the use of a slightly higher capacitor during the fabrication process, as listed in Table 3.2.

Moreover, the proposed WPT system was simulated and measured in the air, and the simulated and measured center frequencies were identical to the tissue case. The only difference was that the simulated and measured |S21| was about 0.3 dB higher in the air. This finding proves the effectiveness of the proposed system against the resonance shift.

3.5 Performance during the Lateral Misalignment

In this section, we conducted a performance evaluation of the proposed system, focusing on its response to lateral misalignment (Δx) within tissue. The results of the assessment demonstrated that the measured efficiency surpassed 50% for Δx values up to |6.5| mm in tissue, as illustrated in Fig 3.8. This outcome indicates that the system is capable of maintaining a satisfactory level of efficiency, even when faced with lateral misalignment within the tissue medium

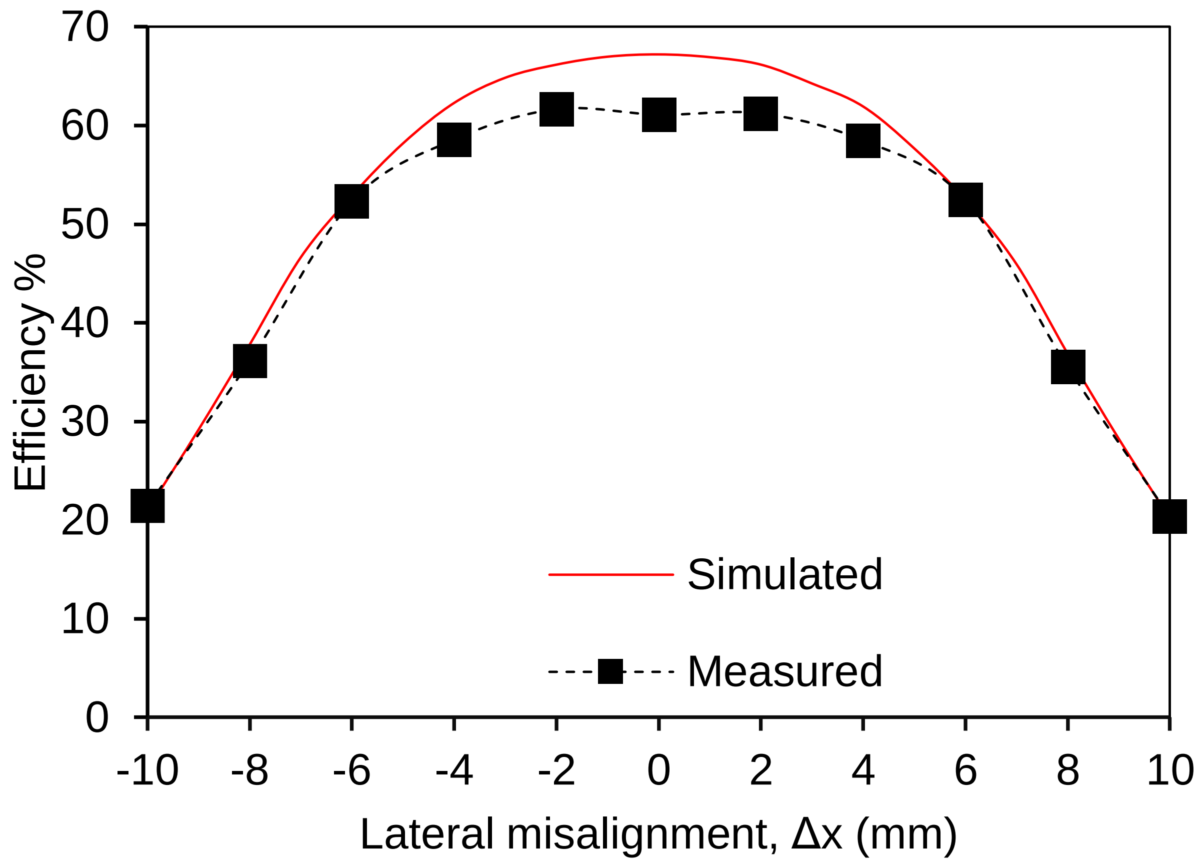

Fig 3. 8 Efficiency performance during the lateral misalignment

3.6 The safety Consideration

Safety of the human body needs to be guaranteed during the use of EM waves. Specific absorption rate (SAR) is a measuring factor for EM wave absorption by the human body. SAR is calculated as [71]

$$SAR = \frac{\sigma}{\rho_{den}} |E|^2 \qquad (3.6.1)$$

where σ is the conductivity of the tissue, ρ_{den} is the density of the tissue, E is the intensity of electric fields. According to the IEEE standard C95.1-1999, the SAR averaged over 1g of cubic tissue (1-g average SAR) must be less than 1.6 W/kg to preserve the safety of the human body [71] as shown in Fig. 8. The maximum 1-g average SAR level of the proposed design is about 1.59 W/kg, i.e., it does not exceed the value defined by the IEEE standard C95.1-1999. Although the proposed WPT system has used a higher frequency than that of [2], the proposed WPT system operated within the safety limit illustrated by IEEE standard C95.1-1999 for 1-g SAR with an input power (166mW).

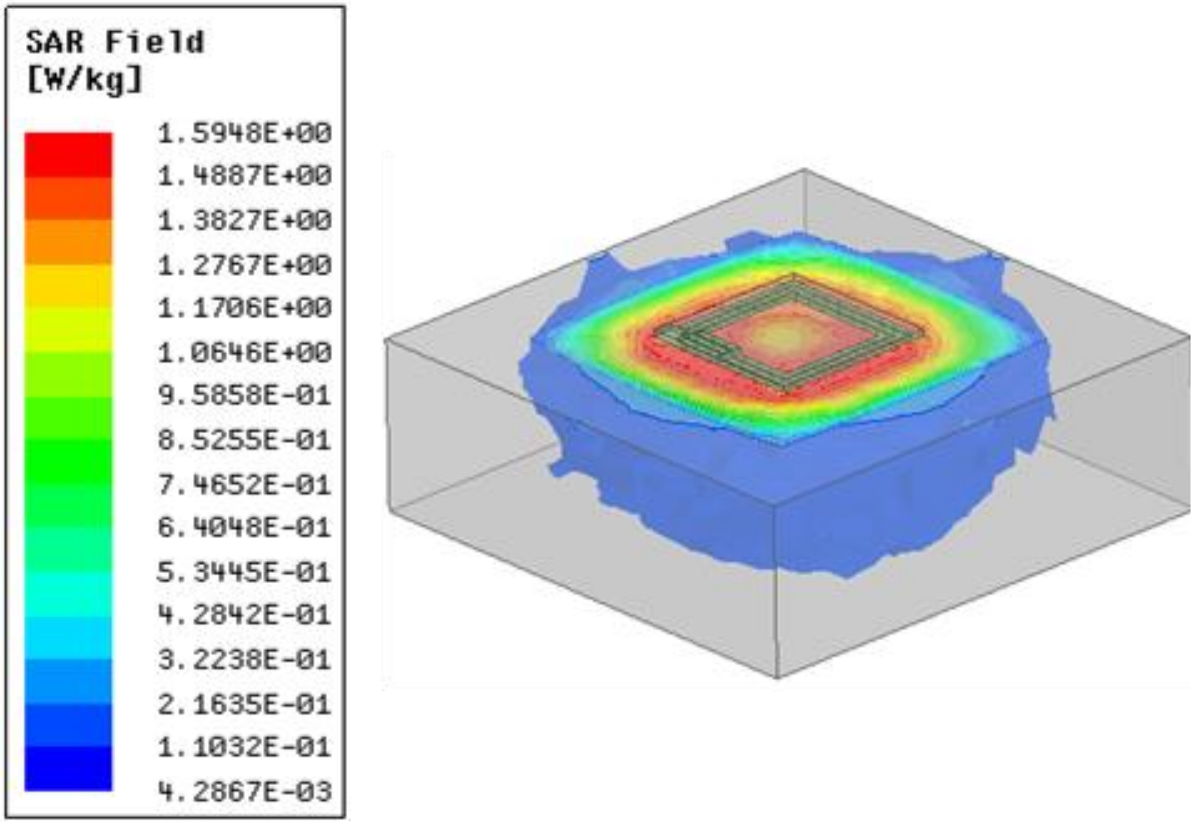

Fig 3. 9 Three-dimensional view of EM Simulated 1-g average SAR distribution at 50 MHz when the input power is set as 22.2 dBm.

Chapter 4 Multi-Ring Resonators Stacked Metamaterial inspired geometry For Miniaturization WPT system.

4.1 Introduction

As mentioned in the previous chapter that we cannot overcome the problem of radiation by using the conventional inductor. The conventional coupled suffers from loss of power in the parallel magnetic field component (Hρ). At this point the use of metamaterial is the best way to help in solving this problem. Metamaterials have a strong ability to control the direction of magnetic fields because of their negative or near-zero permeability. By using this characteristic in near field, it helps to improve the coupling between TX and RX.

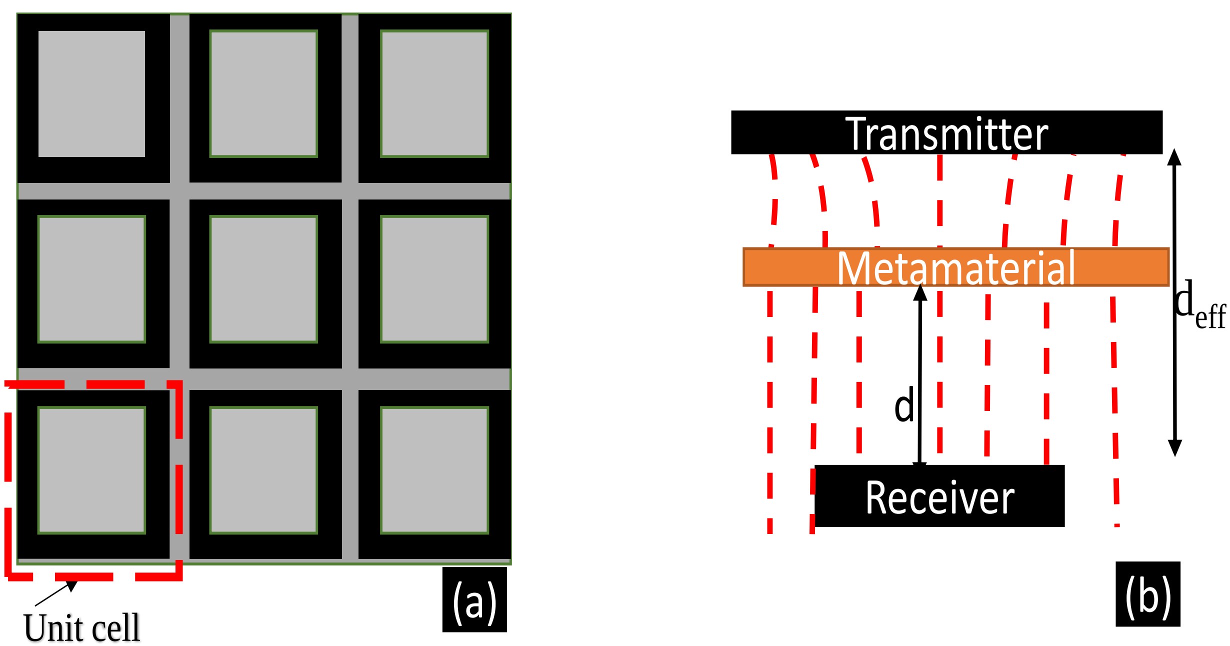

Fig 4. 1 Conventional metamaterial. (a)structure. (b) conventional way to use it in WPT system.

4.2 Conventional Metamaterial

Conventional metamaterial structure is shown in Fig. 4.1 (a). The conventional metamaterial consists of unit cells which are organized in array vertically on the same plane. For example, as shown 3×3. The active routing-based meta-surface[14] enabled the adaptive location of the receiver during operation. In [15] proposed a semidefinite-relaxation-based method to determine the optimum loading reactance of the meta-surface unit cells. The resulting meta-surface showed enhanced efficiency when utilized as a passive relay in a reference WPT system when compared to that WPT system without meta-surface15. In[17,18,19,20,21] further intermediate meta-surface or metamaterials layers with near-zero, negative permeability, or both of them have been exploited to enhance the WPT systems efficiency. Still, current WPT systems based on meta-surface[14,15,16] .Usually, metamaterial slab is used as shown in Fig. 4.1 (b). It is placed in between the TX and RX and this help to focus the magnetic field but it leads to reduce the effective distance. Also, still there is some loss of the magnetic field in the parallel component (Hρ) behind the slab of metamaterial.

4.3 Stacked Metamaterial

In this section, we presented a novel metamaterial-inspired geometry that utilizes a co-axial configuration of stacked unit cells. This innovative design is then employed as a wireless power transfer (WPT) transmitter, referred to as Meta-TX, which transfers power to a WPT receiver embedded in biological tissues. By adopting this approach, the original working distance between the transmitter (TX) and receiver (RX) of the WPT system is maintained. The proposed metamaterial-inspired geometry exhibits near-zero effective permeability, allowing for a higher concentration of magnetic fields to be directed towards the receiver. This enhancement in efficiency and misalignment performance leads to improved power transfer efficiency and performance. This can by using stacked metamaterial attached with the transmitter to work as Meta-Tx as shown in Fig. 4.2.

The effect of using this configuration can be shown as:

The magnetic field and dispersion properties of a small inductive loop can be analyzed. This loop is positioned in the xy-plane and its center is located at z = 0. It behaves as a magnetic dipole, and its magnetic field in the near-field regime (where $\beta r \ll 1$) is discussed in [26].

$$\begin{bmatrix} H_r \\ H_\theta \\ H_\varphi \end{bmatrix} = H_0 \begin{bmatrix} 2\cos\theta \\ \sin\theta \\ 0 \end{bmatrix} \tag{4.3.1}$$

Where r, θ, φ are the representation of the spherical coordinate system.$H_0 = IA/(4\pi r^3)$. Given the assumption of a single turn loop with current I and area A, we can rewrite equation (4.3.1) in the cylindrical coordinate system as follows:

$$\begin{bmatrix} H_\rho \\ H_\varphi \\ H_z \end{bmatrix} = \begin{bmatrix} sin\theta & cos\theta & 0 \\ 0 & 0 & 1 \\ cos\theta & -sin\theta & 0 \end{bmatrix} \times \begin{bmatrix} H_r \\ H_\theta \\ H_\varphi \end{bmatrix} = \mathrm{H}_0 \begin{bmatrix} 3sin\theta \\ 0 \\ 1 + 3cos\theta \end{bmatrix} \qquad (4.3.2)$$

Where ρ, φ, z is the representation of the cylindrical coordinate system. The component Hρ is parallel, it indicates that the magnetic field is aligned with the radial direction in the cylindrical coordinate system. This component cannot generate near-field coupling because the radial direction does not contribute to the coupling between the transmitter and receiver.

To enhance the near-field coupling and improve the magnetic field focusing on the receiver, it is necessary to increase the perpendicular component Hz while minimizing the parallel component Hρ. This can be achieved through the proposed metamaterial-inspired geometry that manipulate the magnetic field distribution. In addition to the two magnetic field components (Hρ and Hz), the electric field also has a component in the cylindrical coordinate system. The electric field component is typically denoted as Er and represents the radial component of the electric field. This component is perpendicular to both the radial direction (ρ) and the z-axis direction. Therefore, when considering the near field coupling and field distribution, it's important to consider both the magnetic field components (Hρ and Hz) and the electric field component (Eφ). By properly manipulating and optimizing these field components, it is possible to enhance the near field coupling and improve the overall performance of the system. If the electric field component in the cylindrical coordinate system is denoted as Eϕ, and kϕ represents the wave vector component in the azimuthal direction, then based on the given information, it is stated that kϕ has a zero value. Therefore, the wave vector can be written as:

$$\vec{\mathrm{K}} = K_\rho a_\rho + K_z a_z \qquad (4.\ 1.3)$$

where kρ represents the wave vector component in the radial direction ($\hat{\rho}$) and kz represents the wave vector component along the z-axis ($\hat{z}$). The wave vector k is a vector quantity that characterizes the direction and magnitude of the wave propagation. This wave equation describes the propagation of electromagnetic waves in a medium with diagonal permittivity and permeability, where the wave's spatial variation and temporal variation are coupled through the permittivity (ε) and permeability (μ) of the medium with ερ = εϕ = εz and μρ = μϕ = μz, so the equation will be as follow:

$$\vec{\mathrm{K}} \times \vec{\mathrm{K}} \times \vec{\mathrm{H}} + \frac{\omega^2}{c^2}\mu\varepsilon \times \vec{\mathrm{H}} = 0 \qquad (4.\ 3.\ 4)$$

ω represents the angular frequency of the wave, and c represents the speed of light in the medium. By substituting from Equations 4. 2,3 to Equation 4. 4 it leads to:

$$\begin{bmatrix} \frac{\omega^2\mu_\rho\varepsilon_\varphi}{c^2} - K_z^2 & 0 & K_\rho K_\rho \\ 0 & \frac{\omega^2\mu_\rho\varepsilon_\varphi}{c^2} & 0 \\ K_z K_\rho & 0 & \frac{\omega^2\mu_z\varepsilon_\varphi}{c^2} - K_\rho^2 \end{bmatrix} \begin{bmatrix} H_\rho \\ 0 \\ H_z \end{bmatrix} = 0 \qquad (4.\ 3.5)$$

To ensure the existence of non-trivial solutions for the magnetic field $\vec{\mathrm{H}}$, the determinant of the coefficient matrix must vanish. Therefore, the dispersion equation in the cylindrical coordinate system for this small inductive loop can be written as:

$$\frac{K_\rho^2}{\mu_z} + \frac{K_z^2}{\mu_\rho} = \frac{\omega^2}{c^2}\varepsilon_\rho \qquad (4.3.6)$$

By utilizing the conditions $|\mu z| < 1$, $|\mu p| \geq 1$, and $|\varepsilon\varphi| \geq 1$, the variance of the magnetic field in the ρ-direction can be minimized, i.e., $k\rho \rightarrow 0$. This implies that the magnetic field is enforced and predominantly oriented in the z-direction. These conditions on the permittivity and permeability values restrict the propagation of the magnetic field in the radial direction (ρ) and promote a stronger field alignment along the z-direction. In Fig 4.2 shows the comparison between the magnetic field distribution of the conventional WPT system using TX and RX and the magnetic field distribution by using the proposed meta-TX and RX. Which shows the effect of the stack configuration on the distribution of magnetic field by increasing the perpendicular component and this increasing the focus of the field.

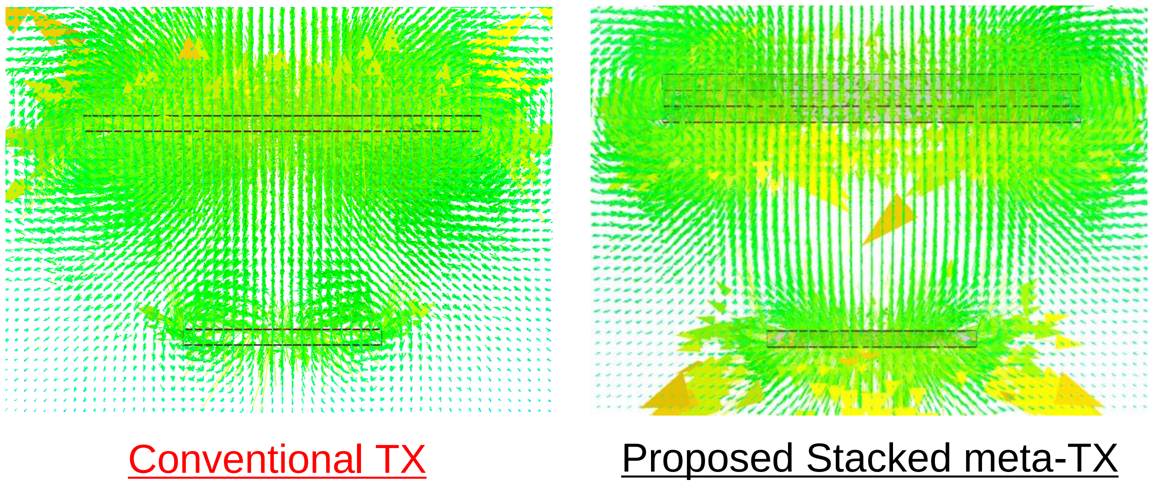

Fig 4. 2 The proposed stacked metamaterial (a) Stacked metamaterial. (b) Split ring resonator (SRR) and its characteristics.

The first developed unit cell of stacked metamaterial by our WPT team is based on split ring resonators (SRR) In [25]. This unit cell is designed by the short inductor theory which we used to solve the problem of resonance shift frequency. By using this metamaterial configuration not only achieved high intensity of magnetic field but also, it helps to mitigates the frequency misalignment problem. Also, reduced the second problem of the tissue which is the radiation. Because each layer shields each other from the radiation. The proposed metamaterial was low magnetic loss as shown in Fig 4.3. the effective permeability is very small < 1. Due to the equation [4.3.5] the imaginary part of the permeability should be near zero or zero. SRR is achieved this condition. and achieve a very good performance (efficiency is 63%) with the conventional size of RX.

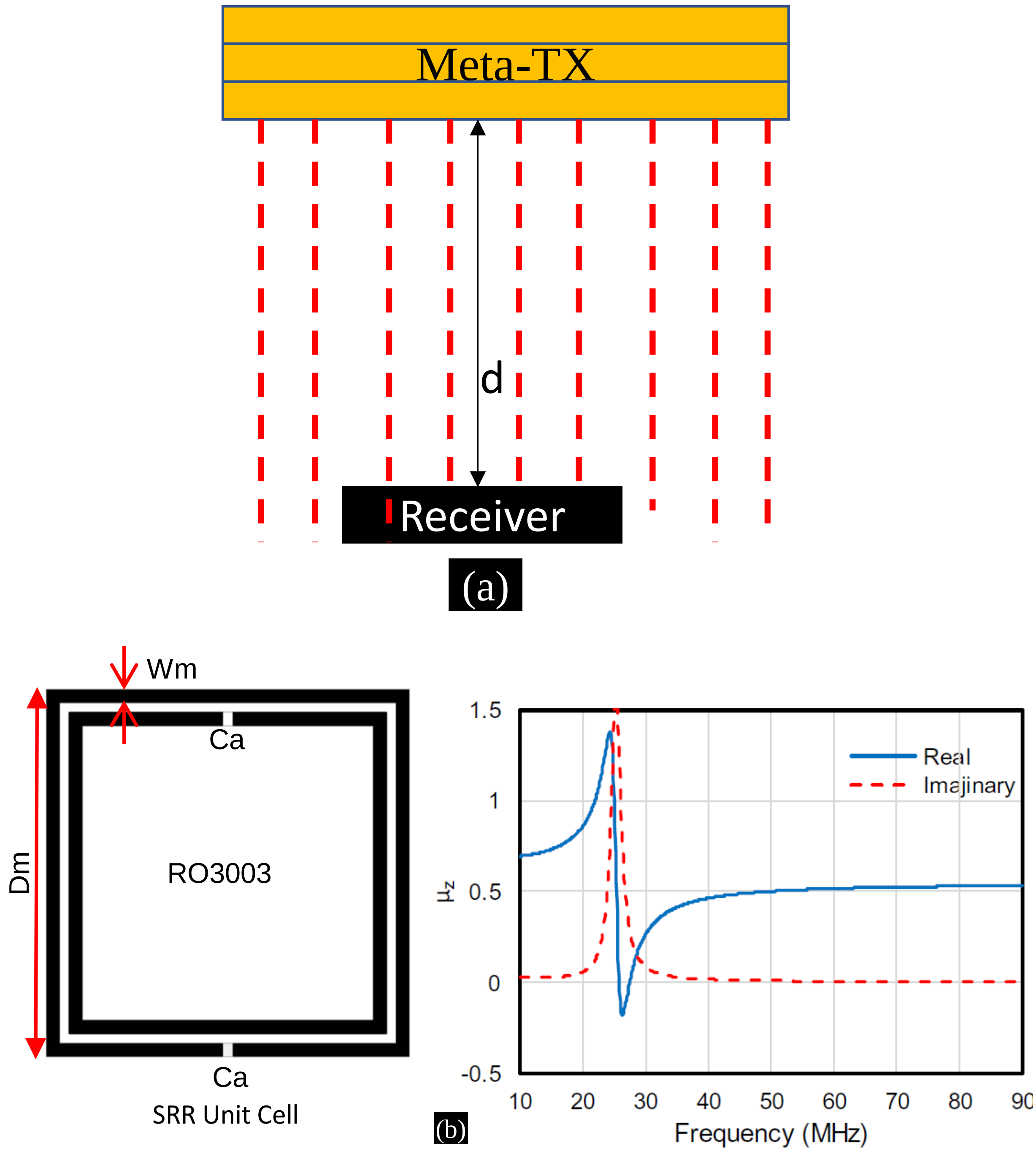

Fig 4. 3 The proposed stacked metamaterial (a) Stacked metamaterial. (b) Split ring resonator (SRR) and its characteristics.

$$\begin{aligned} \mu_z &= \mu_{real} + J\mu_{imaginary} \\ &= \mu_{real}\left(1 + \frac{J\mu_{imaginary}}{\mu_{real}}\right) \end{aligned} \tag{4.3.5}$$

In the field of biomedical applications, minimizing the size of the receiver (RX) is of utmost importance. Initially, the performance of the first unit cell did not meet the desired criteria when using a small RX. As a result, further development was undertaken to create an improved unit cell design. The objective was to enhance the performance specifically for applications requiring a compact RX size.

4.4 The Proposed Stacked metamaterial

In the proposed Multi Ring Resonator (MRR) unit cell, the compensation capacitances (C1, C2, C3, C4) are non-uniform, meaning that they have different values for each element. On the other hand, the Conventional Split Ring Resonator (SRR) unit cell does not exhibit this non-uniformity. The Multi Ring Resonator (MRR) is an innovative unit cell structure, as illustrated in Figure 4.4(a). It offers similar characteristics to the Conventional Split Ring Resonator (SRR) and can be utilized to extract metamaterial properties. Figure 4.4(b) presents a comparison between the Conventional SRR and the proposed MRR. Table I provides a summary of the dimensions and loading capacitance values for both the conventional SRR and proposed MRR unit cells. These values are crucial in determining the characteristics and performance of the unit cells.

To ensure medium-independent characteristics, the loop inductance is carefully selected in both the conventional SRR and proposed MRR unit cells. This allows for consistent behavior and performance regardless of the surrounding medium.

It is worth noting that the specific values of the dimensions, compensation capacitances, and loop inductance will vary based on the design requirements and objectives of the WPT system. The values listed in Table 4.1 serve as reference points for understanding the comparison between the conventional SRR and proposed MRR unit cells.

Table 4. 1 Capacitors Value used for unit cell of SRR and MRR

Parameter	Value	Unit
Dm	20	mm
Wm	0.75	mm
Sm	0.5	mm
Ca	57	pF
C1	40	pF
C2	40	pF
C3	50	pF

The Multi Ring Resonator (MRR) is an innovative unit cell structure, as illustrated in Figure 4.4(a). It offers similar characteristics to the Conventional Split Ring Resonator (SRR) and can be utilized to extract metamaterial properties. Figure 4.4(b) presents a comparison between the Conventional SRR and the proposed MRR.

In our study, we followed the procedure outlined in reference [73] to extract the effective permeability (μz). The real part of the effective permeability (μ') is shown in Figure 4.3(b), while the imaginary part (μ") is depicted in Figure 4.3(c). Both unit cells, the conventional SRR and the proposed MRR, exhibit a real part of the effective permeability (μ') that is less than or equal to 1, indicating the achievement of near-zero permeability.

Equation [4.3.5] in this chapter indicates that the proposed MRR demonstrates lower magnetic loss compared to the Conventional SRR, thanks to the inclusion of an inductor. The inductor introduces a resistance (R) to represent the loss, and as the loops of the MRR are in parallel, the equivalent resistance (R) decreases when the number of parallel loops increases.

To evaluate the performance of the WPT system, we designed a system based on two-unit cells and examined the effects of reducing the size. Our findings indicate that the SRR WPT system topology, with a compact receiver (7x7 mm^2) placed in tissue as the transmitter, shows promising performance. However, further improvements are still required.

To address this, we employed the MRR, as depicted in Fig 4.3.a, which showcases the three-dimensional model of the MRR metamaterial within the tissue. Figure 4.5 also presents coefficient results of the TX, indicating an efficiency comparison and the degree of improvement achieved (the efficiency improved from 54% to 60.94%).

Furthermore, Figure 4.6 provides a comparison of the efficiency ($|S21|^2 \times 100$) between both WPT systems using different sizes of the RX (receiver).

These results highlight the potential of the MRR-based WPT system in achieving improved efficiency compared to the Conventional SRR. The use of the MRR offers advantages such as reduced magnetic loss and enhanced performance in tissue environments. However, further research and optimization are necessary to further enhance the efficiency and effectiveness of the WPT system.

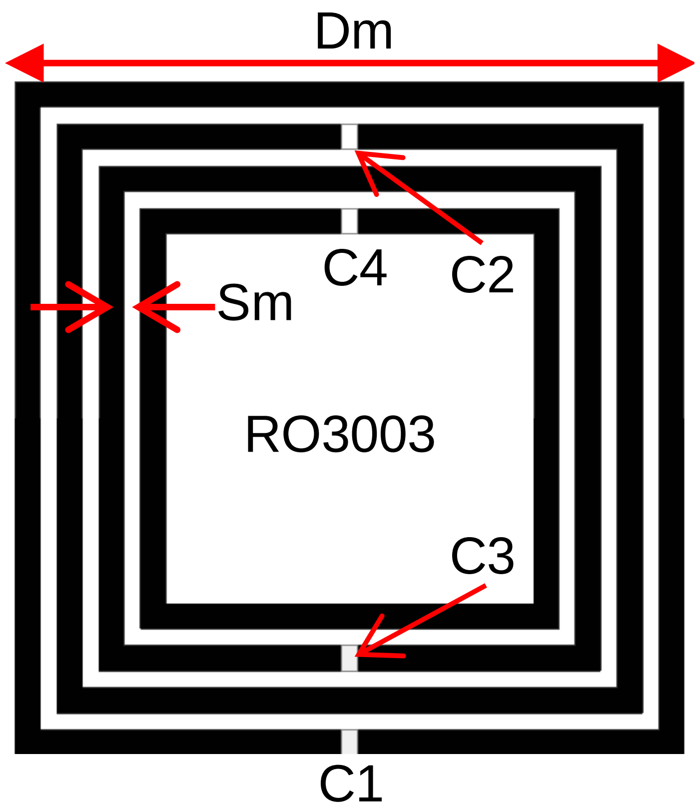
Dm
C4
C2
Sm
RO3003
C3
C1

(a)

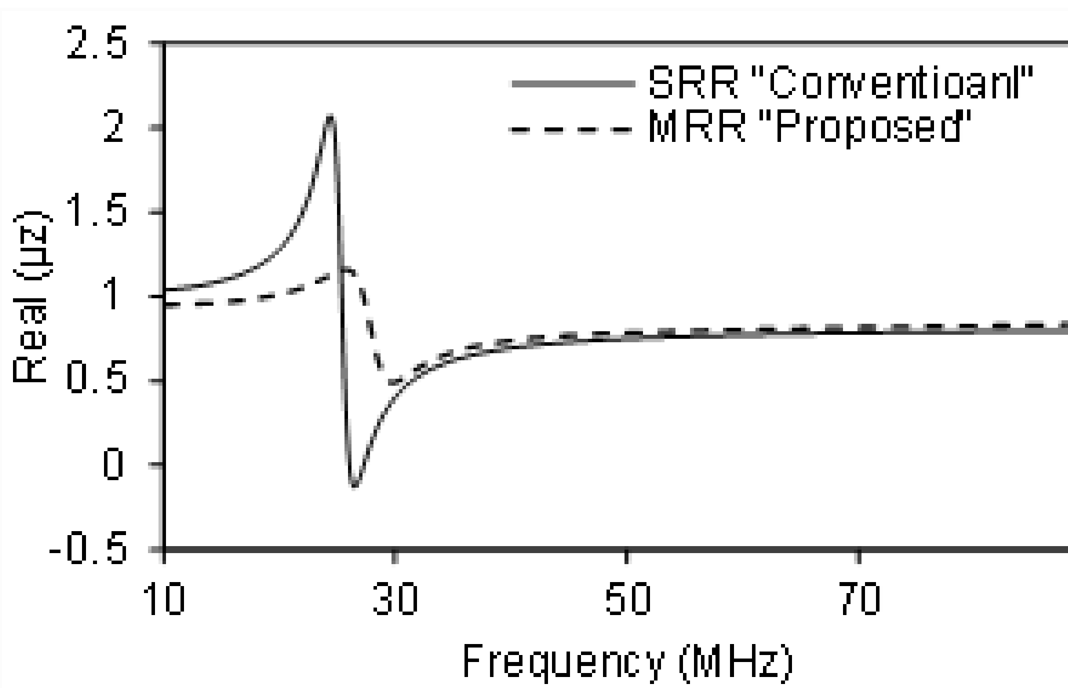
2.5
2
1.5
1
0.5
0
-0.5
Real (μz)
10
30
50
70
90
Frequency (MHz)
SRR "Conventioanl"
MRR "Proposed"

(b)

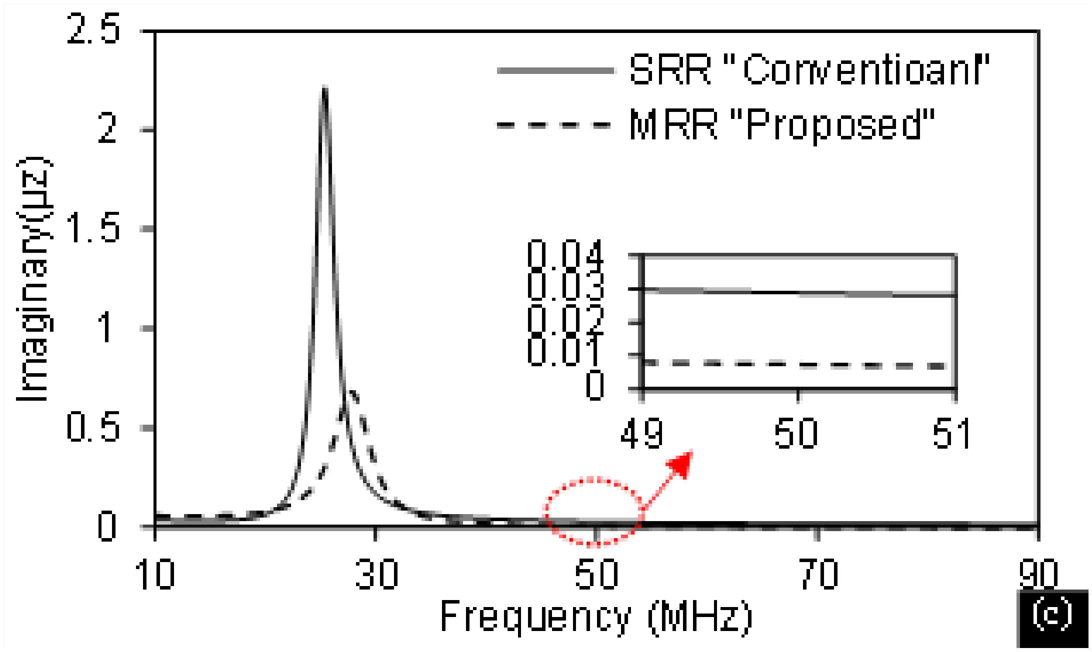

Fig 4. 4 Multi-Ring Resonators (MRR) metamaterial. (a) unit cell structure. (b) the comparison between SRR and MRR Real permeability. (c) the comparison between SRR and MRR imaginary permeability.

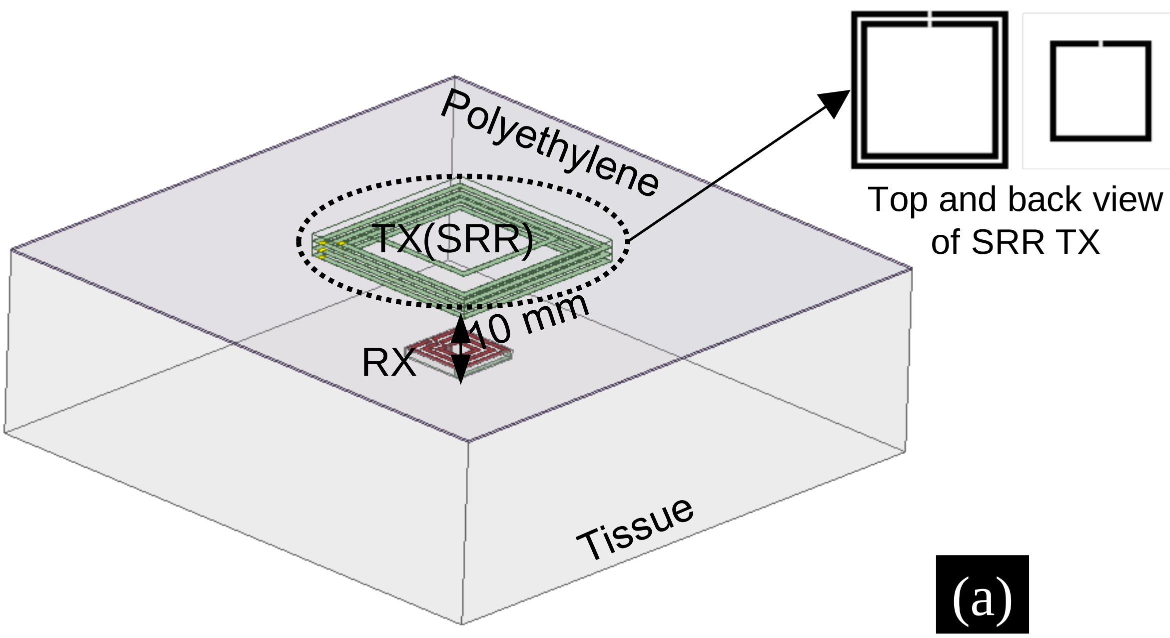

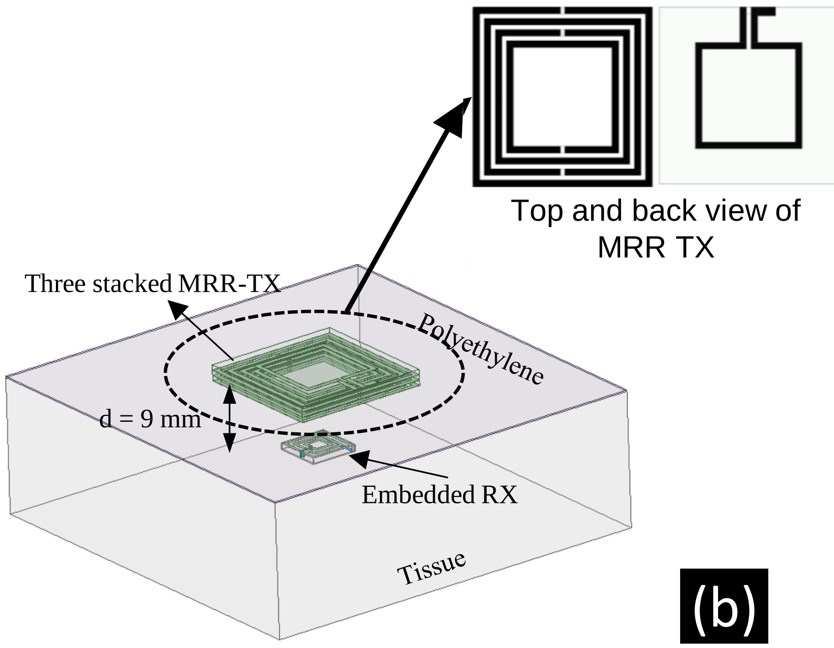

Fig 4. 5 SRR and MRR based WPT system topology in tissue (a) SRR (b)MRR

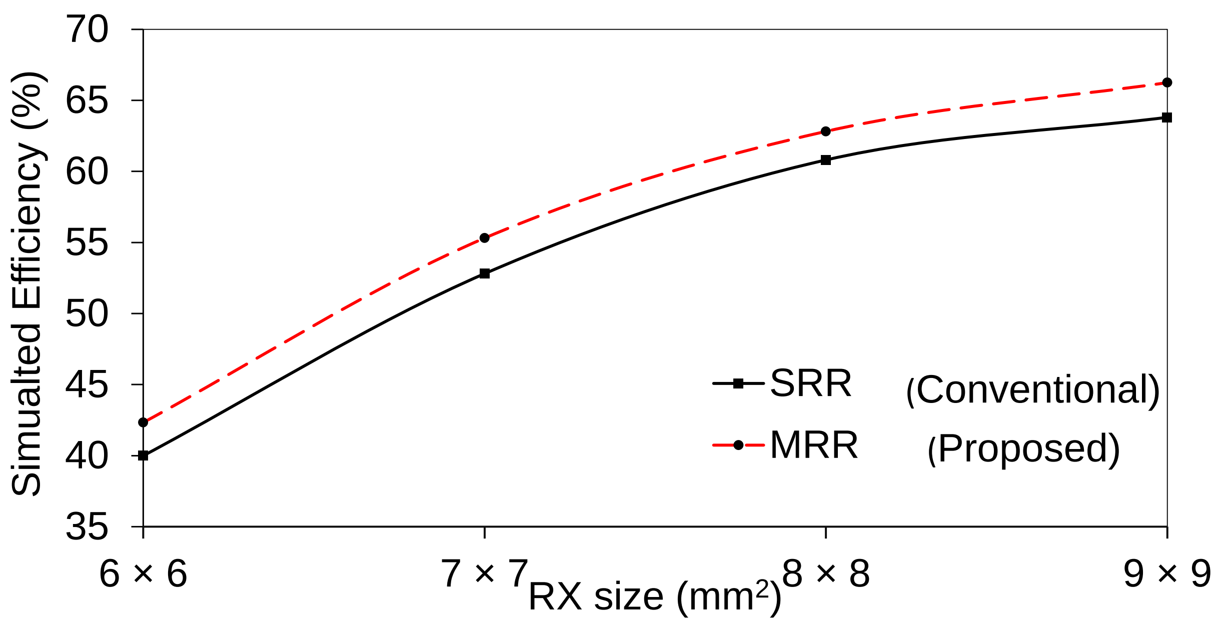

Fig 4. 6 Comparison of simulated efficiency between conventional SRR- and the proposed MRR-based WPT systems with different sizes of RX.

Fig 4. 7(a) displays the proposed stack metamaterial, which is attached to the transmitter in biomedical applications. The embedded millimeter-sized receiver (RX) is located at a depth of 9 mm from the tissue surface. The tissue characteristics used in this study are from [71] at a frequency of 50 MHz, with muscle properties including a dielectric constant of 77, conductivity of 0.68, and dielectric loss tangent of 3.16.

Fig 4.7(b) shows the front and back views of the RX structure, which measures 7×7 mm^2 and contains three turns, each with a width of 0.5 mm and a separation of 0.5 mm. Fig 4.7(c) displays the front view of each layer of the MRR stacked metamaterial, with a size of 20×20 mm2, a resonator width of 0.75 mm, and a separation of 0.5 mm. Additionally, the back view of the inductive feeding network used to feed the entire metamaterial structure is shown in this Fig.

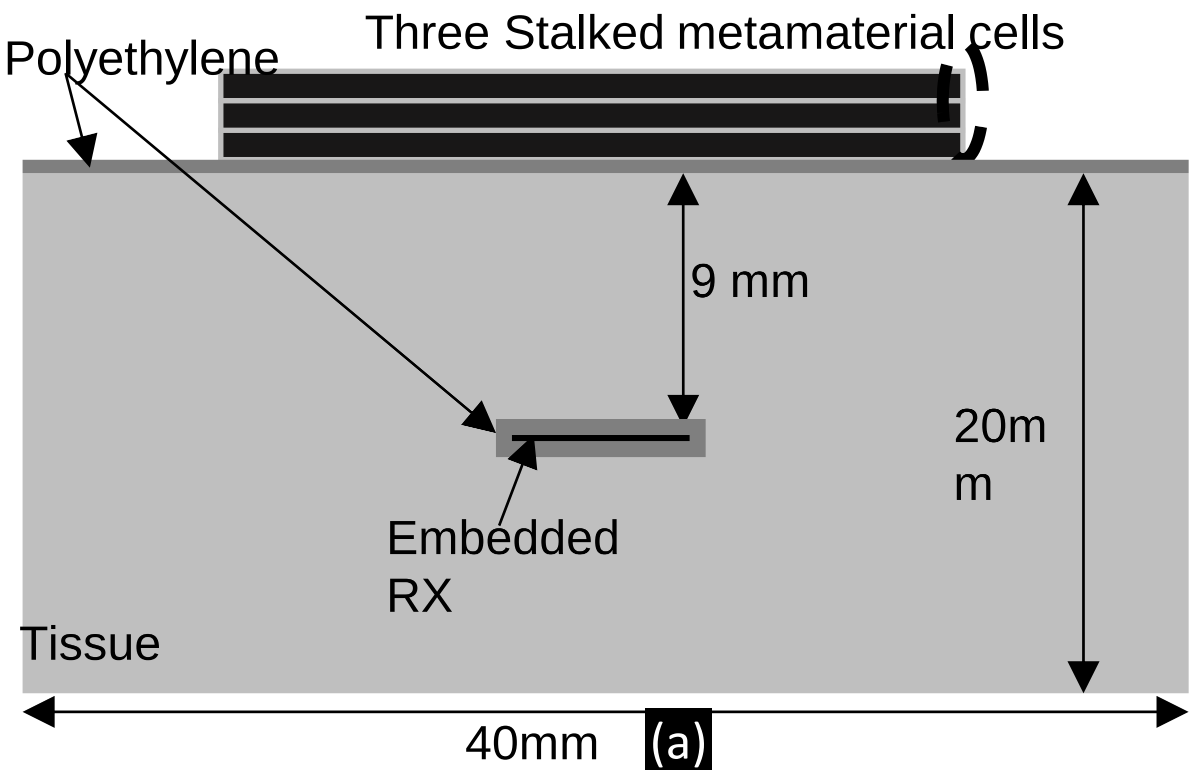

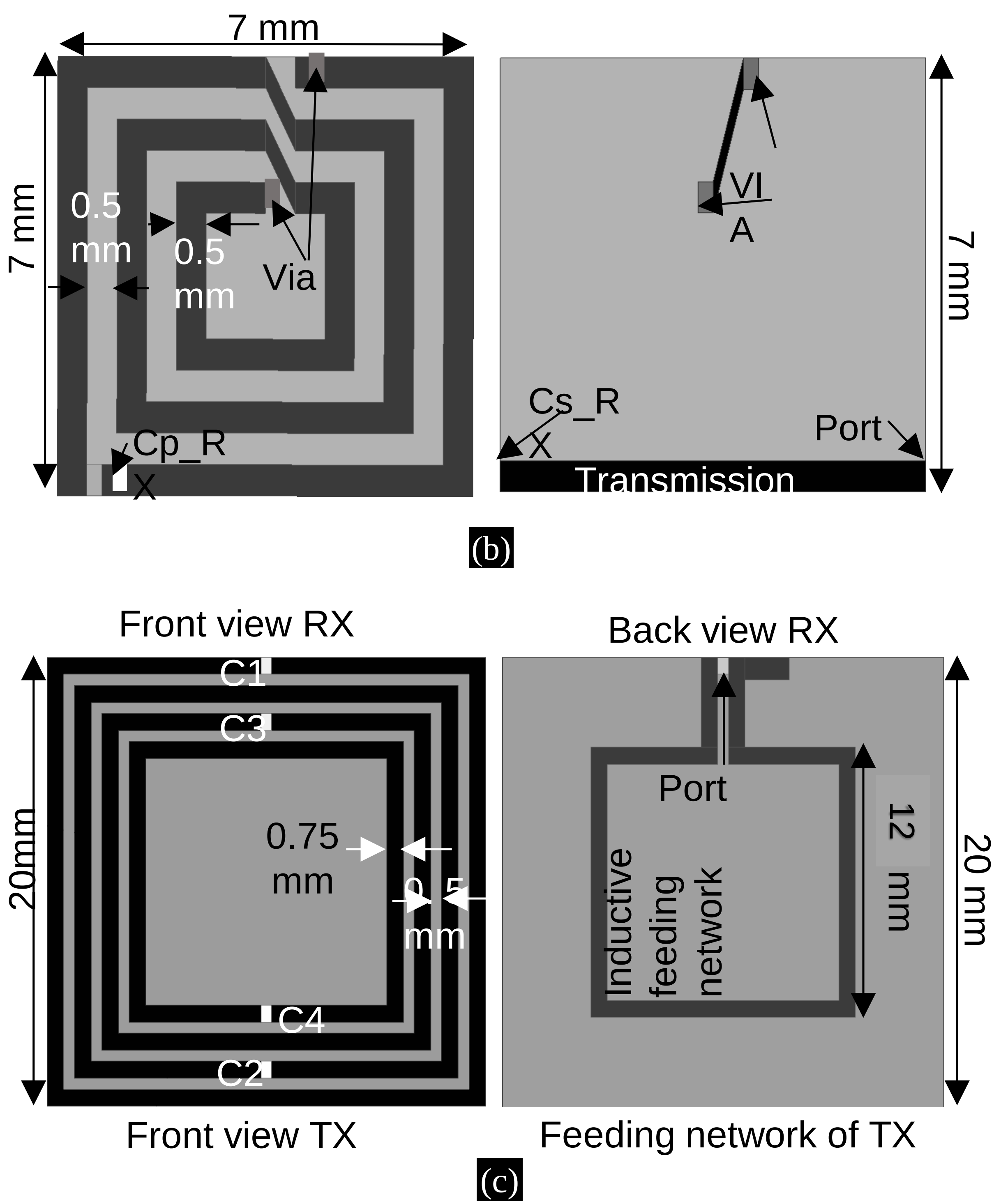

Fig 4. 7 Proposed system (a) Proposed system with embedded RX and stacked metamaterial (b) RX structure (c) Met-TX top view and feeding network.

The Fabrication and measurement of the Proposed WPT System layout was printed on Rogers (RO3003) substrate and fabricated using the MITS FP-21T Precision machine. Fig 4.8(a) shows the fabricated system. We chose to fabricate a 7×7 mm2 size because it is the smallest size achievable with the current technology PCB. With better technology, a smaller size can be realized with an acceptable level of efficiency.

S-parameters were measured using a vector network analyzer (Keysight PNA series, part number: N5222A) in both air and chicken breast. Fig 4.8(b) illustrates the measurement setup in chicken breast, where the RX is placed between two layers of chicken breast inside polyethylene bags to ensure that there is no physical contact between the system and the tissue. The measured and simulated S-parameters for chicken breast mediums are compared in Fig 4.8 (c, d, e), respectively. Efficiency (η) is calculated from the S-parameters as:

$$\eta = |S_{21}|^2$$

The simulated efficiencies at 50 MHz are 61.9% in air and 54% in tissue. The measured efficiency in tissue is 51%. The simulated and measured center frequencies are both 50 MHz. During the fabrication of the proposed WPT system, the capacitors listed in Table 4.1 were used. The system was simulated and measured in the air, and the simulated and measured center frequencies matched those of the tissue case. However, there was a slight difference between the simulated and measured results due to the type of capacitors used in the fabrication process. Nevertheless, this confirms that the proposed system is effective against resonance shift.

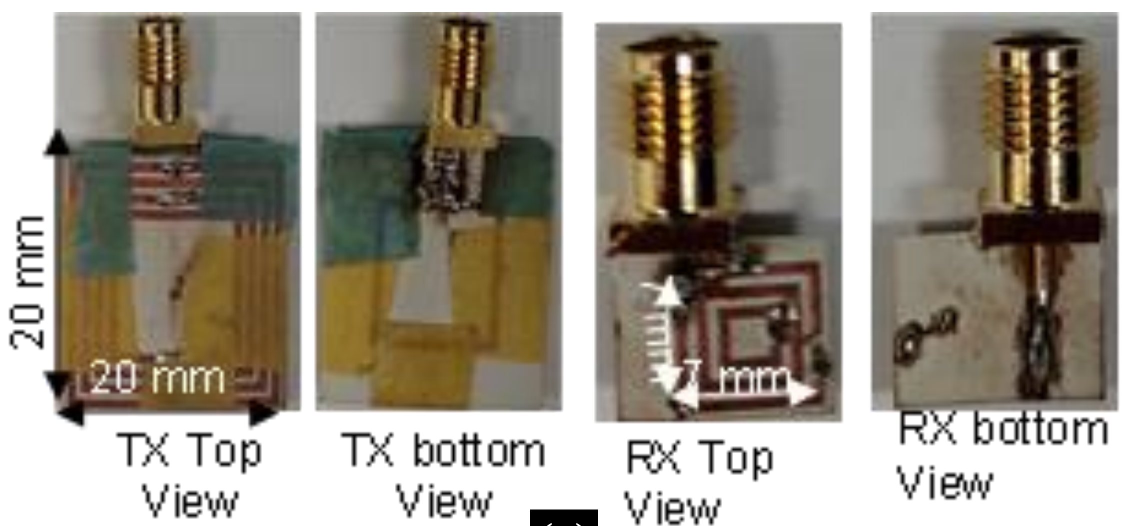

(a)

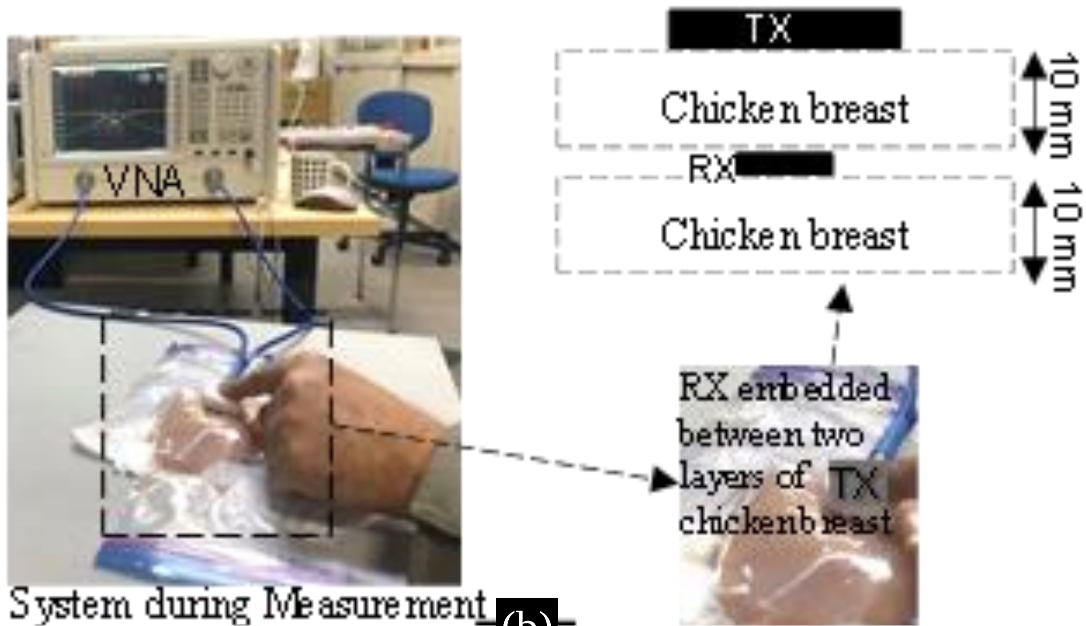
VNA
System during Measurement
TX
Chicken breast
10 mm
RX
Chicken breast
10 mm
RX embedded between two layers of chickenbreast
TX

(b)

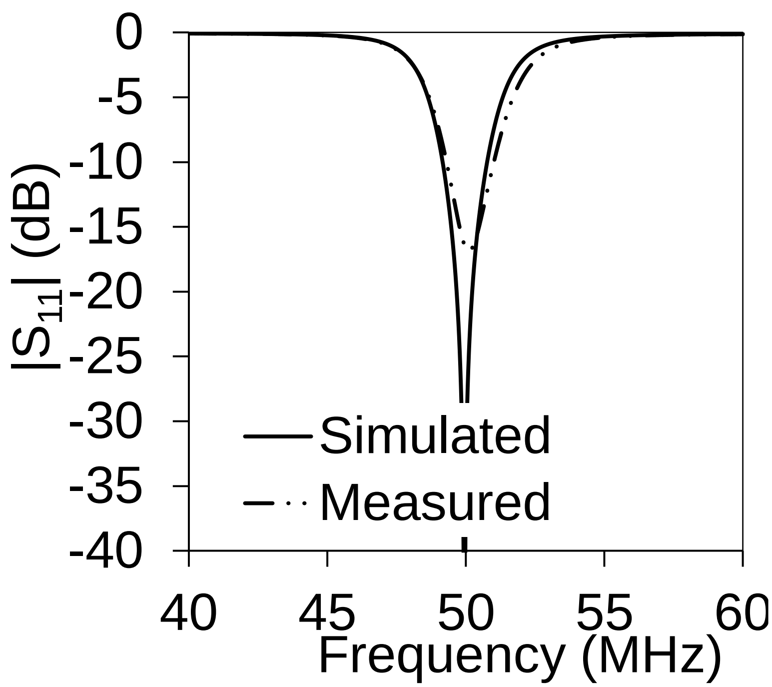
0
-5
-10
-15
-20
-25
-30
-35
-40
|S11| (dB)
40
45
50
55
60
Frequency (MHz)
Simulated
Measured

(c)

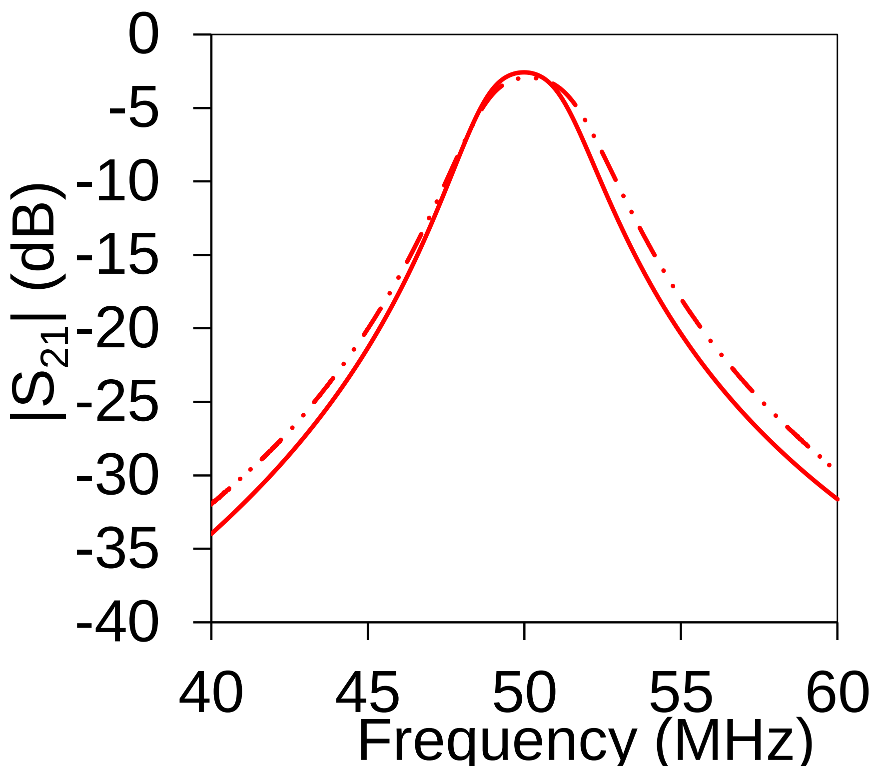

(d)

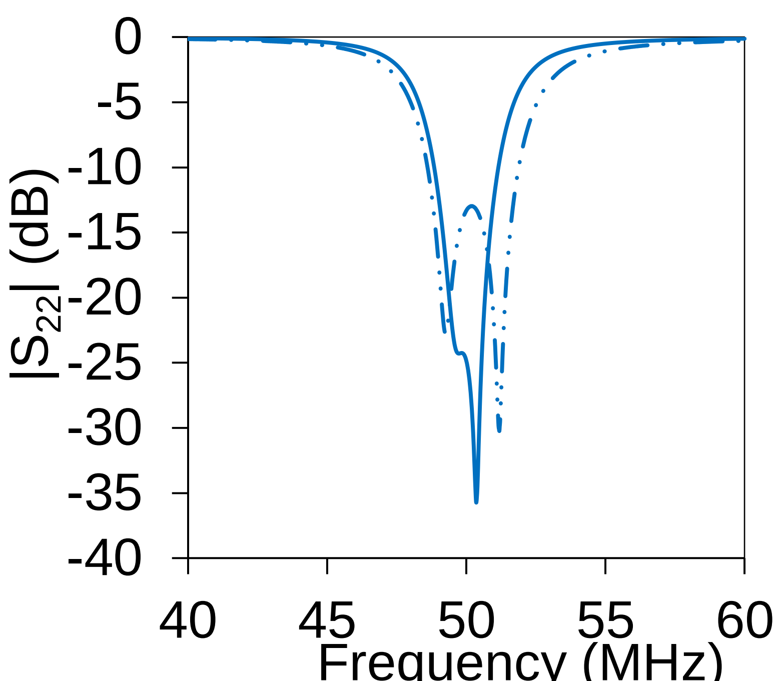

(e)

Fig 4. 8 The fabricated proposed system (a) fabricated Proposed system with embedded RX (b) measurement setup (c) |S11|(d) |S21|(e) |S22|.

Table 4. 2 Capacitors Value USED FOR both Simulation and Fabrication

	TX (for each layer)				RX	
	C1	C2	C3	C4	Cp	Cs
Simulation	40	40	50	50	200	32
Measurement	40	40	50	50	200	32

4.5 The Misalignment performance of the Proposed WPT System

In this section we will discuss about the proposed stacked metamaterial performance while the different misalignment occurred. For TX and RX, we checked the lateral and separation misalignment. Fig 4.9 (a) shows the proposed system when the TX misalignment (Δy) happened. Also, show the comparison between the simulation and the measurement results. From the pointed Fig we found that the proposed system has 54% simulation efficiency and 50% measured efficiency. and this means that our proposed system is working efficiently during the lateral misalignment of TX.

Fig 4.9 (b) shows the Proposed system during the separation misalignment of the TX (d_{out}). Also, it shows the comparison between the simulated and measured efficiency. We found that the results of simulation and the measurement are in a good agreement. Fig 4. 10(c), shows the proposed system when the separation misalignment of RX happened (d) change. It also, shows the simulated efficiency with changing of the d. When the Rx became near of the TX the efficiency is increase. but when the distance increases the efficiency is decrease. For separation misalignment of the RX, our measurement setup put some limitation to make us enable to measure this kind of misalignment in the tissue. Finally, to compare between our proposed system and [10] [11] [7] WPT systems. we used the figure of merit as:

$$\mathrm{FOM} = \eta \times \frac{\mathrm{d}^2}{\sqrt[3]{A_{TX}A_{RX}^2}}$$

where d is the distance between the RX and the tissue surface. there is another parameter used to compare it is misalignment factor. it calculated as (MF= $(\Delta x^2 + \Delta y^2)/d_{TX} * d_{RX}$) [11]. Where, Δx, and Δy are the lateral misalignment in x and y-direction. d_{TX} and d_{RX} are the side lengths of the TX and RX The complete comparison is shown in Table III. as shown in the comparison table the proposed give a good performance.

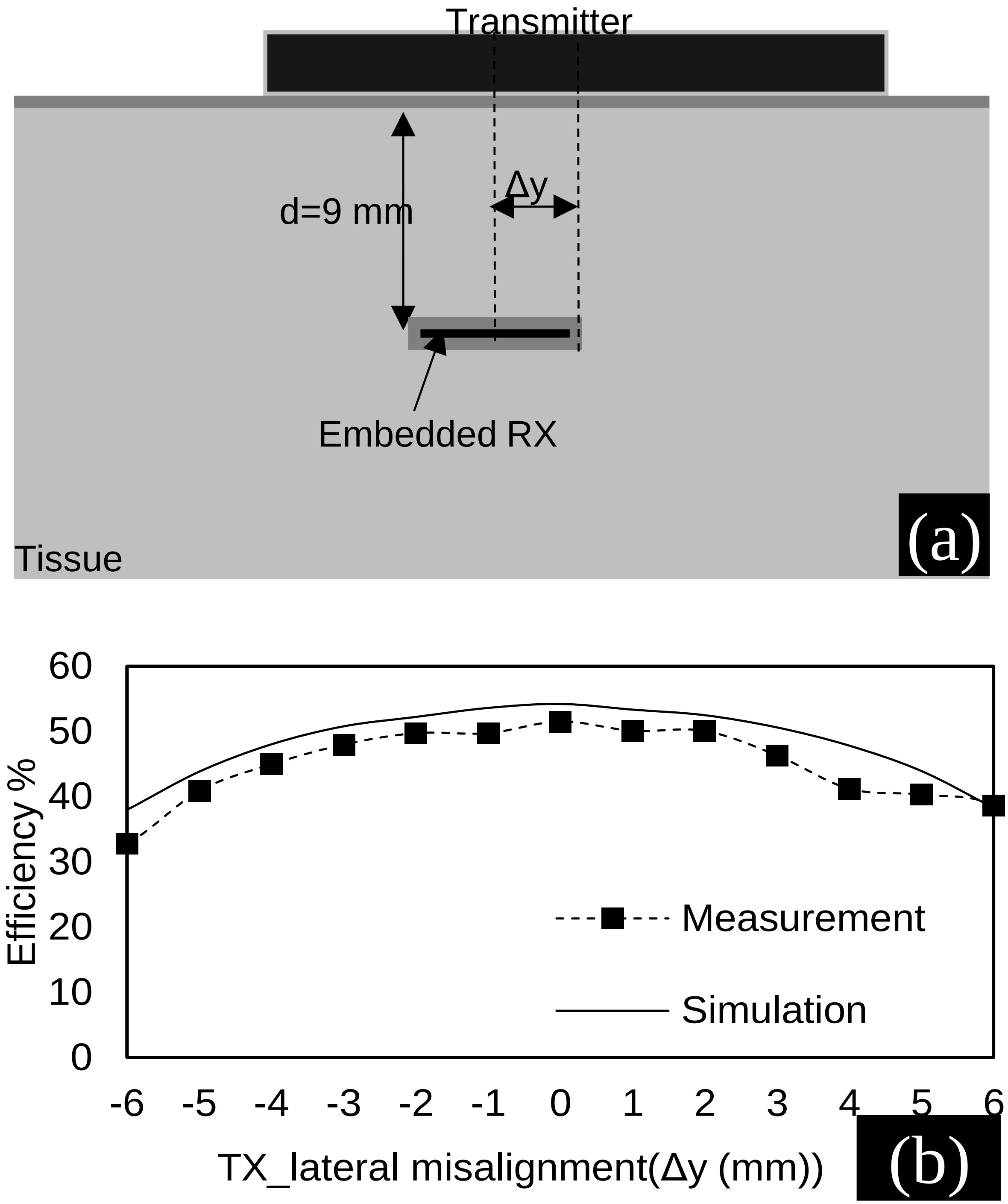

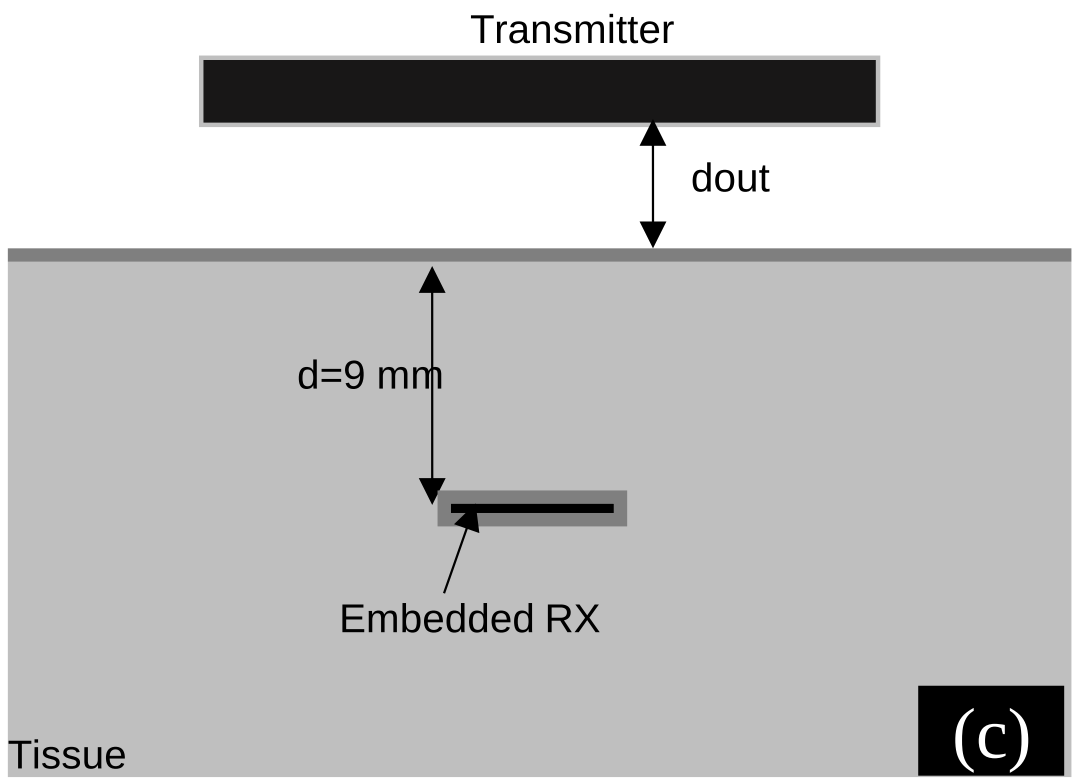

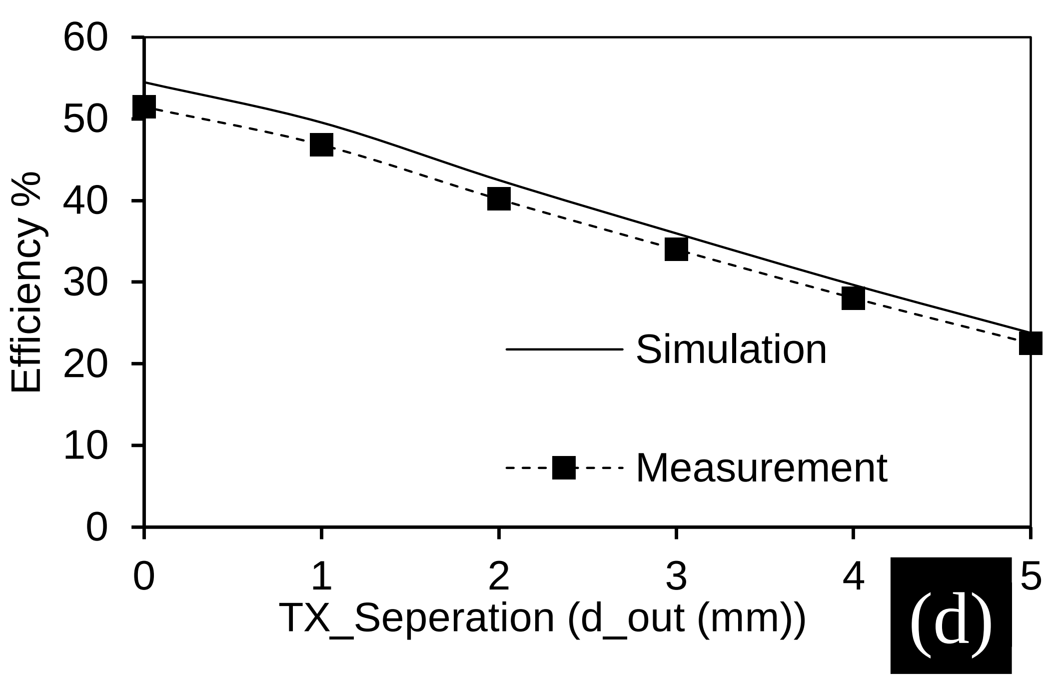

Fig 4. 9 Performance of the proposed system during the misalignment (a)the system during the lateral misalignment (b)Comparison between measured and simulated efficiency during the transmitter lateral misalignment. (c) system during the TX separation misalignment (d)

Comparison between measured and simulated efficiency during the transmitter separation misalignment.

4.6 The safety Consideration of the Proposed WPT System

The IEEE standard C95.1-1999 sets a safety limit for the Specific Absorption Rate (SAR) averaged over 1g of cubic tissue (1-g average SAR) at less than 1.6 W/kg to ensure human body safety. As demonstrated in Fig. 8, the maximum 1-g average SAR level of the proposed WPT design is approximately 1.59 W/kg, which is within the permissible limit of 1.6 W/kg. To achieve this safety condition, the proposed WPT with an integrated rectifier consumes an input power of 21 dBm.

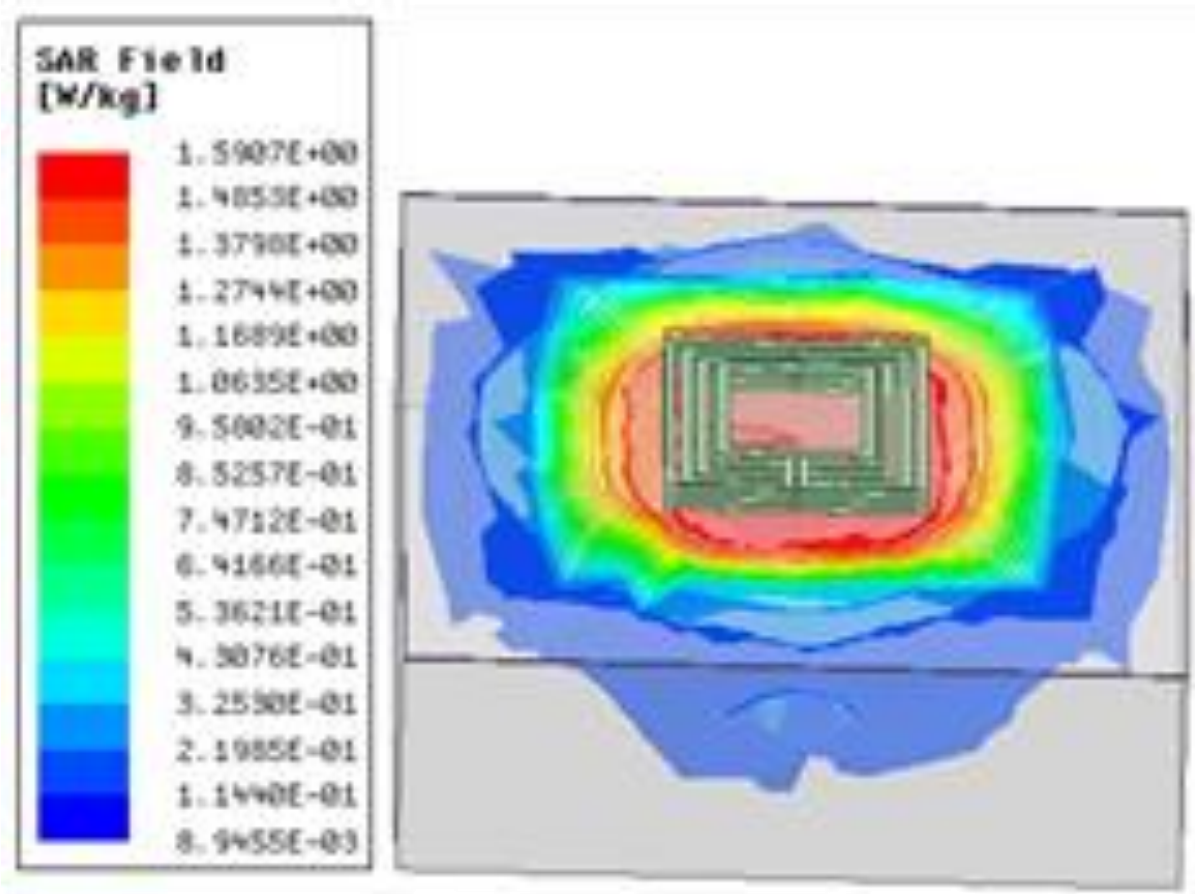

Fig 4. 10 Three-dimensional view of EM Simulated 1-g average SAR distribution at 50 MHz and the input power is set as 130 mW.

We compare between the performance of the proposed MRR metamaterial based WPT system and the performance of the first unit cell SRR based WPT system, and we found that the proposed MRR given the same level of efficiency. However, the size of RX is almost 50% of the conventional RX.

The input power consumed by MRR is low and this because the size of RX is small. So, the ability of gathering power by RX is low.

Table 4. 3 Comparison between Proposed system and the Literature

Ref	Tissue	F_0 (MHz)	TX (mm^2)	RX (mm^2)	d (mm)	η (%)	$\frac{d}{\sqrt{d_{TX} \times d_{RX}}}$	η/η_{max} @MF $= 0.33$	P_{max} (mW)
[39] *	Chicken	50	20×20	10 ×10	10	62	0.7	-	168
This work*	Chicken	50	20×20	7×7	9	54	0.8	71%	130

Chapter 5 Biomedical WPT System with Integrated Matching-less Rectifier, and Isolator for Compactness and Efficiency

5.1 Introduction

Rectifiers are essential components in RF-DC conversion circuits used in wireless power transfer systems. As the AC voltage received by the WPT system is in the form of a sinusoidal waveform, it needs to be converted to a DC voltage to power electronic devices. The rectifier circuit performs this task by using a diode as its principal component.

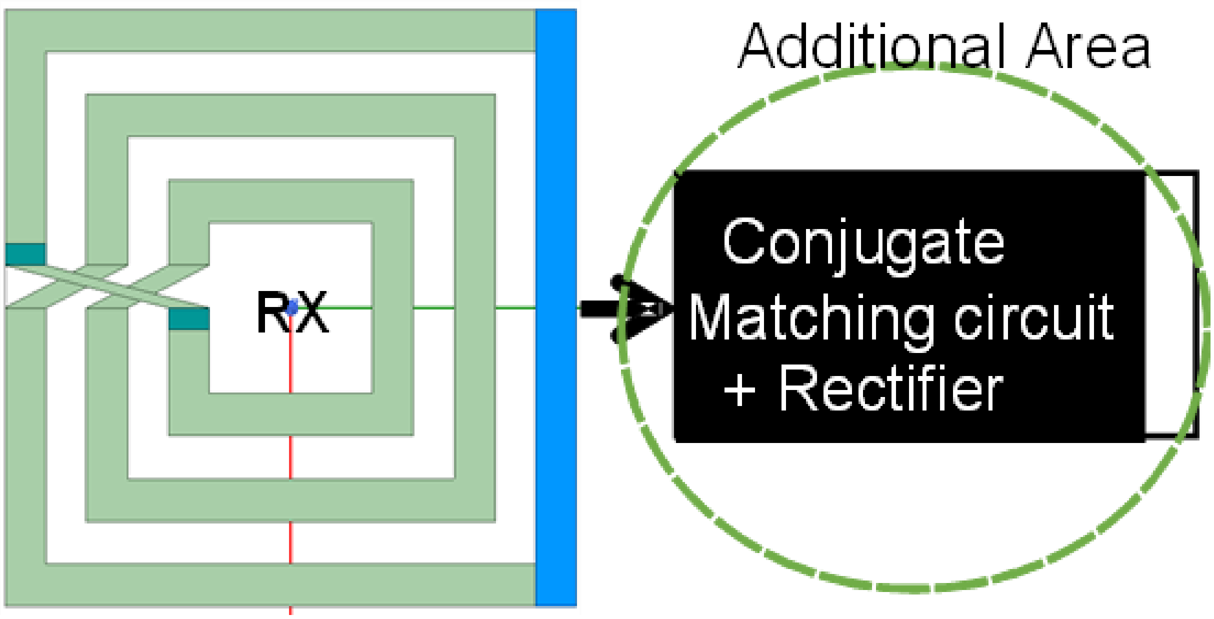

Fig 5. 1 The Conventional RX with outside rectifier

5.2 Conventional Method for Integration Rectifier

The conventional method for integrating a rectifier in a WPT system is to add additional area for the matching circuit and rectifier, as shown in Fig 5.1. In this method, the rectifier is an electrical device that converts the power from the output of the WPT, which is in the form of alternating current (sinusoidal wave form) and has varying power levels, into a direct current, which has a constant power level and flows in one direction. The process is accomplished by using a diode and is known as rectification.

The matching circuit is designed to match the impedance of the load to the impedance of the WPT system, which is usually a resonant circuit. The matching circuit also provides an efficient transfer of power from the WPT to the load. In the conventional method, the matching circuit and rectifier are placed in parallel with the load, as shown in Fig 5.1. The rectifier circuit includes a diode, which allows the current to flow in only one direction, and a capacitor, which smooths out the output voltage.

The drawback of this conventional method is that it requires additional area for the matching circuit and rectifier. This additional area increases the size of the overall system, which can be a limitation in some applications where size is a critical factor. Additionally, the use of a capacitor to smooth out the output voltage can cause some ripple in the output voltage, which may not be desirable for some applications.

5.3 Types of Rectifiers

There are two main types of rectifiers:

5.3.1 Half-wave rectifier:

This type of rectifier allows current to flow in only one direction during the positive half-cycle of the input AC voltage and blocks the current flow during the negative half-cycle. Fig.5.2 shows the circuit diagram and the result wave. It is the simplest type of rectifier and is mainly used in low-power applications.

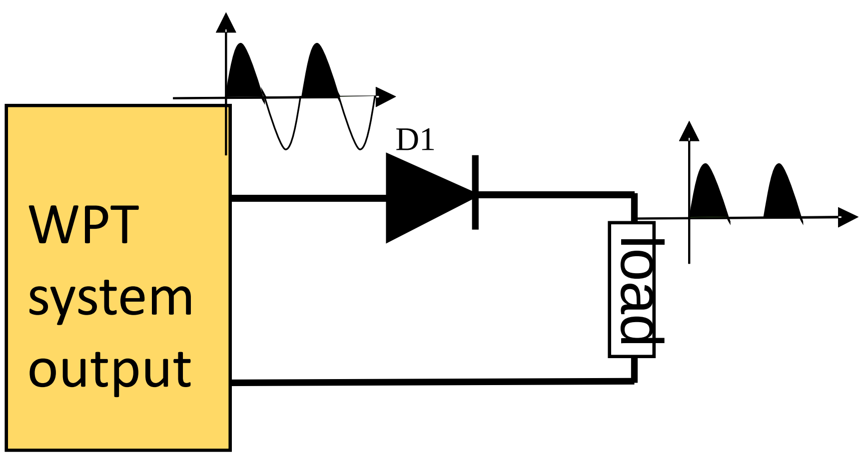

Fig 5. 2 Circuit diagram of Half-wave rectifier

5.3.2 Full-wave rectifier*:*

This type of rectifier allows current to flow in the same direction during both positive and negative half-cycles of the input AC voltage. It is more complex than a half-wave rectifier but provides a smoother output and is more efficient.

Types of Full-wave Rectifiers:

5.3.2.1 Center-tap rectifier:

This type of rectifier uses a center-tapped transformer to convert AC voltage into DC voltage. It uses two diodes and produces a pulsating DC output as shown in Fig.5.3(a).

5.3.2.2 Bridge rectifier:

This type of rectifier uses four diodes arranged in a bridge configuration to convert AC voltage into DC voltage. It is the most common type of full-wave rectifier and produces a smoother DC output. Fig.5.3(b).

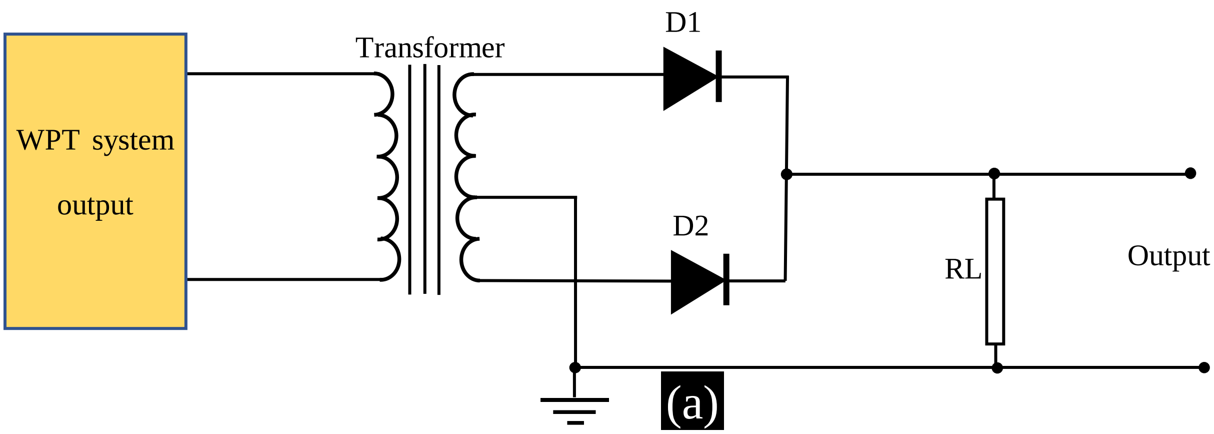

(a)

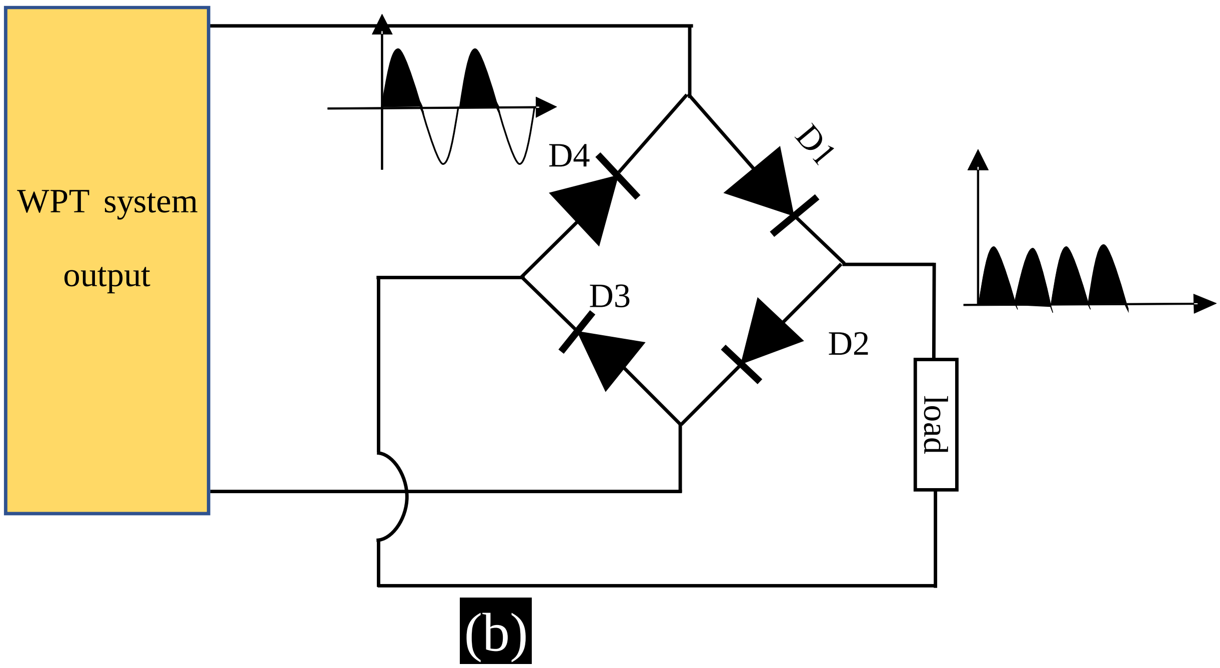

Fig 5. 3 Circuit diagram of full wave rectifier (a) Center tapped rectifier (b)Bridge rectifier

5.3.3 Voltage Doubler

It is a special type of the half wave one where, two diodes are connected as shown in Fig 5.4. which consists of a voltage clamping circuit followed by a half-wave rectifier D1 and C1 act as a compressing circuit and the voltage at the input of D2 becomes doubled in the positive half cycle. Then, the output of D2 equals to that voltage minus the threshold voltages of the two diodes. Input impedance of the rectifier is different from the output impedance of WPT system and this leads degradation of the efficiency if they are attached together without proper matching. Conventionally this impedance matching needs an additional area and circuit, and this is not suitable for the biomedical application. So, we proposed another method which is detailed explain in next section.

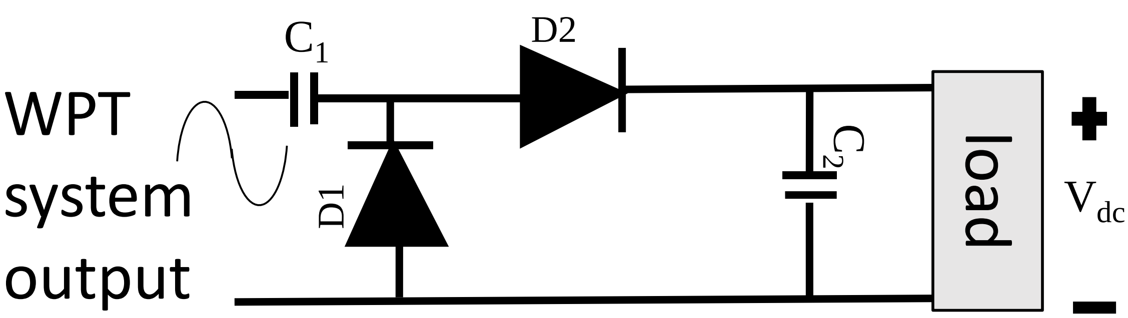

Fig 5. 4 Basic Voltage Doubler Circuit Diagram

5.4 Matching less Integration rectifier

In the previous chapter, the RX that we used has a DGS structure which means that the back side of the substrate is a ground so, we decided to exploit this to integrate the voltage doubler on the same substrate. The metamaterial that we used enables us to realize a matching less rectifier and this because of the highly coupling characteristics. By adding the interconnects of the rectifier to the back side of the RX substrate and simulate to take the parasitic capacitance in our consideration for optimizing the value of RX capacitors. We neglect the effect of the diodes because the diode body is dielectric. We used Advanced Design System (ADS) to design the voltage doubler as shown in Fig 5.4(a). According to the simulated result of the input impedance shown in Fig 4. (b). we change the input impedance of the RX to achieve the condition of the impedance matching as in equation 1:

$$Z_{out}(WPT) = Z_{in}^{*}(rectifier) \tag{5.7.1}$$

With some optimization on the lumped element of the RX and the impedance matching of the output port is the conjugate impedance of the rectifier. We designed the voltage doubler as shown in Fig 5.3. The layout of the voltage doubler using HFSS simulator is shown in Fig 5.4. we do that to check the result at the target frequency 50MHz. After getting the acceptable level of efficiency and S-parameters by optimizing the value of RX capacitors. We take this result and connect it with rectifier on ADS simulator. We choose to allocate the rectifier on this place because the strength of the magnetic field is lower than the center of substrate and does not produce an additional coupling which leads to change in the performance. The chosen input impedance is shown in the Fig 5.5.

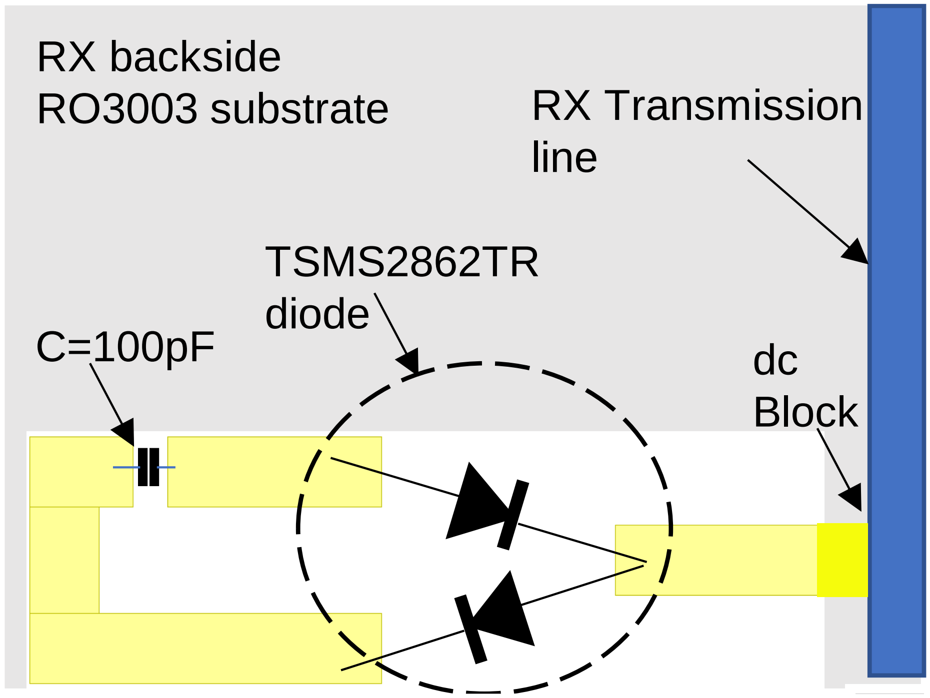

Fig 5. 5 Layout of the rectifier on the simulator (HFSS).

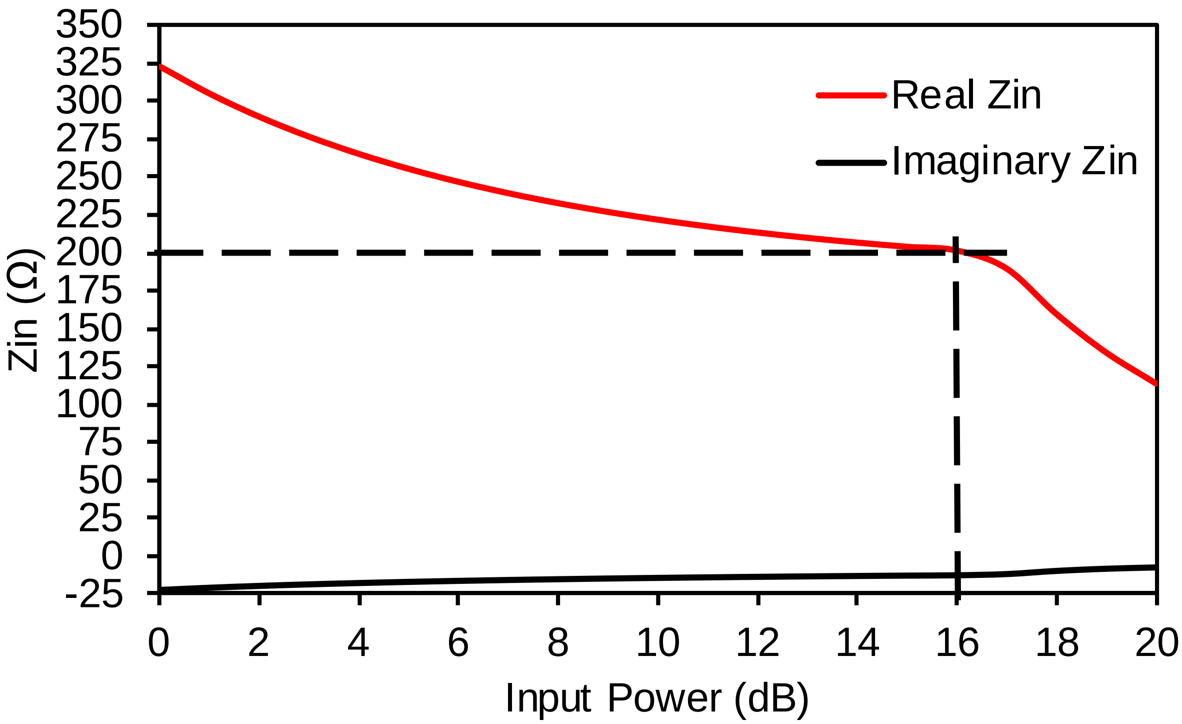

Fig 5. 6 Real and Imaginary of the Impedance of Voltage Doubler

5.4.1 Evaluation of Different Rectifier Loads.

We used the same method for optimizing the capacitors of the RX and the impedance matching of the output port as a conjugate of the rectifier with different load as shown in Table 5.1 to evaluate the performance of the integrated rectifier and WPT system.

Table 5. 1 Designed Lumped Elements for different rectifier loads

Load(Ω)	100	200	300	400	500	1000
C (Pf)	1000	500	330	250	200	100
Cp2 (Pf)	200	200	203	207	211	222
C2 (Pf)	33	32	31	29	26	33

Fig. 5.7 shows the simulation results of efficiency vs. input power for the Wireless Power Transfer (WPT) system. The efficiency is plotted for different loads, and it is observed that the load of 1000 (units) provides the highest efficiency compared to the other loads. This finding indicates that the WPT system operates most efficiently when the load connected to the output port matches the load impedance or power requirements of the system. The results from ADS simulation with the load of 1000 being the most efficient have practical implications for the design and implementation of the WPT system. By using the load of 1000 or closely matching the impedance of the output port to the load impedance, engineers can achieve higher efficiency and more effective power delivery. This optimization of the load impedance is particularly important in real-world applications, as it ensures that the WPT system operates at its highest potential with minimal energy losses.

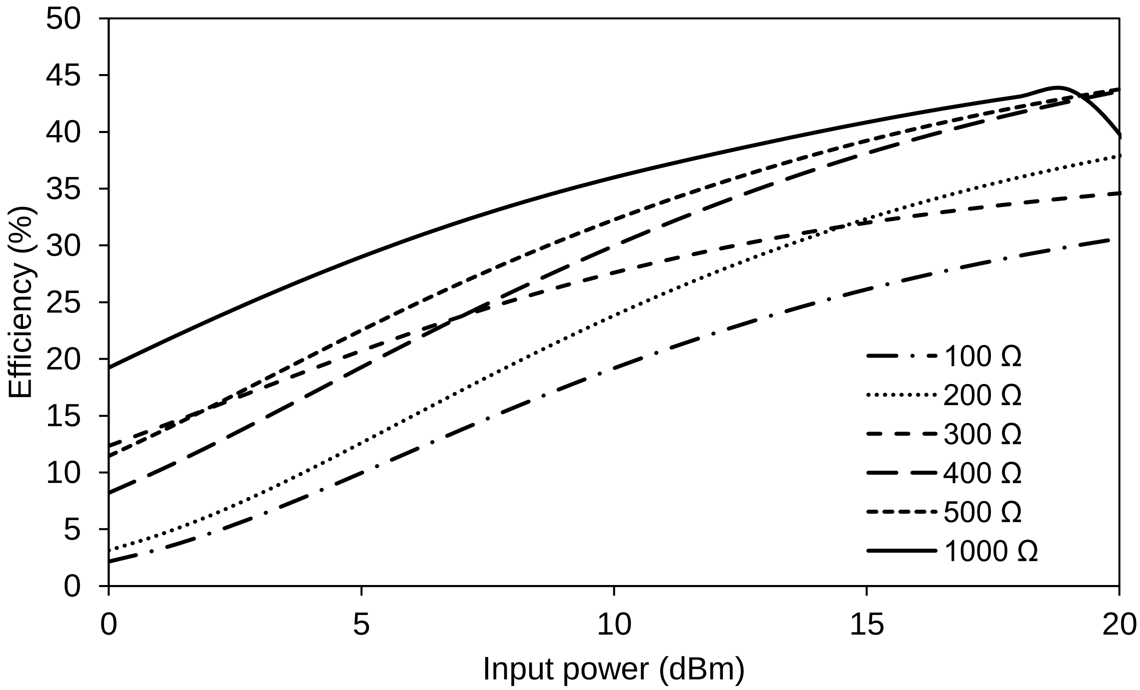

Figure 5. 7 The simulated efficiency versus input power with the variation of the load.

5.5 Fabrication and Measurement

We refabricate the new RX with the integrated Rectifier with the modified value of the capacitors as shown in the table I. The meta-TX is the same without any change. As shown in the Fig. 5.8(a) the Fabricated system in details. Comparison between the size of fabricated system with the area of Japanese 1-yen coin is also shown in the same figure. We achieved RX size is 16% of the area of the compared coin which is the smallest so far.

dc is done by using signal generator and multimeter. The diode we used in the fabrication is Schottky Avago HSMS-2862-TR1(Is=5e-8 A, R_s=5 Ω, Vj=0.65 V, B_v=7 V C_{jo}=0.18 pF). The fabricated is on (RO3003) substrate. We carried out of the measurement on the load of 1kΩ. We need the confirmation that the fabricated system is work and to show the clear version of the fabricated system, so we put the measurement setup in air as shown in Fig.5.8 (b). But we provided the result in the tissue.

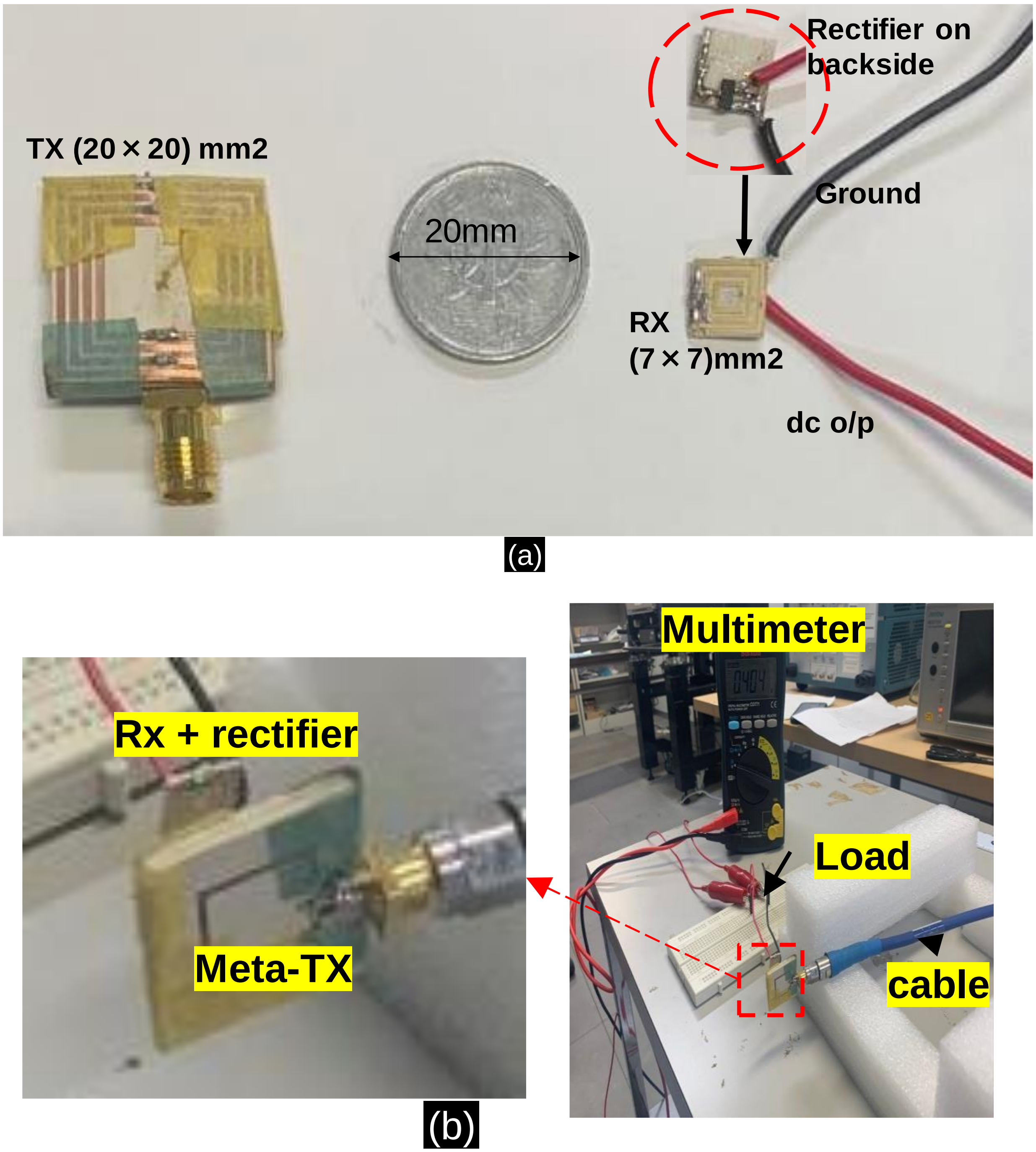

Fig 5. 8 Fabrication System (a)TX, RX +Rectifier (b) measurement setup

Table 5. 2 Loading Capacitors of the fabricated system

	Meta-TX Capacitors(pF)	RX Capacitors(pF)	Rectifier Capacitor (pF)

	C_1	C_2	C_3	C_4	C_{p2}	C_{s2}	C
RF-RF	40	40	50	50	200	32	-
RF-dc	40	40	50	50	222	33	100

The measured and the simulated results are compared in Fig.5.9. where in Fig 5.9. (a) shows the comparison between the measured and simulated reflection coefficient ($|S_{11}|$) vs the input power(dB) and it is in a good agreement. In Fig 5.9. (b) Shows the Comparison between the measured $|S_{11}|$ vs frequency at 2 different input power (0dBm and 20dBm). This Figure show there is no changing between the two values. In Fig 5.9. (c) illustrate the comparison between the simulated and measured dc output voltage. There is a good agreement between them. We only measure until input power 20 dBm because of the limitation of SAR. The peak value of measured dc voltage at (R_L= 1kΩ) is achieved at 18dBm input power is almost 6 V which is almost the same as the simulated result. Fig 5.9. (d) shows the comparison between the measured and simulated efficiency with the variation of the input power. There is a good agreement between them. The system achieved peak simulated efficiency is happened at 18 dBm 44%. While the peak measured efficiency is happened at 19 dBm and it is 39%in tissue. Using the impedance matching of each port is as follow: port 1 is in 50Ω and port 2 is (200+j12) Ω at the operating frequency 50 MHz. we have checked the performance of the WPT system integrated with rectifier when the misalignment happened (separation). $|S_{11}|$ is -4dB at Δz= -5cm and -32dB at perfect alignment. At Δz=5cm is -5dB in air.

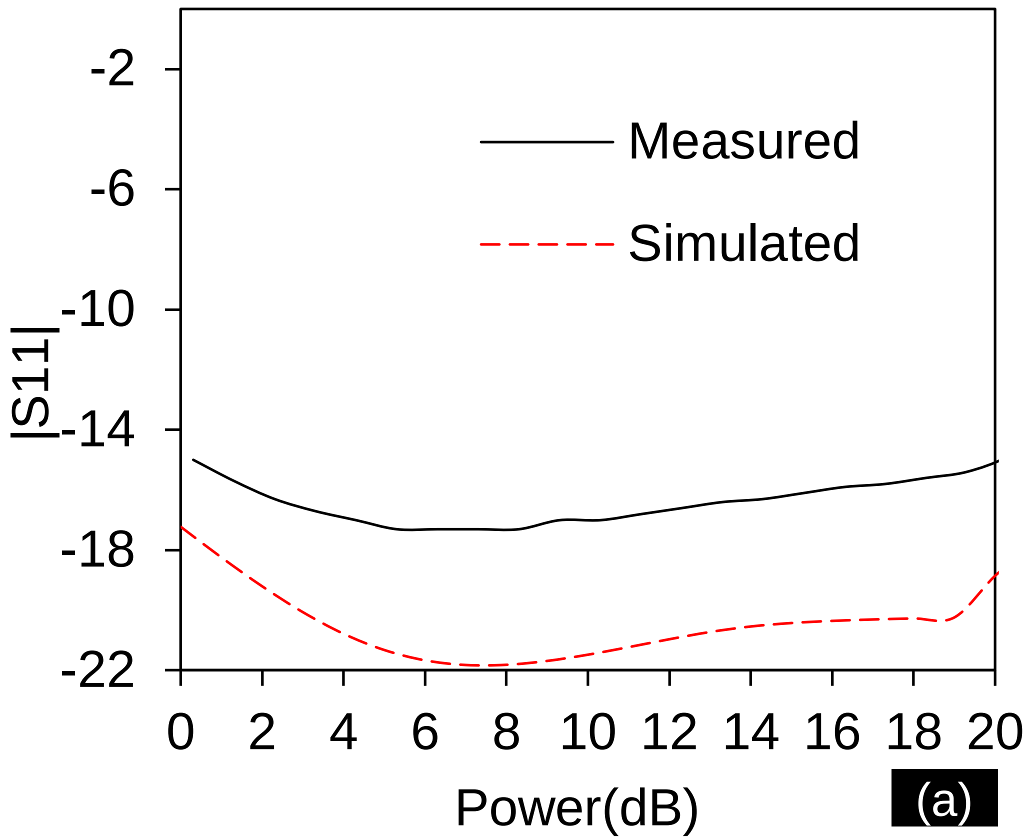

-2
-6
-10
-14
-18
-22
|S11|
Measured
Simulated
0 2 4 6 8 10 12 14 16 18 20
Power(dB)
(a)

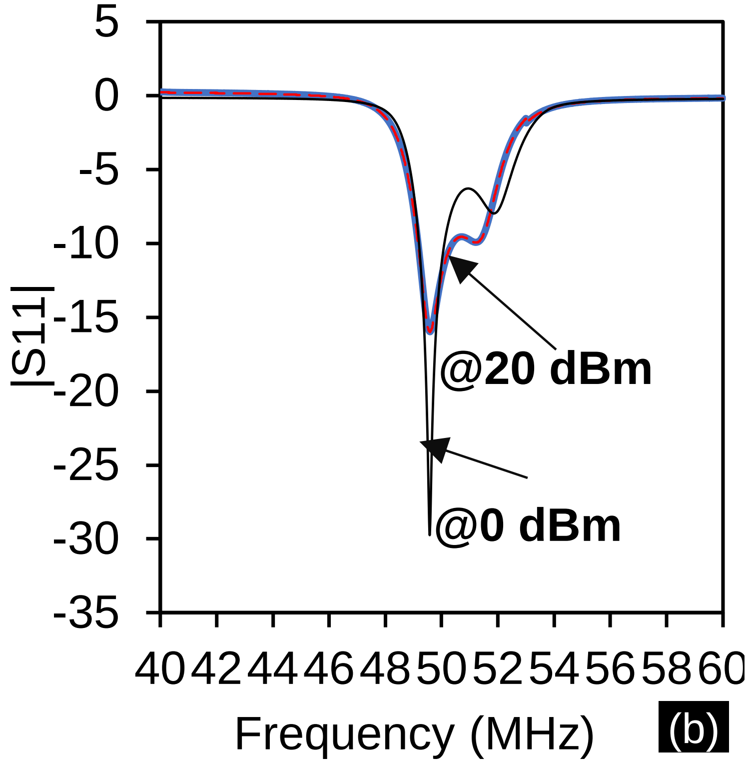

5
0
-5
-10
-15
-20
-25
-30
-35
|S11|
@20 dBm
@0 dBm
40 42 44 46 48 50 52 54 56 58 60
Frequency (MHz)
(b)

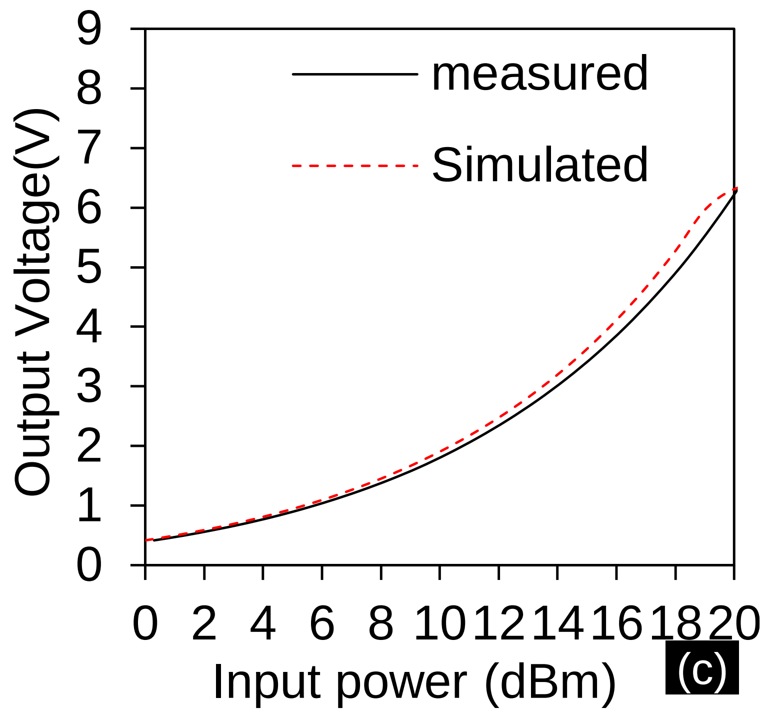

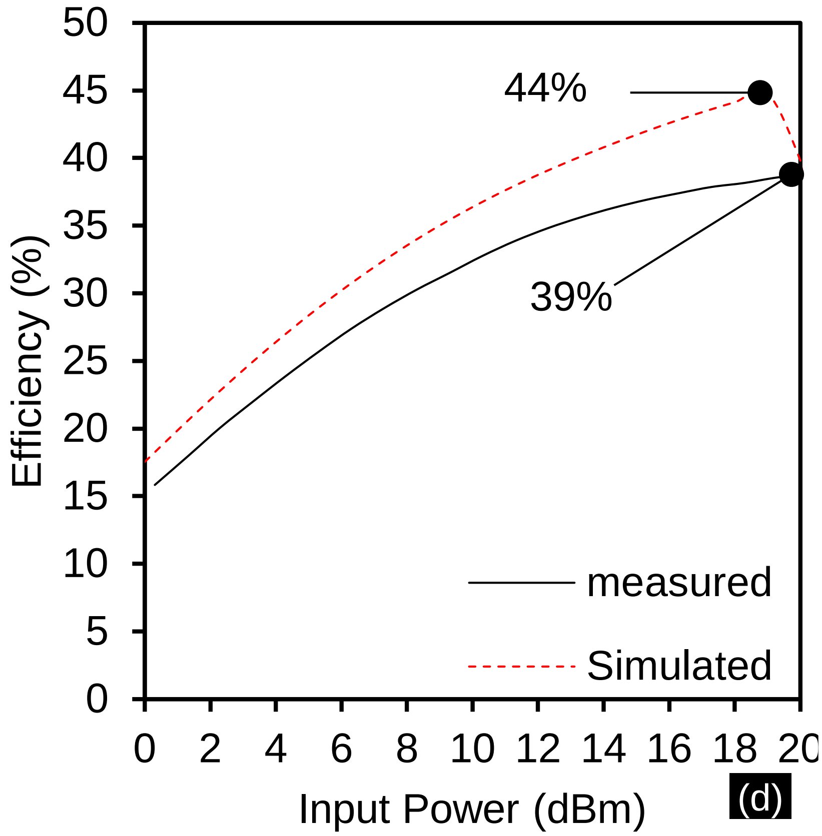

Fig 5. 9 Comparison between measured and simulated results (a) |S11| vs Input power. (b) |S11| vs Frequency. (c) Output dc voltage vs input power. (d) Efficiency vs input power.

5.6 Isolator

In the context of Wireless Power Transfer (WPT) systems, an isolator is a device used to protect the power amplifier and other sensitive components from reflected power as shown in Fig 5.10. WPT systems are designed to transfer power wirelessly from a transmitter to a receiver over a certain distance. However, if there is a mismatch between the load impedance and the characteristic impedance of the transmission line, some of the power will be reflected towards the transmitter. This reflected power can cause damage to the power amplifier and other components.

An isolator is placed between the transmission line and the power amplifier to prevent the reflected power from reaching the amplifier. It is a passive device that allows power to flow from the transmitter to the receiver, but blocks power from flowing back towards the transmitter.

Isolators typically consist of a ferrite circulator or a waveguide-based device. They are designed to work over a specific frequency range and are selected based on the operating frequency of the WPT system.

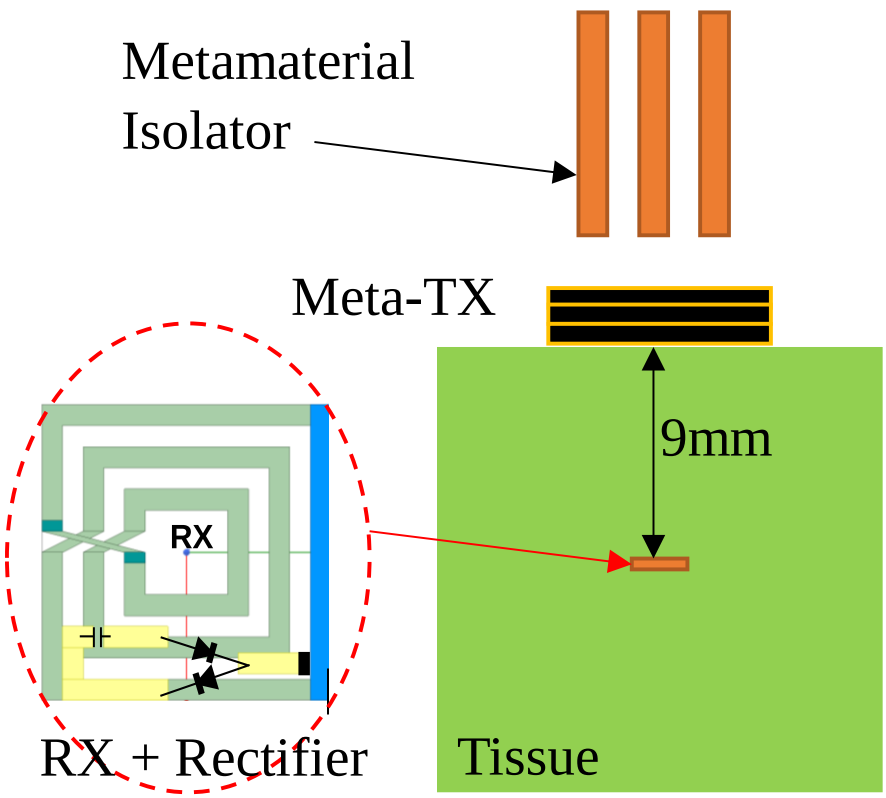

Fig 5. 10 Metamaterial based WPT System with integrated rectifier with metamaterial isolator.

Overall, the isolator plays an important role in protecting the power amplifier and ensuring reliable operation of the WPT system.

That's an interesting application of WPT systems. Indeed, in biomedical applications, it's important to ensure that the performance of the system is stable and that the surrounding devices and electromagnetic fields do not affect it.

The use of a near-zero metamaterial as a shielding layer to reduce electromagnetic field leakage is a novel approach to solving this problem [48-49].

In the context of WPT systems, the term "isolator" can also refer to a different device than the one I described earlier. In this context, an isolator is a device used to transmit power in only one direction while blocking power from flowing in the opposite direction.

In WPT systems, an isolator can be used to protect the power source, such as a battery or power supply, from high voltage and current spikes that may be generated by the load, such as a wireless device or battery charger. The isolator allows power to flow from the source to the load, but blocks power from flowing in the opposite direction, protecting the source from any potential damage.

Isolators used in this context are typically based on magnetic or semiconductor technologies and are designed to operate over a specific frequency range. They are commonly used in WPT systems to improve the efficiency and reliability of power transfer.

5.6.1 Isolator by using metamaterial

Designing a zero characteristics metamaterial as an isolator for use before the transmitter (TX) in a WPT system could provide several benefits.

By using a metamaterial as an isolator, you can create a device that allows power to flow from the source (e.g., a battery or power supply) to the transmitter, while blocking any power or voltage spikes that may be generated by the transmitter from flowing back towards the source. This can help protect the source from damage and improve the efficiency and reliability of the WPT system.

Furthermore, the use of a zero characteristics metamaterial could help reduce any electromagnetic interference (EMI) that may be generated by the transmitter. This can help ensure that the WPT system operates reliably and does not interfere with other electronic devices in the surrounding environment.

To design a zero characteristics metamaterial as an isolator, you would need to carefully select the materials and geometries used in the device. The metamaterial would need to have a refractive index close to zero, which means that it would not interact with electromagnetic waves. This property can be used to create a boundary between the transmitter and the source, effectively isolating the transmitter from any potential interference or voltage spikes generated by the load. Overall, using a near zero characteristics metamaterial as an isolator before the TX in a WPT system could provide a novel and effective approach to improving the efficiency and reliability of the system.

5.6.2 Isolator metamaterial structure

The characteristics of the unit cell of the zero characteristics metamaterial, including its geometry, material composition, and electromagnetic properties, are depicted in Fig 5.11 (a) and (b). The unit cell is the fundamental building block of the stacked metamaterial and plays a crucial role in determining its overall performance as an isolator in a WPT system. When evaluating different configurations of the metamaterial, it's important to consider the practical limitations of the WPT system, such as the available space and the operating frequency range. The number of unit cells can be increased until a satisfactory level of performance is achieved while considering these limitations. Starting with a single unit cell is a good first step, as it allows you to evaluate the basic properties of the metamaterial and its performance. However, if the performance is not satisfactory, increasing the number of unit cells can provide more attenuation of the unwanted signals, resulting in lower power loss and magnetic field leakage. It's important to note that increasing the number of unit cells can also increase the complexity and cost of the metamaterial. Therefore, it's important to balance the desired performance with practical considerations.

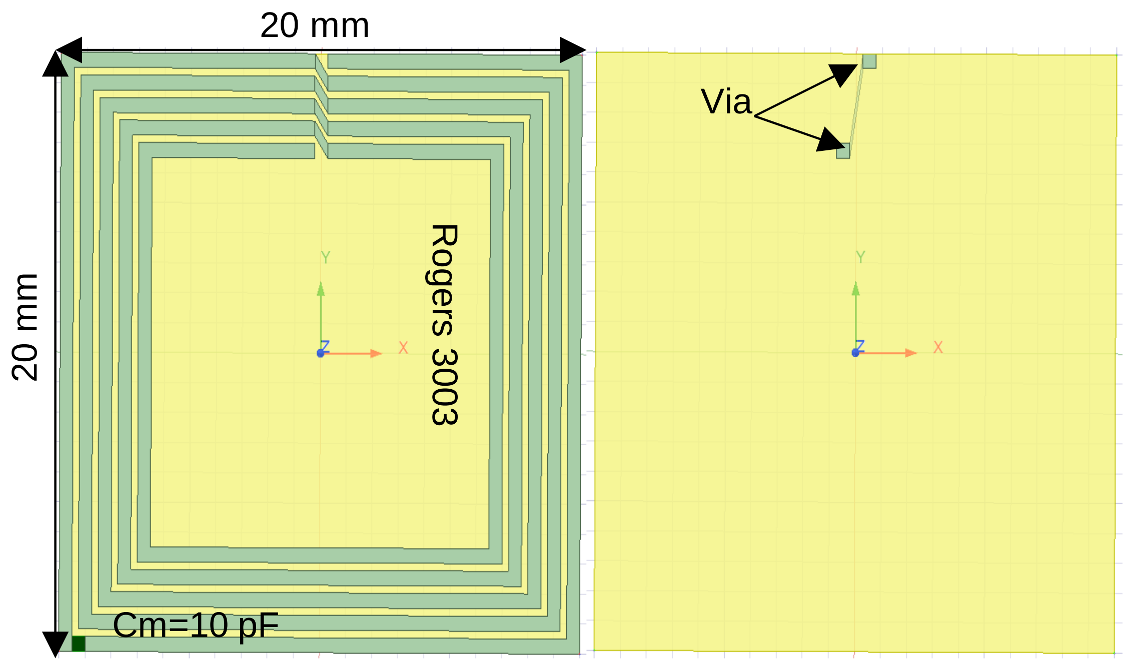

(a)

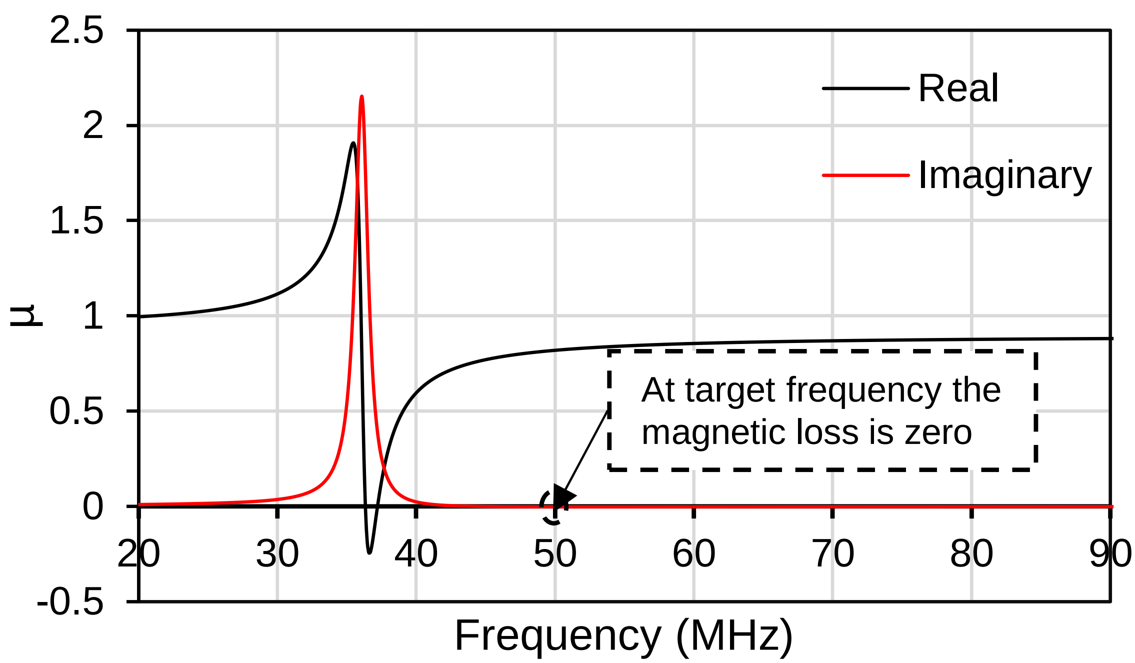

(b)

Fig 5. 11 Metamaterial Isolator (a) unit cell structure (b) its characteristics.

By increasing the number of unit cells in the isolator layer, we were able to decrease the magnetic field leakage and reduce the power loss, as more cells provided better isolation. At low power

(10mW), we observed that using four-unit cells of the isolator layer resulted in a reduction of magnetic field leakage by approximately 40%, and a decrease in power loss by about 10%. Moreover, using six-unit cells further reduced the magnetic field leakage by about 60%, with a similar decrease in power loss. However, increasing the number of unit cells beyond this point did not yield significant improvements. Overall, these results demonstrate the importance of using an appropriate number of unit cells in the isolator layer to achieve optimal performance.

5.6.3 The Effect of Metamaterial Isolator on Magnetic Leakage

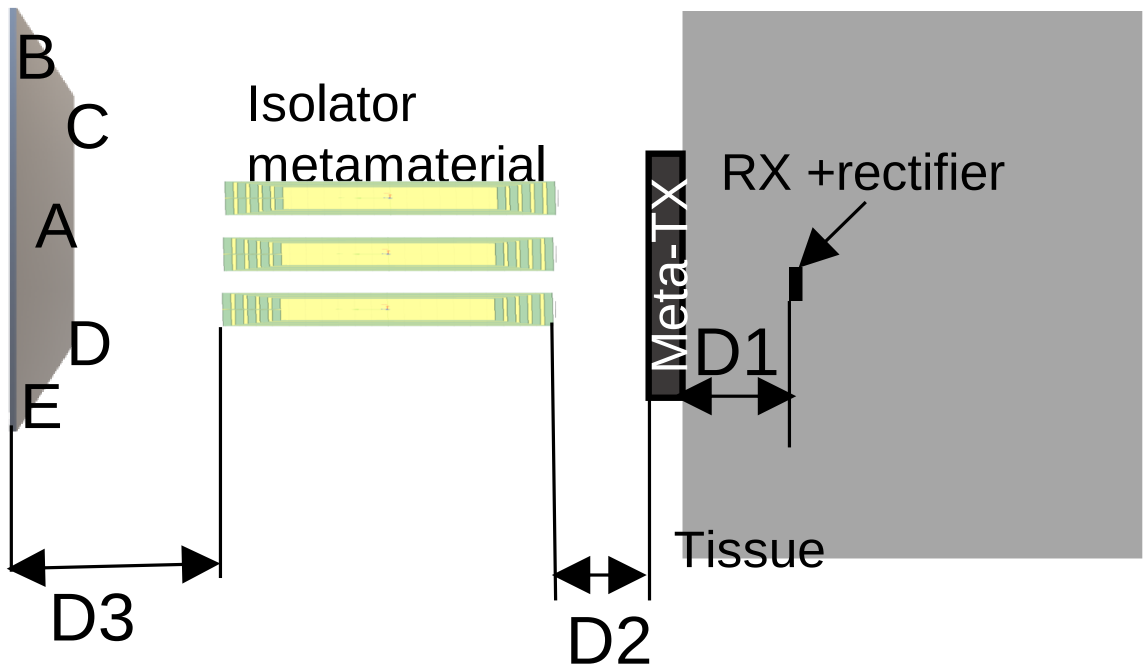

Fig 5. 12 WPT structure with NZ metamaterial Isolator

The purpose of the study was to investigate the effect of the metamaterial isolator on power loss and magnetic field distribution in a WPT system. The simulation was conducted using the HFSS simulator, and the WPT system structure with the metamaterial unit cells was depicted in Fig.5.12. The distance between the RX integrated with the rectifier and Meta-TX was D1=9 mm, and the distance between the WPT system and the isolator unit cell was D2=5mm. The reference plane was D3=15 mm behind the isolator, which was used to display the magnetic field strength at different points (A, B, C, D, and E) with and without the isolator cells.

To begin, we utilize a unit cell with dimensions of 20×20 mm2 and incorporate 3 cells with 10 pf feeding capacitors, as depicted in Fig.5.10. The direction of the magnetic field in our WPT system can be observed in Fig.5.13(a). Without the isolator layer, the original WPT system experiences considerable leakage. However, when the isolator layer is added, the magnetic field vectors from the meta-Tx and the isolator intersect. This results in the cancellation of some vectors, while others are returned, as illustrated in Fig.5.13(b). By employing this approach, any adverse impact on the enclosed equipment is minimized.

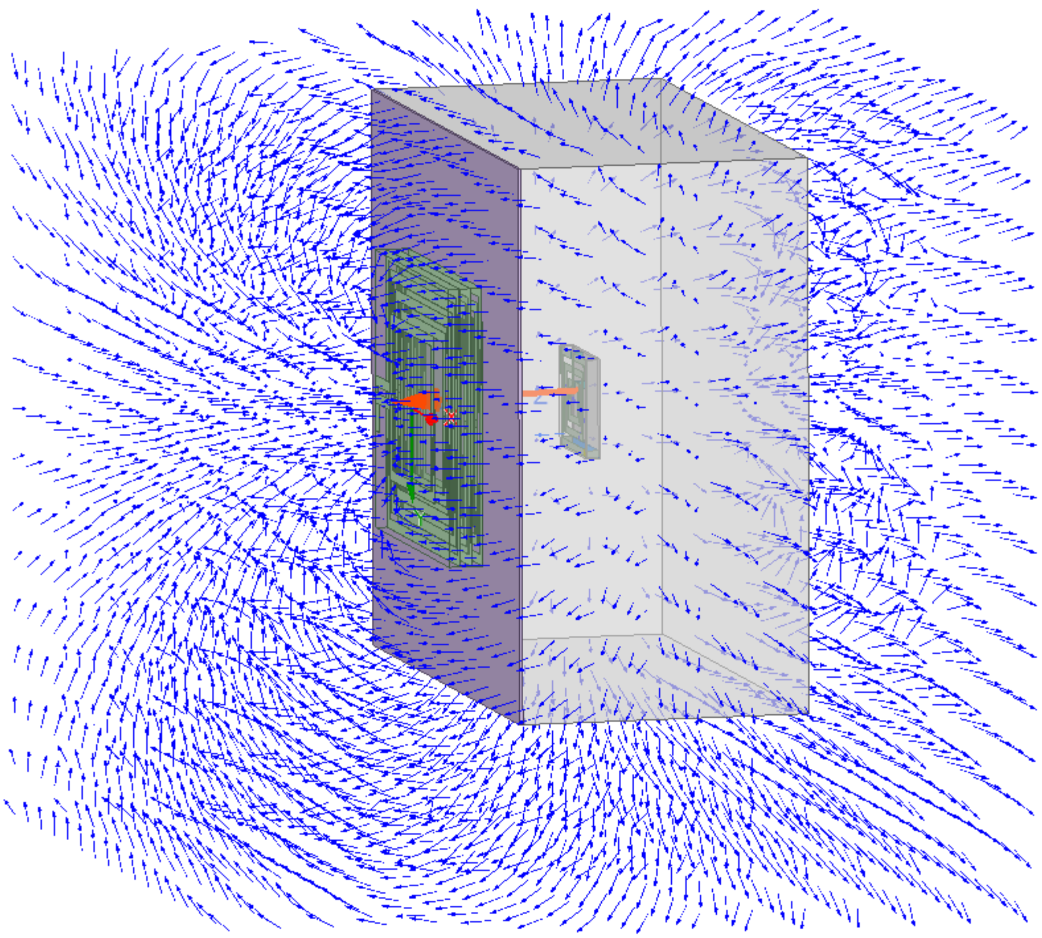

(a)

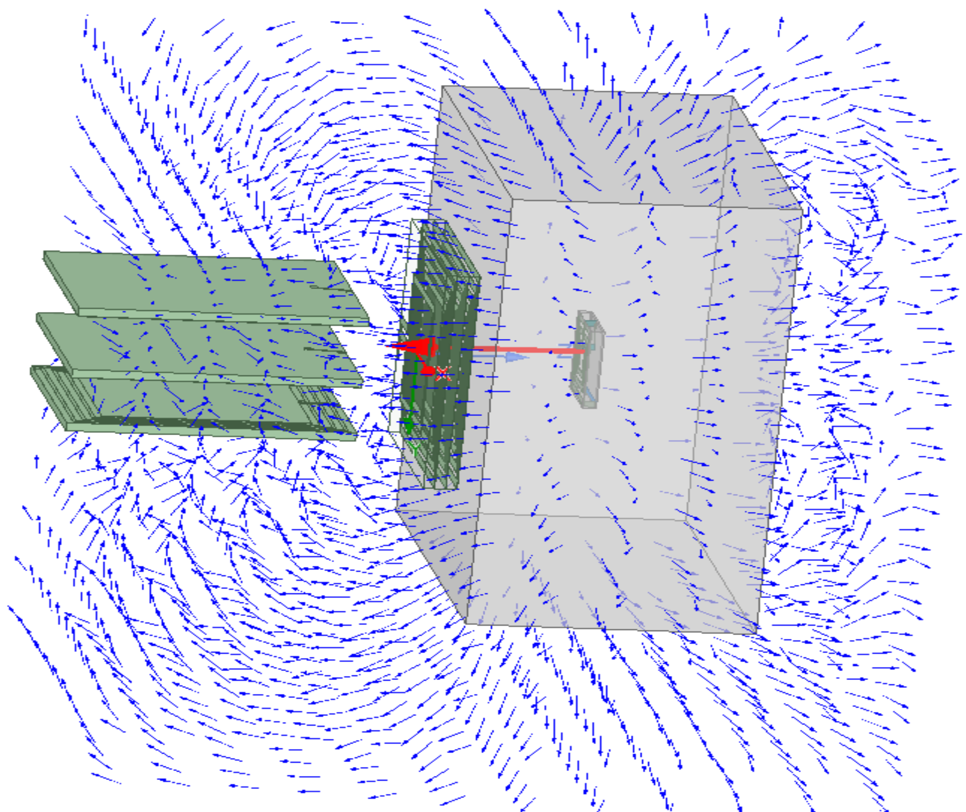
(b)

Fig 5. 13 Magnetic field direction(a) without (b) with NZ metamaterial Isolator

Fig.5.14 illustrates the magnetic strength behind the Meta-TX. In the absence of an isolator, the magnetic field of the WPT system is strong at the edges but weak in the center, as demonstrated in Fig.5.14(a). Conversely, when the system incorporates an isolator, the magnetic field strength in the center and a significant area surrounding it is weaker, as shown in Fig.5.14(b).

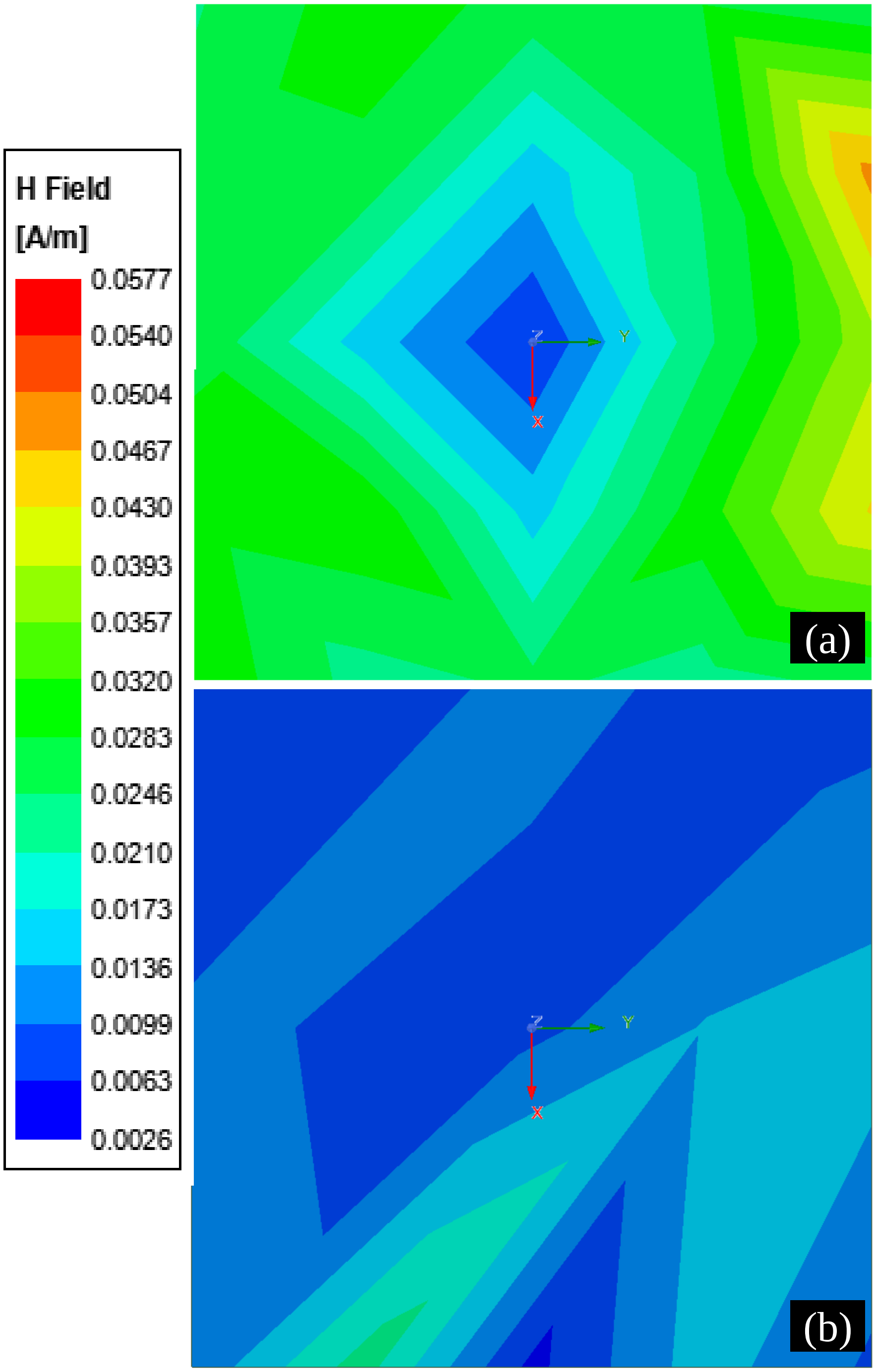

Fig 5. 14 Magnetic field strength (a) with (b) without NZ metamaterial Isolator

5.6.4 The Effect of Metamaterial Isolator on Power losses

The results indicate that the isolator layer effectively reduces the magnetic field leakage in the WPT system. Additionally, Fig.5.13 provides a comparison of the power loss in the system with and without the isolator layer. The simulation data reveals that the power loss in the WPT system with the isolator layer is significantly lower than that without it. Specifically, as the number of unit cells in the isolator layer increases from 3 to 5, the power loss is further reduced. This highlights the effectiveness of increasing the number of unit cells in minimizing power loss in the WPT system. Fig.5.15(a) shows the structure of the WPT system with the isolators.

Fig. 15(b) and (c) simulation results clearly demonstrate that the isolator metamaterial significantly reduces the power losses of the surrounding equipment. Without the isolator, the steel plate experiences power loss, but adding the isolator decreases it. This decrease in power loss is due to the ability of the isolator metamaterial to minimize magnetic field leakage, resulting in reduced power loss in the surrounding equipment. Therefore, using the isolator metamaterial is an effective solution to ensure that the WPT system does not cause external interference in biomedical applications.

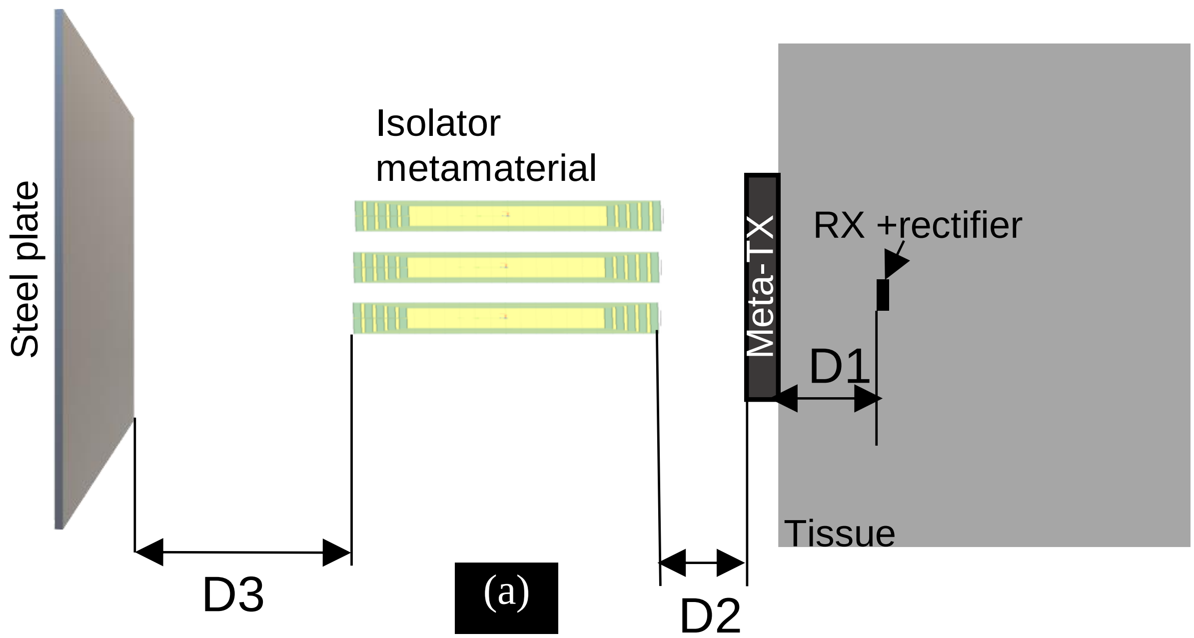

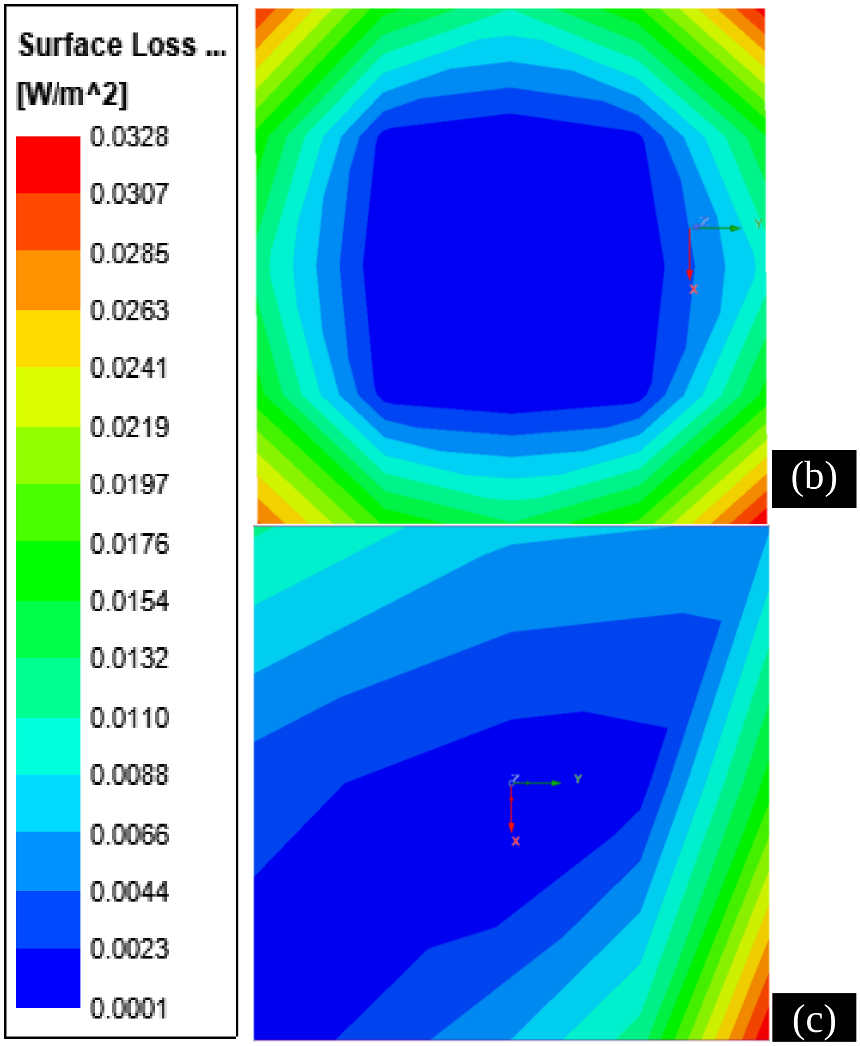

Fig 5. 15 Power losses before TX. (a) the WPT system structure (b) with (c) without NZ metamaterial Isolator

5.6.5 Fabrication and Measurement Results

The unit cell of the isolator metamaterial with dimensions of 20×20 mm2 was fabricated as illustrated in Fig.16(a) using the MITS FP-21T Precision machine on a substrate made of Rogers (RO3003) with a thickness of 0.762 mm and a metal thickness of 17um. The design parameters used for fabrication were D=20 mm, the width of the loops=0.5 mm, the separation between loops=S=0.25 mm, and the feeding capacitor was 10 pF. Fig.16(b) shows the measurement setup, where the isolator metamaterial unit cells were positioned 5mm apart from each other and 5mm away from the WPT system. A reference plane was placed 15mm before the isolator, and a vector network analyzer (Keysight PNA series, part number: N5222A) was used to measure the S-parameters. The results of the comparison between measurements with and without isolators indicate that there was no significant change between them as shown in Fig.5.16(c)

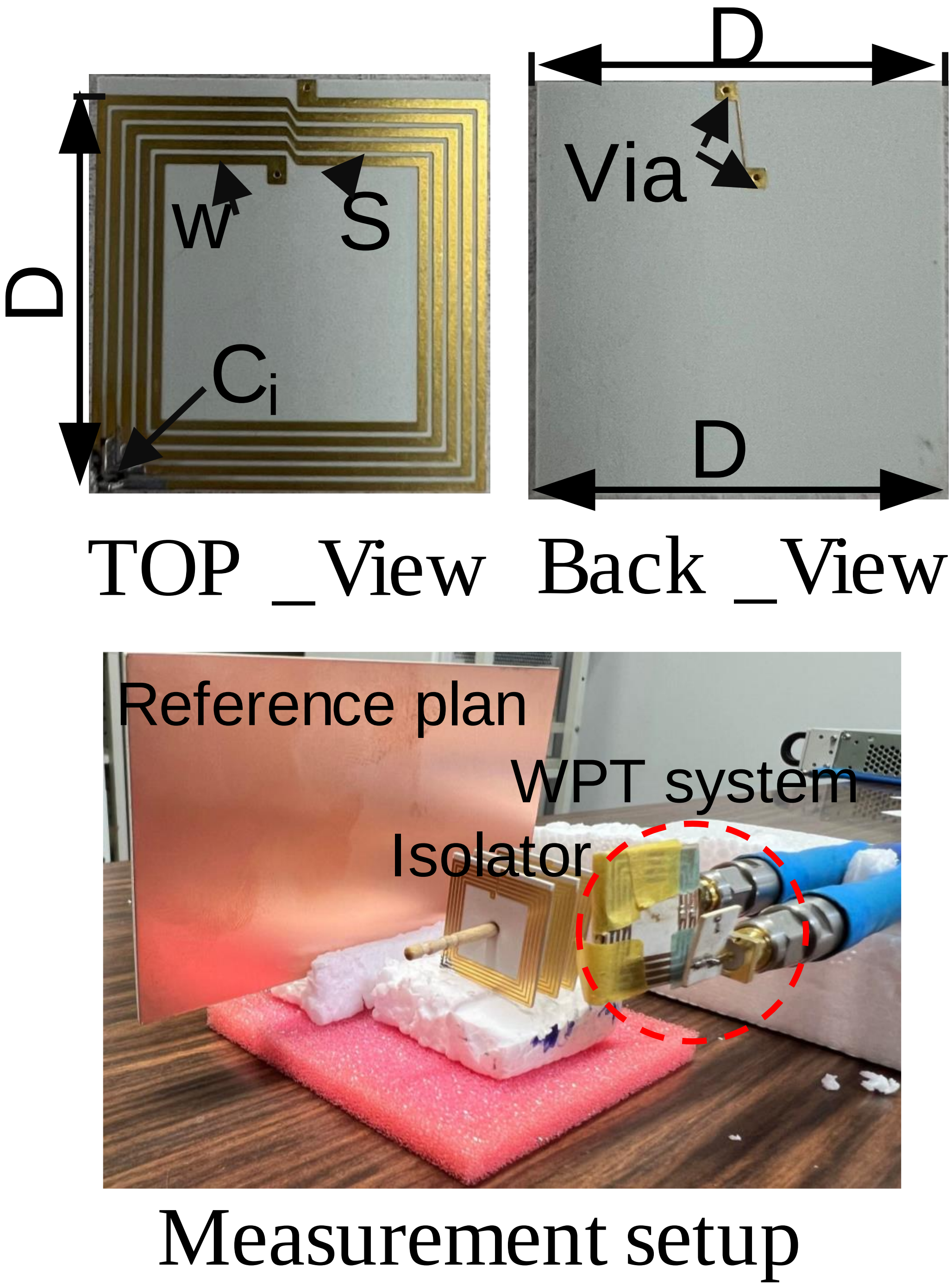

(b)

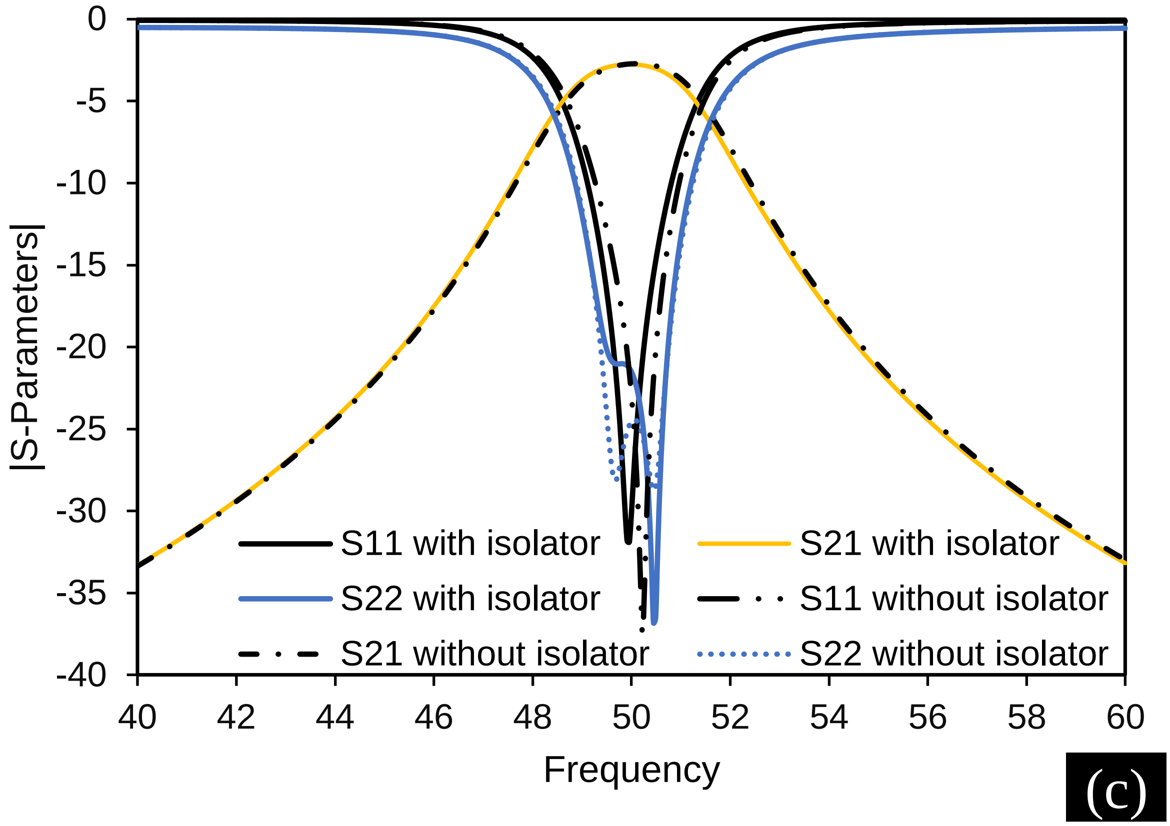

Fig 5. 16 Power losses before TX. (a) the WPT system structure (b) with (c) without NZ metamaterial Isolator

Chapter 6 Conclusion and Future Work

WPT system can eliminate the need for battery replacement surgeries, reduce the risk of infection, and provide a continuous and reliable source of power. However, several challenges must be addressed to ensure the successful implementation of WPT systems for biomedical applications.

One of the primary challenges is to ensure the safety of the patient. The WPT system must operate within the limits of specific absorption rate (SAR) and temperature rise restrictions set by regulatory bodies. The system should also be designed to minimize electromagnetic interference and magnetic field leakage, which can affect the operation of nearby medical devices and cause harm to the patient.

Another challenge is to maximize the efficiency of the WPT system. The efficiency of the system is influenced by various factors such as the distance between the transmitter and receiver coils, the orientation of the coils, and the properties of the surrounding tissues. Therefore, the system should be optimized to maximize power transfer efficiency while minimizing power losses.

Moreover, the size and weight of the WPT system should be minimized to ensure that it can be easily implanted and not cause discomfort to the patient. The system should also be designed to be compatible with different types of implants and medical devices.

6.1 Conclusion

In this thesis, we have proposed a compact WPT system that utilizes a low magnetic loss metamaterial and an isolator metamaterial to reduce magnetic field leakage and power losses. The proposed system was tested with chicken breast tissue and demonstrated good efficiency levels and performance during misalignment. The system also operates within the limits of IEEE C95.1-1995 for the 1-g average SAR.

Overall, the proposed WPT system has the potential to overcome the challenges associated with using WPT systems for biomedical applications. With further research and development, WPT systems could revolutionize the field of implantable medical devices, improving patient safety, and providing a reliable and continuous source of power for these life-saving devices.

In this research, we successfully designed and implemented a MISO-WPT system that is insensitive to tissue properties. Our proposed approach utilized a small electrical-length DGS resonator to achieve this result. The TX of the WPT system was comprised of three cooperative DGS resonators, each utilizing the small electrical-length DGS resonator to improve the kQ-product and maximize efficiency. The dimensions of the fabricated WPT system are summarized in Table III. The system achieved high measured efficiencies of 68% and 62% at 49 MHz in both air and chicken tissue, respectively. This confirmed the effectiveness of our system to tissue properties. For longer lateral sides of the TX, an array configuration can be employed to improve the lateral misalignment performance. Overall, our results demonstrate the potential of the proposed WPT system for efficient and effective power transfer in biomedical applications.

In our study, we introduced a novel metamaterial-inspired transmitter geometry for wireless power transfer (WPT) to an embedded receiver in biological tissue. The proposed geometry consisted of stacked and coaxially aligned unit cells, providing shielding against the tissue. Unlike conventional WPT systems, the proposed geometry showed minimal resonance frequency shift in the presence of an airgap between the transmitter and the tissue. This feature resulted in a more stable efficiency during such misalignment cases compared to the conventional system. Additionally, the proposed system could operate with 2.5 times higher input power while still adhering to the limits of IEEE standard C95.1-1999 for the 1-g averaged SAR. We fabricated and characterized the proposed metamaterial-inspired WPT system in chicken breast tissue, considering both lateral and air-gap misalignment scenarios. The measured results were in good agreement with simulations, validating the effectiveness of our proposed theory.

In addition, we have also developed an integrated matching-less rectifier compact WPT system based on low magnetic loss metamaterial with isolator for biomedical applications. The proposed system uses a stacked MRR metamaterial to reduce magnetic losses and improve system efficiency. The system is designed to be integrated with a compact embedded receiver and a matching-less rectifier located on the backside of the receiver substrate. The proposed system achieves good efficiency levels and operates within the limits of IEEE C95.1-1995 for the 1-g average Specific Absorption Rate (SAR). We have also developed a 3-layer zero characteristics metamaterial isolator to reduce magnetic field leakage and power losses. By using this isolator metamaterial, we have managed to maintain system performance without any adverse effects.

Overall, the results of this thesis demonstrate the potential of WPT systems for biomedical applications and provide valuable insights into the design and optimization of efficient and reliable WPT systems that can operate within the limits of safety standards.

6.2 Future Work

Fig 6. 1 Block diagram of the whole system.

The "inverter," "WPT system," and "rectifier" are three essential components in a Wireless Power Transfer (WPT) system, each playing a crucial role in the overall power transfer process:

- Inverter: An inverter is a device or circuit that converts direct current (DC) into alternating current (AC). In the context of WPT, the inverter is typically a part of the transmitter (TX) and is responsible for generating the AC signal that carries the power to be transmitted wirelessly.
- Wireless Power Transfer (WPT) System
- Rectifier

Together, these components work in harmony to enable efficient and reliable wireless power transfer, providing a convenient and versatile solution for powering electronic devices and systems without the need for physical connections. The total efficiency of the system is calculated as

$$\eta_{total} = \eta_{inverter} \times \eta_{WPT} \times \eta_{rectifier} \tag{6.1}$$

Hence, the inverter can significantly impact the overall system efficiency. While our research has primarily focused on the WPT and rectifier parts, it is essential to recognize the role of the inverter in the overall performance of the system. To achieve optimal overall system efficiency, it is crucial to design and optimize the inverter for high efficiency while considering other components in the WPT system. Additionally, feedback control mechanisms and power management strategies can be employed to adjust the inverter's output power based on load conditions and maximize power transfer efficiency.

Another issue the body is not perfectly flat. In the reality, human body has many curves, and this leads to the formation of air gaps between the transmitter (TX) and the body. Future research could focus on overcoming these limitations, a flexible Meta surface with low magnetic loss will be the suitable solution. Also, the development of WPT systems for specific applications, such as cardiac implants or neural stimulators, and the investigation of new metamaterial designs to further improve system performance.

6.3 Expected result.

- Implementation of a low magnetic loss flexible metasurface-based WPT system for a compact RX for biological applications. This implementation will enable the realization of battery-less bio-friendly and patient-comfortable sensors. The system's efficiency and performance during misalignment will also be evaluated through simulation and experimental results.
- The impact of this proposed WPT system is expected to be significant in the microwave-engineering field in general. The development of a compact and efficient WPT system for biomedical applications could potentially revolutionize the way medical devices are powered, allowing for more comfortable and long-term implantable devices that do not require regular battery replacements. Additionally, the use of metamaterial-based meta surface in WPT systems could pave the way for more innovative and advanced wireless power transfer solutions in various fields.

References

1. J. Garnica, R. A. Chinga, and J. Lin, "Wireless Power Transmission: From Far Field to Near Field," in Proceedings of the IEEE, vol. 101, no. 6, pp. 1321-1331, June 2013.
2. H. Kim, H. Hirayama, S. Kim, K. J. Han, R. Zhang, and J. Choi, "Review of Near-Field Wireless Power and Communication for Biomedical Applications," IEEE Access, vol. 5, pp. 21264-21285, 2017.
3. L. A. Bradshaw, J. K. Ladipo, D. J. Staton, J. P. Wikswo, and W. O. Richards, "The human vector magnetogastrogram and magnetoenterogram," IEEE Transactions on Bio.Engineering, vol. 46, no. 8, pp. 959-970, August 1999.
4. R. R. Harrison, "Designing Efficient Inductive Power Links for Implantable Devices," in Proceeding of IEEE International Symposium on Circuit and Systems, New Orleans, LA, USA, May 2007.
5. R. Jegadeesan, Y. X. Guo, and M. Je, "Electric near-field coupling for wireless power transfer in biomedical applications," in Proceeding of IEEE MTT-S International Microwave Workshop Series on RF and Wireless Technologies for Biomedical and Healthcare Applications, Singapore, 2013, pp. 1-3.
6. M. Soma, D. C. Galbraith, and R. L. White, "Radio-Frequency Coils in Implantable Devices: Misalignment Analysis and Design Procedure," IEEE Transactions on Biomedical Engineering, vol. BME-34, no. 4, pp. 276-282, April 1987.
7. G. L. Barbruni, P. M. Ros, D. Demarchi, S. Carrara, and D. Ghezzi, "Miniaturised wireless power transfer systems for neurostimulation: A review," IEEE Trans. Biomed. Circuits Syst., vol. 14, no. 6, pp. 1160–1178, Dec. 2020.
8. Ahmadi, M. M. & Jullien, G. A. A wireless-implantable microsystem for continuous blood glucose monitoring. *IEEE Trans. Biomed. Circuits Syst.* **3**, 169–180 (2009).
9. S. A. Mirbozorgi, H. Bahrami, M. Sawan, and B. Gosselin, "A Smart Cage with Uniform Wireless Power Distribution in 3D for Enabling Long-Term Experiments with Freely Moving Animals," IEEE Transactions on Biomedical Circuits and Systems, vol. 10, no. 2, pp. 424-434, April 2016.

10. L. Li, H. Liu, H. Zhang, and W. Xue, "Efficient Wireless Power Transfer System Integrating with Metasurface for Biological Applications, " IEEE Trans. Ind. Electron., vol. 65, no. 4, pp. 3230-3239, Apr. 2018.
11. A. Ibrahim and M. Kiani, “A Figure-of-Merit for Design and Optimization of Inductive Power Transmission Links for Millimeter-Sized Biomedical Implants,” IEEE Trans Biomed Circuits Syst, vol. 10, no. 6, pp. 1100-1111, Dec. 2016.
12. R. K. Pokharel, A. Barakat, S. Alshhawy, K. Yoshitomi, and C. Sarris, “Wireless power transfer system rigid to tissue characteristics using metamaterial inspired geometry for biomedical implant applications,” Sci. Rep., vol. 11, pp. 1–10, 2021.
13. K. Finkenzeller, RFID Handbook: Fundamentals and Applications in Contactless Smart Cards and Identification 2nd Ed. New York: Wiley, 2003.
14. G. Sun, B. Muneer, b, and Q. Zhu, “Ultracompact implantable design with integrated wireless power transfer and RF transmission capabilities,” IEEE Trans. Biomed. Circuits Syst., vol. 12, no. 2, pp. 281–291, Feb. 2018.
15. Q. Wang, W. Che, M. Mongiardo, and G. Monti, “Wireless Power Transfer System with High Misalignment Tolerance for Bio-Medical Implants,” IEEE Trans. Circuits Syst. II: Exp. Briefs, vol. 67, no. 12, pp. 3023-3027, Dec. 2020
16. M. M. Ahmadi and G. A. Jullien, “A Wireless-Implantable Microsystem for Continuous Blood Glucose Monitoring,” IEEE Trans. Biomed. Circuits Syst., vol. 3, no. 3, pp. 169-180, June 2009.
17. T. Ohira, "The kQ product as viewed by an analog circuit engineer", *IEEE Circuits Syst. Mag.*, vol. 17, no. 1, pp. 27-32, Feb. 2017.
18. U. Jow and M. Ghovanloo, “Optimization of Data Coils in a Multiband Wireless Link for Neuroprosthetic Implantable Devices,” IEEE Trans. Biomed. Circuits Syst., vol. 4, no. 5, pp. 301-310, Oct. 2010.
19. S. Chalise, F. Tahar, M. R. Saad, A. Baraket, K. Yoshitomi, and R. K. Pokharel, “High Efficiency Wireless Power Transfer System Using Spiral DGS Resonators Through Biological Tissues,” in Proc. IEEE Int. Microwave Biomedical Conf., Philadelphia, PA, Jun. 2018, pp. 43-45.

20. H. Vihvelin, J. R. Leadbetter, M. Bance, J. A. Brown, and R. B. A. Adamson, “Compensating for Tissue Changes in an Ultrasonic Power Link for Implanted Medical Devices,” IEEE Trans. Biomed. Circuits. Syst., vol. 10, no. 2, pp. 404-411, Apr. 2016.
21. M. Meng and M. Kiani, “Design and Optimization of Ultrasonic Wireless Power Transmission Links for Millimeter-Sized Biomedical Implants,” IEEE Trans. Biomed. Circuits. Syst., vol. 11, no. 1, pp. 98-107, Feb. 2017.
22. N. Nguyen, N. Ha-Van, and C. Seo, “Midfield Wireless Power Transfer for Deep-Tissue Biomedical Implants,” IEEE Antennas Wirel. Propag. Lett., vol. 19, no. 12, pp. 2270-2274, Dec. 2020.
23. U. Jow and M. Ghovanloo, “Design and Optimization of Printed Spiral Coils for Efficient Transcutaneous Inductive Power Transmission,” IEEE Trans. Biomed. Circuits. Syst., vol. 1, no. 3, pp. 193-202, Sep. 2007.
24. M. Kiani, U. Jow, and M. Ghovanloo, “Design and optimization of a 3-coil inductive link for efficient wireless power transmission,” IEEE Trans. Biomed. Circuits. Syst., vol. 5, no. 6, pp. 579–591, Dec. 2011.
25. D. Pivonka, A. Yakovlev, A. Poon, and T. Meng, “A mm-sized wirelessly powered and remotely controlled locomotive implant,” IEEE Trans. Biomed. Circuits Syst, vol. 6, no. 6, pp. 523–532, Dec. 2012.
26. G. Wang, P. Wang, Y. Tang and W. Liu, "Analysis of dual band power and data telemetry for biomedical implants", *IEEE Trans. Biomed. Circuits Syst.*, vol. 6, no. 3, pp. 208-215, Jun. 2012.
27. U. Jow and M. Ghovanloo, "Optimization of data coils in a multiband wireless link for neuroprosthetic implantable devices", *IEEE Trans. Biomed. Circuits Syst.*, vol. 4, no. 5, pp. 301-310, Oct. 2010.
28. R. Jegadeesan, K. Agarwal, Y. Guo, S. Yen, and N. V. Thakor, “Wireless Power Delivery to Flexible Subcutaneous Implants Using Capacitive Coupling,” IEEE Transactions on Microwave Theory and Techniques, vol. 65, no. 1, pp. 280-292, January 2017.
29. iP. Chen, H. Yang, R. Luo, and B. Zhao, “A tissue-channel transcutaneous power transfer technique for implantable devices,” IEEE Trans. Power Electron., vol. 33, no. 11, pp. 9753–9761, Nov. 2018.

30. E. Abramov, I. Zeltser, and M. M. Peretz, “A network-based approach for modeling resonant capacitive wireless power transfer systems,” in CPSS Transactions on Power Electronics and Applications, vol. 4, no. 1, pp. 19-29, March 2019.
31. J. Alberto, U. Reggiani, and L. Sandrolini, “Magnetic near field from an inductive power transfer system using an array of coupled resonators,” in Proceeding of Asia-Pacific International Symposium on Electromagnetic Compatibility, Shenzhen, 2016, pp. 876-879.
32. Pozar, David M. Microwave Engineering. Hoboken, NJ: Wiley, 2012.
33. L. Huang, A.P. Hu, A.K. Swain, and Y. Su, “Z-Impedance Compensation for Wireless Power Transfer Based on Electric Field,” IEEE Trans. Power Electronics, Vol. 31, No. 11, November 2016.
34. S. Kim, J. Bito, S. Jeong, A. Georgiadis, and M. M. Tentzeris, “A flexible hybrid printed RF energy harvester utilizing catalyst-based copper printing technologies for far-field RF energy harvesting applications,” in Proceeding of IEEE MTT-S International Microwave Symposium, Phoenix, AZ, 2015, pp. 1-4.
35. S. Fan et al., “A 2.45-GHz Rectifier-Booster Regulator with Impedance Matching Converters for Wireless Energy Harvesting,” IEEE Transactions on Microwave Theory and Techniques, vol. 67, no. 9, pp. 3833-3843, September 2019.
36. A. Barakat, K. Yoshitomi, and R. K. Pokharel, “Design Approach for Efficient Wireless Power Transfer Systems During Lateral Misalignment,” IEEE Transactions on Microwave Theory and Techniques, vol.66, no.9, pp.4170-4177, September 2018.
37. A. Pacini, A. Costanzo, S. Aldhaher, and P. D. Mitcheson, “Load- and Position-Independent Moving MHz WPT System Based on GaN-Distributed Current Sources,” IEEE Transactions on Microwave Theory and Techniques, vol. 65, no. 12, pp.5367-5376, December 2017.
38. S.A. Mirbozorgi, H. Bahrami, M. Sawan, and B. Gosselin, “A Smart Multicoil Inductively Coupled Array for Wireless Power Transmission,” IEEE Transactions on Industrial Electronics, vol.61, no.11, pp.6061-6070, November 2014.
39. D. Liu and S. Georgakopoulos, “Cylindrical Misalignment Insensitive Wireless Power Transfer Systems,” IEEE Transactions on Power Electronics, vol.33, no.11, pp.9331-9343, November 2018.

40. J. Lee, Y. Lim, W. Yang, and S. Lim, “Wireless Power Transfer System Adaptive to Change in Coil Separation,” IEEE Transactions on Antennas and Propagation, vol.62, no.2, pp.889-897, February 2014.
41. X.Y. Zhang, C.-D. Xue, and J.-K. Lin, “Distance-Insensitive Wireless Power Transfer Using Mixed Electric and Magnetic Coupling for Frequency Splitting Suppression,” IEEE Transactions on Microwave Theory and Techniques, vol.65, no.11, pp. 4307-4316, November 2017.
42. F. Tahar, R. Saad, A. Barakat, and R.K. Pokharel, “1.06 FoM and Compact Wireless Power Transfer System Using Rectangular Defected Ground Structure Resonators,” IEEE Microwave and Wireless Components Letters, vol.27, no.11, pp.1025-1027, November 2017.
43. S. Hekal et al., “Compact Wireless Power Transfer System Using Defected Ground Bandstop Filters,” IEEE Microwave and Wireless Components Letters, vol.26, no.10, pp.849-851, October 2016.
44. W. Zhou, S. Sandeep, P. Wu, P. Yang, W. Yu, and S. Y. Huang, “A Wideband Strongly Coupled Magnetic Resonance Wireless Power Transfer System and Its Circuit Analysis,” IEEE Microwave and Wireless Components Letters, vol. 28, no. 12, pp. 1152-1154, December 2018.
45. F.L. Cabrera and F.R. de Sousa, “Backscatter Efficiency Modeling of Inductive Links Applied to Wireless Power Transfer Systems,” IEEE Transactions on Microwave Theory and Techniques, vol.66, no.5, pp. 2386-2392, May 2018.
46. S. Raju, R. Wu, M. Chan, and C. P. Yue, “Modeling of Mutual Coupling Between Planar Inductors in Wireless Power Applications,” IEEE Transactions on Power Electronics, vol.29, no.1, pp.481-490, January 2014.
47. T. Imura and Y. Hori, “Maximizing Air Gap and Efficiency of Magnetic Resonant Coupling for Wireless Power Transfer Using Equivalent Circuit and Neumann Formula,” IEEE Transactions on Industrial Electronics, vol.58, no.10, pp.4746-4752, October 2011.
48. V. B. Gore and D. H. Gawali, "Wireless power transfer technology for medical applications," Proceeding of Advances in Signal Processing Conference, Pune, 2016, pp. 455-460.
49. M. R. Basar, M. Y. Ahmad, J. Cho, and F. Ibrahim, "Stable and High-Efficiency Wireless Power Transfer System for Robotic Capsule Using a Modified Helmholtz Coil," IEEE Transactions on Industrial Electronics, vol. 64, no. 2, pp. 1113-1122, February 2017.

50. C. Yang, C. Chang, S. Lee, S. Chang, and L. Chiou, “Efficient Four-Coil Wireless Power Transfer for Deep Brain Stimulation,” IEEE Trans. Microw. Theory Techniq., vol. 65, no. 7, pp. 2496-2507, Jul. 2017.
51. S. Alshhawy, A. Barakat, K. Yoshitomi, and R. K. Pokharel, “Separation-Misalignment Insensitive WPT System Using Two-Plane Printed Inductors,” IEEE Microw. Wireless Compon. Lett., vol. 29, no. 10, pp. 683-686, Oct. 2019.
52. A. Barakat, K. Yoshitomi, and R. K. Pokharel, “Design Approach for Efficient Wireless Power Transfer Systems During Lateral Misalignment,” IEEE Trans. Microw. Theory Techniq., vol. 66, no. 9, pp. 4170-4177, Sep. 2018.
53. O. Abdelatty, X. Wang, and A. Mortazawi, “Position-Insensitive Wireless Power Transfer Based on Nonlinear Resonant Circuits,” IEEE Trans. Microw. Theory Techniq., vol. 67, no. 9, pp. 3844-3855, Sept. 2019.
54. Y. Li, J. Hu, X. Li, and K. E. Cheng, “A Flexible Load-Independent Multi-Output Wireless Power Transfer System Based on Cascaded Double T-Resonant Circuits: Analysis, Design and Experimental Verification,” IEEE Trans. Circuits Syst. I: Reg. Papers, vol. 66, no. 7, pp. 2803-2812, July 2019.
55. A. Barakat, K. Yoshitomi, and R. K. Pokharel, “Design and Implementation of Dual-Mode Inductors for Dual-Band Wireless Power Transfer Systems,” IEEE Trans. Circuits Syst. II: Exp. Briefs, vol. 66, no. 8, pp. 1287-1291, Aug. 2019.
56. Y. Cho et al., “Thin Hybrid Metamaterial Slab with Negative and Zero Permeability for High Efficiency and Low Electromagnetic Field in Wireless Power Transfer Systems,” IEEE Trans. Electromagn. Compat., vol. 60, no. 4, pp. 1001-1009, Aug. 2018.
57. A. Barakat, K. Yoshitomi, and R. K. Pokharel, “Design Approach for Efficient Wireless Power Transfer Systems During Lateral Misalignment,” IEEE Transactions on Microwave Theory and Techniques, vol.66, no.9, pp.4170-4177, September 2018.
58. C. Lu et al., “Investigation of Negative and Near-Zero Permeability Metamaterials for Increased Efficiency and Reduced Electromagnetic Field Leakage in a Wireless Power Transfer System,” IEEE Trans. Electromagn. Compat., vol. 61, no. 5, pp. 1438-1446, Oct. 2019.

59. B. Wang, W. Yerazunis, and K. H. Teo, “Wireless Power Transfer: Metamaterials and Array of Coupled Resonators,” in Proceedings of the IEEE, vol. 101, no. 6, pp. 1359-1368, June 2013.
60. K. Dautov, M. Hashmi, G. Nauryzbayev, and N. Nasimuddin, “Recent Advancements in Defected Ground Structure-Based Near-Field Wireless Power Transfer Systems,” IEEE Access, vol. 8, pp. 81298-81309, 2020.
61. T. Shaw and D. Mitra, “Wireless Power Transfer System Based on Magnetic Dipole Coupling with High Permittivity Metamaterials,” IEEE Antennas Wirel. Propag. Lett., vol. 18, no. 9, pp. 1823-1827, Sept. 2019.
62. W. Lee and Y. -K. Yoon, “Tunable Metamaterial Slab for Efficiency Improvement in Misaligned Wireless Power Transfer,” IEEE Microw. Wireless Compon. Lett., vol. 30, no. 9, pp. 912-915, Sep. 2020.
63. B. Wang, W. Yerazunis, and K. H. Teo, “Wireless Power Transfer: Metamaterials and Array of Coupled Resonators,” in Proc. IEEE, vol. 101, no. 6, pp. 1359-1368, Jun. 2013.
64. S. Hekal et al., "A novel technique for compact size wireless power transfer applications using defected ground structures", IEEE Trans. Microw. Theory Techn., vol. 65, no. 2, pp. 591-599, Feb. 2017.
65. M. Fantuzzi, A. Costanzo, S. Tedjini and P. Lemaitre-Auger, "Low-cost UHF near-field power transmission for RFID applications", Proc. 47th Eur. Microw. Conf., pp. 212-215, 2017.
66. S.S. Mohan, M. del Mar Hershenson, S.P. Boyd, and T.H. Lee, “Simple accurate expressions for planar spiral inductances,” IEEE Journal of Solid-State Circuits, vol.34, no.10, pp.1419-1424, October 1999.
67. W.B. Kuhn and N.M. Ibrahim, “Analysis of current crowding effects in multiturn spiral inductors,” IEEE Transactions on Microwave Theory and Techniques, vol. 49, no. 1, pp. 31–38, January 2001.
68. U.-M. Jow and M. Ghovanloo, “Modeling and optimization of printed spiral coils in air saline and muscle tissue environments,” IEEE Trans. Biomed. Circuits Syst., vol. 3, no. 5, pp. 339-347, Oct. 2009.
69. Johnson, R. C. Antenna Engineering Handbook (3rd edn.) 2-6–2-7 (McGraw Hill, 1992).

70. D. Hui, Z. Yisheng, and Z. Baishan, “Research on the electromagnetic radiation of a PCB planar inductor,” in Proceedings of Asia-Pacific Microwave Conference, Suzhou, December 2005, pp. 1-3.
71. S. Verma, D. Rano and M. S. Hashmi, "A novel miniaturized band stop filter using fractal type defected ground structure (DGS)", Proc. IEEE Asia–Pac. Microw. Conf., pp. 799-802, 2017.
72. [online]Available: niremf.ifac.cnr.it/tissprop/htmlclie/htmlclie.php.
73. IEEE standard for safety levels with respect to human exposure to radio frequency electromagnetic fields, 3 KHz to 300 GHz. IEEE Standard C95.1, 1999 edn (1999).
74. A. B. Numan and M. S. Sharawi, “Extraction of Material Parameters for Metamaterials Using a Full-Wave Simulator [Education Column],” IEEE Antennas Propag. Mag., vol. 55, no. 5, pp. 202-211, Oct. 2013.

List of Publications and Awards

Journal

1. **S. Alshhawy**, A. Barakat, K. Yoshitomi, and R. K. Pokharel," Integrated Matching Less Rectifier Compact WPT System Based on Low Magnetic Loss Metamaterial with Isolator for Biomedical Application" IEEE Journal of Electromagnetics, RF and Microwaves in Medicine and Biology. (Submitted)
2. **S. Alshhawy**, A. Barakat, K. Yoshitomi, and R. K. Pokharel, "Compact and Efficient WPT System to Embedded Receiver in Biological Tissues Using Cooperative DGS Resonators," in IEEE Transactions on Circuits and Systems II: Express Briefs, vol. 69, no. 3, pp. 869-873, March 2022.
3. Pokharel, R.K., Barakat, A., **Alshhawy, S**. et al. Wireless power transfer system rigid to tissue characteristics using metamaterial inspired geometry for biomedical implant applications. Sci Rep 11, 5868 (2021).
4. **S. Alshhawy**, A. Barakat, K. Yoshitomi, and R. K. Pokharel, "Separation-Misalignment Insensitive WPT System Using Two-Plane Printed Inductors," IEEE Microwave and Wireless Components Letters, vol. 29, no. 10, pp. 683-686, October 2019.

Conference

1. **S. Alshhawy**, A. Barakat, R. K. Pokharel and K. Yoshitomi, "Low Magnetic Loss Metamaterial Based Miniaturized WPT System for Biomedical Implants," 2022 IEEE/MTT-S International Microwave Symposium - IMS 2022, 2022, pp. 275-278.
2. **S. Alshhawy,** A Barakat, K Yoshitomi, RK Pokharel "Design methodology of compact and high efficiency metamaterial-assisted WPT system through biological tissues ". IEICE Tech. Rep., vol. 121, no. 303, MW2021-86, pp. 11-14, Dec. 2021.
3. A. Barakat, **S. Alshhawy**, K. Yoshitomi, and R.K. Pokharel, "Highly Isolated Dual-Band WPT System for Concurrent Transfer of Wireless Power and Data to Biomedical Implants," in Proceeding of URSI-Japan Radio Science Meeting, Tokyo, Japan, September 2019.

4. A. Barakat, **S. Alshhawy**, K. Yoshitomi, and R. K. Pokharel, “Triple-Band Near-Field Wireless Power Transfer System Using Coupled Defected Ground Structure Band Stop Filters,” in Digest of IEEE MTT-S International Microwave Symposium, Boston, MA, USA, June 2019, pp. 1411-1414.
5. Takashi Miyamoto, Ramesh Pokharel, Kuniaki Yoshtomi, Adel Barakat, **Shimaa Alshhawy**, Jiang Xin “Design of Metamaterial Inspired Transmitter for Misalignment Insensitive Wireless Power Transfer System through Biological Tissues”. IEICE Tech. Rep., vol. 120, no. 422, MW2020-97, pp. 33-38, March 2021.
6. Mohd Khairi Bin Zulkalnain, **Shimaa Alshhawy**, Kan Terazawa, Adel Barakat, Ramesh Pokharel “Near-field Metamaterial-based WPT system with FSK Demodulation in CMOS Technology”. IEICE Tech. Rep., vol. 122, no. 35, MW2022-21, pp. 32-35, May 2022.

Awards

1. **Shimaa Alshhawy**, “WPT System Based on Low Loss Metamaterial for Biomedical Application with Integrated Matching Less Rectifier” 3rd Thailand-Japan Microwave Student Workshop Presentation Award, November 14, 2022.
2. Excellent Student Award of IEEE Fukuoka Section 2019.